—Physics-compatible discretization—

Mass, kinetic energy, enstrophy, vorticity and helicity conservation in CFD.

R.F. Wijland

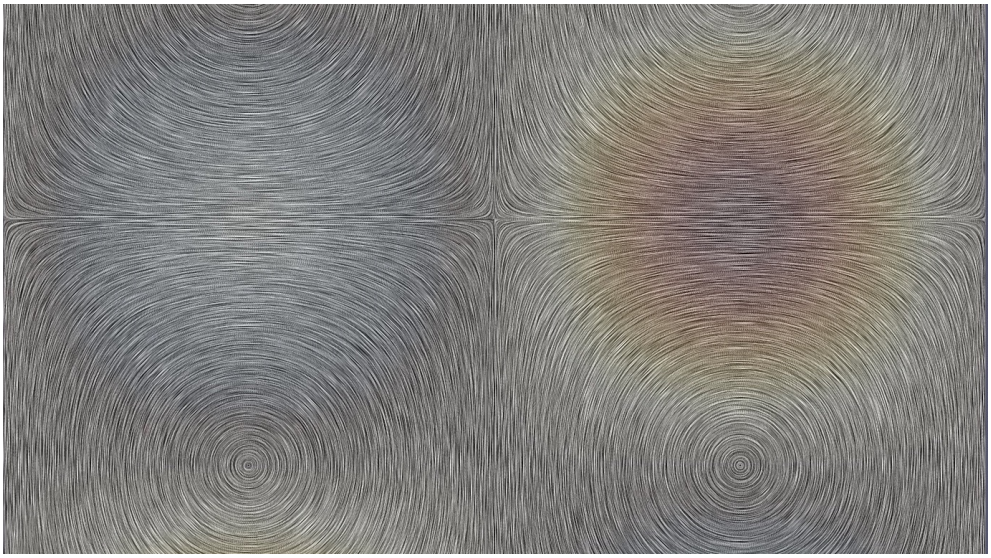

Thesis for *Master of Science* degree in Aerospace Engineering, Aerodynamics and Wind Energy department.

June 24, 2025

Supervisor: Marc Gerritsma

TU Delft Delft University of Technology

Preface

It started with a spark of interest to work on methods that are breaking new ground in numerical analysis by incorporating more physics than traditional methods do. Followed by literature study, on-paper analysis, computer programming for numerical simulations and more. The result lies before you: this thesis. It is not purely a report on a research project, but also the personal closing piece of a Master of Science education.

Without the intent of being unoriginal, this is the place for some special thanks. Particularly because of all (personal) challenges on the way to this result. First of all, I would like to thank my family for their enduring support. Then I would like to thank my supervisor Marc Gerritsma, with special reference to his patience and understanding. Finally, I want to acknowledge other scholars for their contributions to the development of the numeric methods and methodologies that are topic of this work or closely relate to it. In particular Arthur Palha, who was open for some valuable discussions and advice both in person and over email. Further thanks to Gonzalo de Diego for sharing some of his own experiences.

A motivation for studying and developing new computational fluid dynamics (CFD) methods which solve the basic flow equations lies in that traditional methods have their limits. Even when computations are made with a high level of refinement, which is facilitated by increasingly powerful computers, there are limits to the reliability of solutions. Especially after a longer simulated time. This may be improved by incorporating more of the physics into CFD methods, which is a higher-level goal of this work.

Finally, I want to express that I feel honored by anyone reading this thesis and hope its content will be appreciated. There is some re-use of text from my own project plan and literature study in a few places. These documents were not made publicly available.

R.F. Wijland, 2025

Abstract

This MSc thesis is centered around better capturing the physics of Navier-Stokes flow problems with the following two CFD methods that preserve integral invariants. The 2D mass, kinetic energy, enstrophy and total vorticity conserving (MEEVC) method presented in [25] is the cornerstone of this work. It was constructed with mimetic concepts in mind and its favorable properties were a reason to use it as inspiration for developing a novel 3D mass, kinetic energy and helicity conserving (MEHC) method in this work. This method has a separate equation for the evolution of helical density in its formulation, a feature which is possibly unique in CFD.

Analysis and construction of both the MEEVC and MEHC methods is an important topic in this work. In that light the continuous equations independent of any discretization are also studied. Many derivations are included. One thing these derivations demonstrate is a close relation between angular momentum and vorticity. Both the 2D MEEVC and the 3D MEHC method use a system solved for vorticity in addition to a system solved for velocity and pressure. Another key feature they share is that variables are ordered in a DeRham complex with conforming function spaces chosen for them. This enables velocity field solutions that are point-wise divergence-free. The temporal discretization of both methods is characterized by its ability to conserve first- and second-order invariants, as well as that the variables are staggered in time such that the system of equations is decoupled and linearized.

Taylor-Green test problems were executed on a computer with the MEEVC and the MEHC method in respectively 2D and 3D. The results obtained with the MEEVC method confirmed efficacy but also indicated potential limitations to certain conservation properties. A successful implementation of the MEHC method could not be achieved: simulation results were obtained but eventually diverged. The method's conservation properties are only proven analytically. Possible causes are identified to aid any future work.

Contents

Chapter 1

Introduction

For capturing the physics of incompressible fluid flows more accurately in CFD, two specific methods are considered in this work. The most important is the existing mass, energy, enstrophy and vorticity conserving (MEEVC) method [25] for 2D flow which will be documented and verified. Furthermore the novel mass, energy and helicity conserving (MEHC) method for 3D flow is proposed here as a possible idea for further work, although it has problems. The higher goal is to have discrete methods that are compatible with the physical laws that are encoded in the continuous Navier-Stokes equations, whereby most attention is devoted to conservation of corresponding integral invariants in numerical simulations. Such integral invariants are quantities that do not change over time when conditions are appropriate. An example can be the flow's kinetic energy. Invariants have important physical meaning, but discrete methods commonly violate some of them. This essentially indicates that a simulation employing such a method does not correspond to the true flow problem.

This aim of physical compatibility contrasts with that of certain classic schemes which are designed with the prime strive of relatively high accuracy compared to computational cost. Mimetic methods 'mimic' (geometric) properties of the governing differential equations where possible, which can lead to more comparable behavior upon solving. Most mimetic methods use the mathematical language of differential geometry and the coupling with algebraic topology for discrete equivalents. The MEEVC method was developed by thinking in mimetic concepts.

Verstappen and Veldman [32] illustrate how the aforementioned classi-

cal discretization approach can fail to conserve energy while one that better captures the properties of the continuous problem is successful. They first show that a certain finite-difference approximation of the convective operator which is constructed for minimal local truncation error (at up to second order accuracy) leads to violation of kinetic energy conservation. This is solved when they instead use a discrete operator that retains symmetries of the continuous differential operators. An important improvement, as failing to conserve energy can mean that solutions have too much damping or grow exponentially in time. One may be able to suppress such problems to some extend by adding correction terms to the discrete formulation. Yet this will not restore compliance to the conservation laws that are encoded in the governing equations of the original physical problem. Any of such incompatibility generally leads to unrealistic results, or even numerical blowup of the simulation. According to Perot [26], a complete failure like the latter is however unusual for a numeric scheme that sufficiently meets classic mathematical measures of accuracy and stability. This however makes it a tricky problem: the flaws in physical modeling are generally hard to spot from simulation results, especially for complex flows. Results may converge and look realistic while they are not. This effectively undermines the reliable application of such a method in academic as well as corporate contexts. Both scholars and engineers must be able to trust a method before they can draw conclusions from its results. It is therefore worthwhile to develop methods that preserve properties of the original (continuous) problem, instead of focussing only on the aforementioned mathematical criteria.

1.1 Definition and context of conservation

In this thesis a lot is about 'conservation', so it is important to provide a bit more detail here on what is meant by it. All this will show is that conservation can have quite different contexts and that one should always check what authors exactly mean when they claim that a CFD method has particular conservation properties.

In the most straightforward definition, conservation means that an integral quantity remains strictly invariant over time. Conservation of such 'invariants' occurs in physics when conditions are appropriate, this may for example require (the limit of) inviscid fluid and certain boundary conditions.

A more broad definition (that is used less often in this work) actually refers to the correct balance of an integral quantity: it can change in time, but it does so correctly in equilibrium with convective fluxes and dissipation. This means that a quantity, for example kinetic energy, does not decay or grow at a different rate than that which can be expected from physics.

It is possible to differentiate between local and global as well as primary and secondary conservation, as explained in the following using Perot [26] as an important source. Global conservation of an integral quantity means that it is conserved over the entire domain. Local conservation instead refers to the domain subdivided in parts. For example individual integration over each computational cell. Local conservation also requires that the flux crossing the shared boundary of any two adjacent cells is the same on both sides (as this can differ in finite element methods where each cell has its own basis functions). Note that local conservation throughout the domain also implies global conservation. Besides differentiating on the spatial behavior of conservation, one can also differentiate based on the types of variables involved. Conservation of primary unknowns applies to variables that are direct unknowns in the discrete problem formulation, in CFD velocity is typically one of the variables in that role. Secondary unknowns are derived from the primary ones. When velocity is a primary variable and vorticity is computed by taking the curl of velocity, then vorticity is a secondary variable. In that case conservation of total vorticity is a secondary conservation property. Many methods have local conservation of primary variables, while secondary conservation is much less common. Conservation of primary variables is often directly imposed through the formulation, while secondary conservation more indirectly results from how the system is constructed. The (large) effort to achieve the latter may be worth it as *"secondary conservation is important for physically realistic solutions"* [26], also see [17].

1.2 Importance of particular conservation properties

With the previous section explaining the definitions of conservation, here is the place to discuss why it is so important that the MEEVC and MEHC CFD methods have their conservation properties. The corresponding inte-

gral quantities can be found in Section 2.2 with Table 2.1 in particular.

For incompressible flow there should be strong mass conservation: the mass contained within a fixed domain (or any part of it) should be invariant over time. When this is violated it is obviously unphysical in itself, but it can also affect the correctness of results indirectly as demonstrated in [4]. There the authors show that the velocity results of long-time simulations can become less accurate when mass is conserved weakly. Furthermore, [8] shows that conservation properties such as conservation of kinetic energy can also be lost when a CFD method does not (strongly) conserve mass.

Kinetic energy, enstrophy (in 2D) and helicity (in 3D) are important in describing the organization of a flow, as stated by for example Rebholz [27]. Hence they should be conserved as appropriate. That is there should be no (excess) creation or destruction. Otherwise the quality of the solution may suffer and especially when kinetic energy conservation fails one can expect numerical dissipation (or diffusion) to occur. When this leads to incorrectly increasing energy then solutions may keep growing until numeric overflow causes the simulation to blow up after some finite time. Numerical dissipation also has particularly negative effects in direct numerical simulation (DNS) of turbulent flow, where the correct balance between convection and dissipation is paramount. When that balance is correct it leads to the right energy cascade, which is related to that of helicity [24]. Helicity also has an important role in turbulence because it suppresses the nonlinear term and thereby the energy transfer to smaller scales, see [7] and supporting references in that paper. Accurate computation of turbulent flows is relatively challenging, but nevertheless important in for example (engineering of) aircraft high-lift systems [28].

In building a new or selecting an existing conserving method, one may have to choose between different conservation properties when not all can be satisfied. One can then consider the types of flow problems the method intends to solve. According to Perot, *"kinetic energy conservation is often more important than momentum conservation"* [26] in practice. Similarly one can also consider vorticity, enstrophy (in 2D) and helicity (in 3D) conservation important in strongly vortical flows including turbulence (in 3D). For such or otherwise strongly rotating flows it is believed that CFD formulations employing both velocity and vorticity equations with corresponding variables yield higher accuracy in general [1]. This is plausible from the fact

that the angular momentum of an infinitesimal spherical element is directly proportional to the local vorticity in incompressible flows (Section 2.1.4).

1.3 Research question and content of the thesis

It is clarifying to present the *main research question* of the work:

> How does the MEEVC discretization [25] work, does it indeed perform as promised and what could be a conserving 3D method based on the same (mimetic) design principles?

Emphasis will be put on the 2D part, as also developing a successful new 3D discretization is ambitious.

Chapter 2 contains an overview and investigation of the governing equations in order to increase understanding. This includes their derivation and proofs that they dictate invariants under appropriate conditions, which was valuable content to create because little of it was found in literature. An alternative derivation of the vorticity transport equation starting from a conservation of momentum statement is a special example of this and can be found in Section 2.1.4. The chapter ends with mathematical descriptions of Taylor-Green vortex flows in Section 2.3, as the numerical tests in this work aim to solve such flows.

Chapter 3 then focusses on the discrete MEEVC method and Chapter 4 on the numeric results computed with it. Section 3.1 not only presents the MEEVC scheme, but also explains its construction in quite some detail. Then Section 3.2 contains analytic proofs of the MEEVC method's discrete conservation properties, whilst Section 4.2 demonstrates the quality of these properties in actual numeric simulations. Both Sections 4.1 and 4.2 demonstrate convergence on the 2D Taylor-Green problem.

The new 3D method follows in Chapter 5 and overall conclusions with respect to the entire thesis in Chapter 6. The 3D method is derived using inspiration from the 2D MEEVC method in the first sections of Chapter 5 and the resulting formulation is summarized in Section 5.2.3. Its MEHC properties are only proven on paper with algebraic analysis in Section 5.3. Section 5.4 then critically reviews what has been achieved considering the properties, theoretical (in)correctness and problematic test results of the novel method.

Chapter 2

The continuous world in 2D and 3D

This chapter provides some preliminaries: the (Navier–Stokes) equations describing fluid flow physics, their conservation properties and an exact solution for Taylor-Green flow suitable as benchmark. Discrete formulations and more related to numerical computations will be treated in other chapters. The fluid is assumed to be incompressible and, in certain cases, inviscid.

Equations describing the conservation of momentum and mass laws are presented in Section 2.1, including derivations into desired formulations. Proofs of the integral invariants (conservation properties) of these equations can be found in Section 2.2. These proofs can also provide insights and understanding for the discrete work. Details on the Taylor-Green flow are subject of Section 2.3; including solutions, initial and boundary conditions.

2.1 Governing partial differential equations

The equations discussed in this section originate from physical laws (or postulates) stating conservation of mass and momentum. In short, these imply a fixed (and small) group of particles has:

- Constant mass: mass cannot be created or destroyed.
- Balance of momentum: the rate of change of momentum must be balanced by net forces applied (like pressure, viscous or body forces).

In this work, mass density is commonly set to $\rho = 1$ and viscosity μ is considered to be a (non-specified) constant in space and time. Therefore the

kinematic viscosity ($\nu := \mu/\rho$) is a constant as well.

An overview of the set of continuous partial differential equations (PDEs) used for the 2D MEEVC formulation [25, (6)] and for 3D are:

$$\left.\begin{aligned} &\frac{\partial \vec{u}}{\partial t} + \omega \times \vec{u} + \nabla \bar{p} = -\nu \nabla \times \omega \\ &\frac{\partial \omega}{\partial t} + \frac{1}{2}(\vec{u} \cdot \nabla)\omega + \frac{1}{2}\nabla \cdot (\vec{u}\omega) = \nu \nabla^2 \omega \\ &\nabla \cdot \vec{u} = 0 \end{aligned}\right\} \quad \text{2D (MEEVC),} \tag{2.1}$$

and

$$\left.\begin{aligned} &\frac{\partial \vec{u}}{\partial t} + \vec{\omega} \times \vec{u} + \nabla \bar{p} = -\nu \nabla \times \vec{\omega} \\ &\frac{\partial \vec{\omega}}{\partial t} + (\vec{u} \cdot \nabla)\vec{\omega} = (\vec{\omega} \cdot \nabla)\vec{u} + \nu \nabla^2 \vec{\omega} \\ &\nabla \cdot \vec{u} = 0 \end{aligned}\right\} \quad \text{3D.} \tag{2.2}$$

Here, the total pressure $\bar{p}$ relates to the static pressure p by:

$$\bar{p} := \frac{1}{2}\vec{u} \cdot \vec{u} + p. \tag{2.3}$$

If desired, a scalar function ϕ_f representing a conservative body force field $\vec{g} = \nabla \phi_f$ can easily be added, so that $\bar{p} := \frac{1}{2}\vec{u} \cdot \vec{u} + p - \phi_f$. This is however uninteresting for the current work. Lastly, one may see that the $\vec{\omega} \times \vec{u}$-term also appears in opposite order and sign later in this text because for any two vectors $\vec{b} \times \vec{a} = -\vec{a} \times \vec{b}$.

One may note that there are some clear differences between the 2D (2.1) and 3D (2.2) continuous formulations. Most of these are in their respective vorticity transport equations as will be detailed in Section 2.1.3. Three differences are highlighted here:

- In 3D both the velocity $\vec{u}$ and vorticity $\vec{\omega}$ vectors have three components, while in 2D velocity has two and vorticity is effectively a scalar. The latter means that vorticity is treated as a scalar or where mathematically appropriate the corresponding vector that has only one of its components nonzero.
- The 'vortex stretching' term $(\vec{\omega} \cdot \nabla)\vec{u}$ appears only in the 3D vorticity transport equation that is included in (2.2) on the second line. An interpretation of this term is explained in Section 2.1.3 below.

- Another difference is that the 2D vorticity transport equation, that is the second in (2.1), uses a skew-symmetric decomposition of its convective part. This allows the discrete MEEVC formulation to achieve conservation of enstrophy as demonstrated in Section 3.2. In 3D on the other hand, enstrophy is generally not conserved anyway so (2.2) does not employ a skew-symmetric formulation. Furthermore no other reason was found to prefer one there as well.

Finally, it should be remarked that (2.2) is not definitive for the 3D MEHC method and that modifications can be found in Chapter 5.

2.1.1 Balance of linear momentum equation

Conservation of momentum ($\rho\vec{u}$), see [33, (2-19)], in differential form and for incompressible flow is:

$$\rho\frac{\mathrm{D}\vec{u}}{\mathrm{D}t} = \rho\vec{g} + \nabla\cdot\sigma_{ij}, \tag{2.4}$$

where σ_{ij} is the stress tensor. Also, the material derivative is used, which is the temporal derivative of any property f of a material (or fluid) element in the flow field. It is given by [33, p. 17, (1-8)]:

$$\frac{\mathrm{D}f}{\mathrm{D}t} = \frac{\partial f}{\partial t} + (\vec{u}\cdot\nabla)f. \tag{2.5}$$

This property f can be a quantity like temperature, but also the velocity field itself like in (2.4).

The viscous part of the stress tensor is a function of flow kinematics. For common air flows, it is usual to assume the fluid is continuous, isotropic (properties independent of direction) and Newtonian. The latter means viscous stress linearly depends on the strain rate. Stokes proposed a general deformation law for this situation [33, (2-27)]:

$$\sigma_{ij} = -p\delta_{ij} + \mu\left(\frac{\partial u_i}{\partial x_j} + \frac{\partial u_j}{\partial x_i}\right) + \underbrace{\lambda\delta_{ij}\left(\nabla\cdot\vec{u}\right)}_{=0}, \tag{2.6}$$

where δ_{ij} is the Kronecker delta function ($\delta_{ij} = 1$ if $i = j$, otherwise $\delta_{ij} = 0$) and λ the coefficient of bulk viscosity. The latter is however not important, as its term drops out here because of $\nabla\cdot\vec{u} = 0$, see (2.1) and (2.2).

A form of the Navier-Stokes equations [33, (2-30)] is obtained by substituting (2.6) for σ_{ij} in (2.4), under assumption of constant viscosity μ. Further neglecting body forces ($\vec{g} = 0$) results in:

$$\rho \frac{\mathrm{D}\vec{u}}{\mathrm{D}t} = -\nabla p + \mu \nabla^2 \vec{u}, \tag{2.7}$$

$$\Updownarrow$$

$$\frac{\partial \vec{u}}{\partial t} + (\vec{u} \cdot \nabla)\vec{u} = -\frac{\nabla p}{\rho} + \nu \nabla^2 \vec{u}, \tag{2.8}$$

where $\nu = \mu/\rho$ is the kinematic viscosity and $\nabla^2 = \nabla \cdot \nabla = \Delta$ the Laplace operator. Equation (2.8) is equivalent to (2.7) divided by ρ and with $\mathrm{D}\vec{u}/\mathrm{D}t$ expanded according to (2.5). The term $(\vec{u} \cdot \nabla)\vec{u}$ represents the convective derivative.

Equation (2.8) is rewritten in a format equivalent to its 2D variant in the MEEVC paper, that is the first in (2.1), as follows. Known vector identities are used here, several of them thanks to suggestions in [35]. A general rule (for vector fields $\vec{a}$ and $\vec{c}$) is [23, A1. Vector Identities, p. 363, (8)]:

$$\nabla(\vec{a} \cdot \vec{c}) = \vec{a} \cdot \nabla\vec{c} + \vec{c} \cdot \nabla\vec{a} + \vec{a} \times (\nabla \times \vec{c}) + \vec{c} \times (\nabla \times \vec{a}). \tag{2.9}$$

Now let $\vec{a} = \vec{c} = \vec{u}$, then $\nabla(\vec{u} \cdot \vec{u}) = 2\vec{u} \cdot \nabla\vec{u} + 2\vec{u} \times (\nabla \times \vec{u})$. Recognizing $\vec{\omega} = \nabla \times \vec{u}$, rearranging and dividing by 2 gives:

$$\vec{u} \cdot \nabla\vec{u} = \frac{1}{2}\nabla(\vec{u} \cdot \vec{u}) - \vec{u} \times \vec{\omega}. \tag{2.10}$$

Substituting this into (2.8) gives:

$$\frac{\partial \vec{u}}{\partial t} + \frac{1}{2}\nabla(\vec{u} \cdot \vec{u}) - \vec{u} \times \vec{\omega} = -\frac{\nabla p}{\rho} + \nu \nabla^2 \vec{u}. \tag{2.11}$$

Then setting the constant density to $\rho = 1$, rearranging and introducing the total pressure defined by (2.3), gives:

$$\frac{\partial \vec{u}}{\partial t} + \vec{\omega} \times \vec{u} + \nabla \bar{p} = \nu \nabla^2 \vec{u}, \tag{2.12}$$

where $\vec{\omega} \times \vec{u} = -\vec{u} \times \vec{\omega}$ was used (by definition of the cross product). The last step is to rewrite the viscous term by using the following identity [23, A1. Vector Identities, p. 363, (10)]:

$$\nabla \times (\nabla \times \vec{a}) = \nabla(\nabla \cdot \vec{a}) - \nabla^2 \vec{a}.$$

Substitution of $\vec{a} = \vec{u}$, while noting that $\nabla \cdot \vec{u} = 0$ from (2.2) and $\vec{\omega} = \nabla \times \vec{u}$, yields $\nabla^2 \vec{u} = \nabla \times \vec{\omega}$. From that,

$$\frac{\partial \vec{u}}{\partial t} + \vec{\omega} \times \vec{u} + \nabla \bar{p} = -\nu \nabla \times \vec{\omega}. \tag{2.13}$$

This result equals the first equation in (2.2) and is called the 'rotational formulation' of conservation of momentum because of $\vec{\omega} \times \vec{u}$. Its 2D equivalent is the first equation in (2.1), which has scalar-valued vorticity ω; in that case a vector with only one nonzero component.

Using the rotational formulation as the starting point for discretization in this work has its reasons as follows. Considering the resulting discrete formulations in Chapters 3 and 5, the derivatives applied to the variables are admissible in the sense that the result is square-integrable in most cases. This is an important aspect of the design philosophy of the MEEVC method [25] and thereby also of the MEHC method proposed here. Furthermore, according to [20] discretization from the rotational form can lead to methods that have better (energy) conservation properties (see also [8]), are relatively stable and have relatively low computational burden. They can however suffer from lower accuracy.

2.1.2 Mass conservation: the divergence-free constraint

For an incompressible flow, conservation of mass implies the divergence-free constraint on the velocity field must hold (as derived below):

$$\mathrm{div}(\vec{u}) = \nabla \cdot \vec{u} = 0. \tag{2.14}$$

This equation must be valid locally, at any point, so that conservation of mass does *not only* apply at global level. Many CFD methods do not achieve this.

The following derivation of (2.14) is based on [33, Section 2.3] and more detail can be found in that textbook. It starts with the simple notion of an infinitesimally small group of particles with volume $\mathcal{V}$ and mass $m = \rho\mathcal{V}$. Conservation of mass in a Lagrangian framework thereby implies

$$m = \rho\mathcal{V} = \text{constant},$$

so its time derivative must be zero:

$$\frac{\mathrm{D}m}{\mathrm{D}t} = \rho\frac{\mathrm{D}\mathcal{V}}{\mathrm{D}t} + \mathcal{V}\frac{\mathrm{D}\rho}{\mathrm{D}t} = 0. \tag{2.15}$$

The rate of change in volume can be related to the extensional strain rates:

$$\frac{\mathrm{D}\mathcal{V}}{\mathrm{D}t} = (\epsilon_{xx} + \epsilon_{yy} + \epsilon_{zz})\mathcal{V} = \left(\frac{\partial u}{\partial x} + \frac{\partial v}{\partial y} + \frac{\partial w}{\partial z}\right)\mathcal{V} = (\nabla \cdot \vec{u})\mathcal{V},$$

using kinematic relations $\epsilon_{xx} = \partial u/\partial x$, $\epsilon_{yy} = \partial v/\partial y$ and $\epsilon_{zz} = \partial w/\partial z$. Substituting this expression for the time derivative of $\mathcal{V}$ into (2.15) and dividing the result by $\mathcal{V}$ itself yields the continuity equation:

$$\frac{\mathrm{D}\rho}{\mathrm{D}t} + \rho\nabla \cdot \vec{u} = 0. \tag{2.16}$$

Then it is obvious that for an incompressible flow, where ρ is considered a nonzero material constant, the flow field must satisfy

$$\nabla \cdot \vec{u} = 0,$$

that is (2.14), at any location. Hence this equation is incorporated in both the 2D (2.1) and 3D (2.2) formulations.

2.1.3 Vorticity transport equation

First in this section, the vorticity transport equation is derived by taking the curl of the linear momentum equation; to state it simply. This is done for the 3D case and the result is then reduced to 2D. It must be remarked that an alternative derivation of the vorticity transport equation starting from angular momentum conservation can be found in Section 2.1.4 for the general 3D case.

Derivation of the 3D vorticity transport equation

The 3D vorticity transport equation is derived here by taking the curl of (2.11). Thanks to linearity of the curl, each term is considered separately:

- It is assumed that any of the higher-order partial derivatives present is continuous, also if its order of differentiation is changed, so that this order does not matter by Clairaut's Theorem [29, Sec. 14.3, pp. 916–917]. It is justified to assume this continuity because only smooth flows without shocks are considered in this work. Application of the theorem to the following two cases yields:

$$\nabla \times \frac{\partial \vec{u}}{\partial t} = \frac{\partial}{\partial t}(\nabla \times \vec{u}) = \frac{\partial \vec{\omega}}{\partial t} \tag{2.17}$$

and, remembering that ν = constant,

$$\nabla \times (\nu \nabla^2 \vec{u}) = \nu \nabla^2 (\nabla \times \vec{u}) = \nu \nabla^2 \vec{\omega}. \tag{2.18}$$

- The curl of the gradient of any scalar field ϕ is zero (assuming all its second-order derivatives exist), that is $\nabla \times \nabla \phi = 0$ [23, A1. Vector Identities, p. 363, (11)]. Therefore:

$$\frac{1}{2} \nabla \times \nabla (\vec{u} \cdot \vec{u}) = 0 \tag{2.19}$$

and

$$\nabla \times \left(-\frac{\nabla p}{\rho} \right) = -\frac{\nabla \times \nabla p}{\rho} = 0. \tag{2.20}$$

These results are obtained by noting that both $\vec{u} \cdot \vec{u}$ and the pressure p are scalar fields. Furthermore, ρ = constant (incompressible flow) is employed in the latter.

- A final identity to use is, for any two vector fields $\vec{a}$ and $\vec{c}$: $\nabla \times (\vec{a} \times \vec{c}) = \vec{c} \cdot \nabla \vec{a} - \vec{a} \cdot \nabla \vec{c} + \vec{a} \nabla \cdot \vec{c} - \vec{c} \nabla \cdot \vec{a}$ [23, A1. Vector Identities, p. 363, (7)]. Now substitute $\vec{a} = \vec{u}$ and $\vec{c} = \vec{\omega}$ and multiply with -1 to obtain:

$$-\nabla \times (\vec{u} \times \vec{\omega}) = -(\vec{\omega} \cdot \nabla) \vec{u} + (\vec{u} \cdot \nabla) \vec{\omega}. \tag{2.21}$$

Note that some of the terms on the right hand side have dropped out. The third because $\nabla \cdot \vec{\omega} = \nabla \cdot (\nabla \times \vec{u}) = 0$ by the identity [23, A1. Vector Identities, p. 363, (12)]. The fourth because $\nabla \cdot \vec{u} = 0$ by (2.14).

With above results, the curl of (2.11) is assembled:

$$\underbrace{\frac{\partial \vec{\omega}}{\partial t} + (\vec{u} \cdot \nabla) \vec{\omega}}_{\frac{\mathrm{D}\vec{\omega}}{\mathrm{D}t}} = (\vec{\omega} \cdot \nabla) \vec{u} + \nu \nabla^2 \vec{\omega}. \tag{2.22}$$

This is the vorticity transport equation for 3D in (2.2).

On the right hand side of (2.22), the viscous diffusion term $\nu \nabla^2 \vec{\omega}$ is accompanied by the less-familiar 'vortex stretching term' $(\vec{\omega} \cdot \nabla) \vec{u}$ [13]. This inner product measures the change in the velocity vector over its field in the direction the vorticity vector points. In context of the vorticity transport equation, this means a contribution to the temporal derivative of vorticity

that can correspond to rotating and stretching the vorticity vector. A rotation leads to bending of the vorticity field lines while stretching means the local vorticity increases. The latter occurs if the instantaneous velocity field is such that velocity increases in the pointing direction of the vorticity vector. It will follow below that the vortex stretching term is not present in the 2D case. Then vorticity is always perpendicular to the planar velocity, so there is no change in velocity in the direction of the vorticity vector.

Derivation of the 2D vorticity transport equation

The 2D vorticity transport equation is now derived from (2.11) like (2.22) was earlier in this text, but then under assumption of planar flow. The primary result of that will be rewritten into the form used for the MEEVC method [25].

2D planar flow can be described in a 3D basis as follows. An orthonormal basis $(\vec{i}, \vec{j}, \vec{k})$ exists in which the velocity field can be represented in terms of the first two basis vectors only. Because vorticity is defined as the curl of the velocity field, it is always perpendicular to it and hence represented completely in terms of the remaining basis vector. So, let

$$\vec{u} = \begin{bmatrix} u \\ v \\ 0 \end{bmatrix} \quad \text{and} \quad \vec{\omega} = \begin{bmatrix} 0 \\ 0 \\ \omega \end{bmatrix}. \tag{2.23}$$

Note that this is a 3D representation of the 2D case, where $\vec{u}$ is usually represented in two-entry vector format and $\omega = \nabla \times \vec{u}$ in scalar format.

Substituting from (2.23) into (2.11) and taking the curl of this equation differs in two particular aspects compared to the 3D situation treated earlier in this Section 2.1.3. One is that the resulting 'vector' of equations is only nonzero in the $\vec{k}$-component, making it effectively a single equation. The other is that the first term on the right-hand side of (2.21) will be zero as demonstrated in the following. First compute $\vec{u} \times \vec{\omega}$ with $\vec{u}$ and $\vec{\omega}$ from (2.23):

$$\vec{u} \times \vec{\omega} = \begin{vmatrix} \vec{i} & \vec{j} & \vec{k} \\ u & v & 0 \\ 0 & 0 & \omega \end{vmatrix} = \omega \begin{bmatrix} v \\ -u \\ 0 \end{bmatrix}. \tag{2.24}$$

Because the result is a product of a scalar and a vector, its curl can be computed with aid of the identity $\nabla \times (\phi \vec{a}) = \phi \nabla \times \vec{a} + \nabla \phi \times \vec{a}$ [23, A1. Vector

Identities, p. 363, (5)]:

$$\begin{aligned}
\nabla \times (\vec{u} \times \vec{\omega}) &= \nabla \times \left(\omega \begin{bmatrix} v \\ -u \\ 0 \end{bmatrix} \right) \\
&= \omega \begin{vmatrix} \vec{i} & \vec{j} & \vec{k} \\ \frac{\partial}{\partial x} & \frac{\partial}{\partial y} & \frac{\partial}{\partial z} \\ v & -u & 0 \end{vmatrix} + \begin{vmatrix} \vec{i} & \vec{j} & \vec{k} \\ \frac{\partial \omega}{\partial x} & \frac{\partial \omega}{\partial y} & \frac{\partial \omega}{\partial z} \\ v & -u & 0 \end{vmatrix} \\
&= \omega \begin{bmatrix} \frac{\partial u}{\partial z} = 0 \\ \frac{\partial v}{\partial z} = 0 \\ -\frac{\partial u}{\partial x} - \frac{\partial v}{\partial y} = -\nabla \cdot \vec{u} = 0 \end{bmatrix} + \begin{bmatrix} u \frac{\partial \omega}{\partial z} = 0 \\ v \frac{\partial \omega}{\partial z} = 0 \\ -u \frac{\partial \omega}{\partial x} - v \frac{\partial \omega}{\partial y} = -\vec{u} \cdot \nabla \omega \end{bmatrix} \\
&= \begin{bmatrix} 0 \\ 0 \\ -(\vec{u} \cdot \nabla)\omega \end{bmatrix},
\end{aligned}$$

where $\nabla \cdot \vec{u} = 0$ by (2.14) and derivatives with respect to z are zero because of the 2D situation. The curls of other terms in (2.11) are similar to the 3D situation. Hence the result is similar to (2.22), but note that it is now a single (scalar) equation and that there is no vortex stretching term $(\vec{\omega} \cdot \nabla)\vec{u}$:

$$\underbrace{\frac{\partial \omega}{\partial t} + (\vec{u} \cdot \nabla)\omega}_{\frac{\mathrm{D}\omega}{\mathrm{D}t}} = \nu \nabla^2 \omega. \tag{2.25}$$

The convective term in (2.25) can be rewritten by substituting $\phi = \omega$ and $\vec{a} = \vec{u}$ in the identity $\nabla \cdot (\phi \vec{a}) = \phi \nabla \cdot \vec{a} + \vec{a} \cdot \nabla \phi$ [23, A1. Vector Identities, p. 363, (4)] and rearranging:

$$\vec{u} \cdot \nabla \omega = \nabla \cdot (\vec{u}\omega) - \omega \nabla \cdot \vec{u}. \tag{2.26}$$

This reduces to $\vec{u} \cdot \nabla \omega = \nabla \cdot (\vec{u}\omega)$ because $\nabla \cdot \vec{u} = 0$ by (2.14). So then one can write, by trivial summation:

$$(\vec{u} \cdot \nabla)\omega = \frac{1}{2}(\vec{u} \cdot \nabla)\omega + \frac{1}{2}\nabla \cdot (\vec{u}\omega). \tag{2.27}$$

Finally substituting this in (2.25) yields

$$\frac{\partial \omega}{\partial t} + \frac{1}{2}(\vec{u} \cdot \nabla)\omega + \frac{1}{2}\nabla \cdot (\vec{u}\omega) = \nu \nabla^2 \omega, \tag{2.28}$$

which is the 2D vorticity transport equation [25, (6)] of the MEEVC method. In its discrete formulation, the two terms $\frac{1}{2}(\vec{u} \cdot \nabla)\omega$ and $\frac{1}{2}\nabla \cdot (\vec{u}\omega)$ cancel each other in the proof of discrete enstrophy conservation (Section 3.2.4).

2.1.4 Vorticity and angular momentum

While (2.13) is derived from (2.4) and therefore clearly relates to linear momentum, taking its curl to derive the vorticity transport equation (2.22) in Section 2.1.3 did not show (2.22) relates to angular momentum. An alternative 'direct' derivation, based on Chatwin [9], is presented in the following and provides that insight. It applies Newton's second law to a small fluid element by balancing its angular momentum rate of change with moments of forces acting on it. It will also follow that there is a close relation between vorticity and angular momentum. Theoretical arguments for including the vorticity transport equation next to linear momentum in the MEEVC formulation [25] can be drawn from this section later.

Properties and angular momentum of a small element

A small, fixed group of fluid particles enclosed in a volume τ has constant mass m,

$$m = \int_m \mathrm{d}m = \int_\tau \rho \, \mathrm{d}\tau. \tag{2.29}$$

At this point incompressible flow is allowed, that is $\rho = \rho(\vec{r})$, where $\vec{r}$ is the position vector with respect to some origin. The center of gravity g of the fluid element (not to be confused with the body force vector $\vec{g}$) is located at $\vec{r} = \vec{r}_g$, that is

$$\vec{r}_g \int_\tau \rho \, \mathrm{d}\tau = \int_\tau \vec{r} \rho \, \mathrm{d}\tau. \tag{2.30}$$

In this derivation it is generally more convenient to use a position vector with respect to the center of gravity rather than the origin. Therefore let

$$\vec{s} = \vec{r} - \vec{r}_g. \tag{2.31}$$

Note from the definition of the center of gravity (2.30) that:

$$\int_\tau \vec{s} \rho \, \mathrm{d}\tau = \vec{0}, \tag{2.32}$$

which is a relation that will be useful later. Finally the *angular momentum* of the fluid element can be formulated as:

$$\vec{H} = \int_\tau \vec{s} \times \vec{u} \rho \, \mathrm{d}\tau. \tag{2.33}$$

In order to derive a differential equation, the velocity field in the small element is approximated by a spatial linear expansion around its center of gravity:

$$\vec{u}\left(\vec{s}\right) = \vec{u}\big|_g + \left(\vec{s}\cdot\nabla\right)\vec{u}\big|_g + \mathcal{O}\left(|\vec{s}|^2\right), \tag{2.34}$$

where the last term indicates the order of the truncation error that is neglected when cutting off the series after its linear term. This way velocity (at a given point in time) is described in terms of its value and spatial gradient at g. Substituting this into (2.33) yields the following expression for angular momentum:

$$\vec{H} \approx \underbrace{\int_\tau \vec{s}\times\vec{u}\big|_g \rho\,\mathrm{d}\tau}_{=0} + \int_\tau \vec{s}\times\left(\left(\vec{s}\cdot\nabla\right)\vec{u}\big|_g\right)\rho\,\mathrm{d}\tau, \tag{2.35}$$

where the first integral is zero because it amounts to (2.32) multiplied by a vector that is constant over the domain of integration. Note that upon assuming constant density, the remaining integral's integrand scales with arm length squared and the velocity gradient. Approximate linear momentum on the other hand, with integrand $\vec{u}\big|_g\rho$, scales with velocity when density is constant. Therefore strong velocity gradients or a large elements increase the relative importance of considering angular momentum. In component notation, the nonzero part of (2.35) is

$$\vec{H} \approx \epsilon_{ijk}\left.\frac{\partial u_k}{\partial x_l}\right|_g \int_\tau s_j s_l \rho\,\mathrm{d}\tau = \epsilon_{ijk}\left.\frac{\partial u_k}{\partial x_l}\right|_g T_{jl}. \tag{2.36}$$

In the last step the volume integral of the product of arm lengths and density is expressed by the symmetric matrix T_{jl}, which will frequently appear in the remaining derivation.

A few useful relations for working with component notation as in (2.36) are as follows. The cross products of any vectors $\vec{a}$ and $\vec{b}$ can be expressed with the Levi-Civita tensor ϵ_{ijk} as

$$(\vec{a}\times\vec{b})_i = \epsilon_{ijk}a_j b_k \quad \text{or} \quad \vec{a}\times\vec{b} = \epsilon_{ijk}\vec{e}_i a_j b_k, \tag{2.37}$$

where the vectors $\vec{e}_i$ form a standard basis. The Levi-Civita tensor is defined

depending on permutations of (1, 2, 3), see for example [18, (A.11)]:

$$\epsilon_{ijk} = \begin{cases} +1 & \text{if } (i,\, j,\, k) \text{ is } (1,\, 2,\, 3),\, (2,\, 3,\, 1) \text{ or } (3,\, 1,\, 2) \text{ 'even'} \\ -1 & \text{if } (i,\, j,\, k) \text{ is } (3,\, 2,\, 1),\, (1,\, 3,\, 2) \text{ or } (2,\, 1,\, 3) \text{ 'odd'} \\ 0 & \text{if } i = j,\, j = k \text{ or } i = k \text{ 'not a permutation'}. \end{cases} \tag{2.38}$$

Two other useful operations expressed in component notation are the dot poduct as

$$\vec{a} \cdot \vec{b} = a_i b_i \tag{2.39}$$

and the gradient of a vector field as

$$\nabla \vec{a} = \frac{\partial a_i}{\partial x_j}. \tag{2.40}$$

A description of vorticity employing aforementioned expressions is

$$\omega_i = \left(\nabla \times \vec{u}\right)_i = \epsilon_{ijk} \frac{\partial u_k}{\partial x_j}, \tag{2.41}$$

which will turn out useful later.

Relation between angular momentum and vorticity in a special case

In case of a *spherical (or other appropriately symmetric) element* τ*, with spherically symmetric density*, angular momentum becomes proportional to vorticity as will be demonstrated here. Another consequence of aforementioned assumption is that T_{jl} can be expressed in terms of the element's mass moment of inertia. This will be derived first in the following, which aims to enhance understanding.

Spherical symmetry in any property, for example density, means that it only depends on distance with respect to a particular origin. In other words, the property is constant over the surface of any sphere centered at this origin. This especially simplifies descriptions in terms of polar coordinates, as it implies independence of the two angular coordinates. Still, Cartesian coordinates will be used in the following as spherical symmetry implies any plane through the origin is a mirror-symmetry plane.

Recall from (2.36) that in general

$$T_{jl} := \int_\tau s_j s_l \rho \, \mathrm{d}\tau. \tag{2.42}$$

Now consider a point with location $\vec{s} = \vec{a} = [a_1\ a_2\ a_3]^{\mathrm{T}}$ and density $\rho = \rho_a$. In a spherical element there must always be another point with $\vec{s} = \vec{b} = [a_1\ {-a_2}\ a_3]^{\mathrm{T}}$. As mentioned above, spherical symmetry impies that any plane through the center of the element is a mirror-symmetry plane, so also the $s_1 s_3$-plane. Therefore $\rho_a = \rho_b$, so it becomes clear that $a_1 a_2 \rho_a$ is cancelled by $b_1 b_2 \rho_b = a_1(-a_2)\rho_a$ upon performing the integration in T_{12}. Because such cancelling contributions exist for any point in τ, it can be concluded from this example that $T_{jl} = 0$ for $j \neq l$. It is therefore equivalent to write

$$T_{jl} = \delta_{jl} \int_{\tau} s_j s_l \rho \, \mathrm{d}\tau, \tag{2.43}$$

where δ_{jl} is the well-known Kronecker delta function: $\delta_{jl} = 1$ if $j = l$ and $\delta_{jl} = 0$ otherwise. There are also non-spheric, for example cuboidal (box), elements that have symmetries such that T_{jl} reduces to the above in case of a spherically symmetric density distribution. Note that (2.43) effectively reduces T_{jl} to a vector, for a sphere or cube even a scalar as then it does not matter which coordinate is in the integrand.

Now consider a general mass inertia tensor for comparison against T_{jl}. For any rigid body with continuous mass distribution it is given by [3, p. 545, (20.37)]:

$$\begin{bmatrix} I_{xx} & -I_{xy} & -I_{xz} \\ -I_{yx} & I_{yy} & -I_{yz} \\ -I_{zx} & -I_{zy} & I_{zz} \end{bmatrix} = \begin{bmatrix} \int\limits_m (y^2+z^2)\,\mathrm{d}m & -\int\limits_m xy\,\mathrm{d}m & -\int\limits_m xz\,\mathrm{d}m \\ -\int\limits_m yx\,\mathrm{d}m & \int\limits_m (x^2+z^2)\,\mathrm{d}m & -\int\limits_m yz\,\mathrm{d}m \\ -\int\limits_m zx\,\mathrm{d}m & -\int\limits_m zy\,\mathrm{d}m & \int\limits_m (x^2+y^2)\,\mathrm{d}m \end{bmatrix},$$

where the notation $(x,\ y,\ z)$ is used in place of $(s_1,\ s_2,\ s_3)$ for the sake of better readability. Considering that it is equivalent to integrate over τ by using $\mathrm{d}m = \rho\,\mathrm{d}\tau$, the similarities with T_{jl} (2.42) are obvious. Further it must be remarked that I_{xx}, I_{yy} and I_{zz} are the principal moments of inertia. The product of each with angular acceleration about the corresponding axis produces the related torque around that same axis. The other terms (I_{xy}, I_{xz}, etcetera) are called products of inertia and relate angular acceleration about one axis to torque around another.

To avoid confusion, it must be remarked that vorticity equals twice the *average* angular velocity a fluid element (as in general it can distort). This definition is explained in the textbook of White [33, pp. 19–20]. However, in

case the element does not deform, it equals twice the angular velocity of a solid body rotation. Such as in the context of what is discussed here.

The mass inertia tensor at the center of gravity of a sphere with spherically symmetric density distribution simplifies in similar way as T_{jl} did from (2.42) to (2.43): all products of inertia are zero, while all moments of inertia are equal ($I = I_{xx} = I_{yy} = I_{zz}$). Hence the inertia tensor effectively reduces from second to zeroth order (scalar). Remember x, y and z in the inertia tensor correspond to the axes s_1, s_2 and s_3, so I_{xx} and T_{11} are

$$I_{xx} = \int_\tau (s_2^2 + s_3^2)\rho \, \mathrm{d}\tau \quad \text{and} \quad T_{11} = \int_\tau s_1^2 \rho \, \mathrm{d}\tau. \tag{2.44}$$

Here it does not matter which coordinate s_i is in the integrand, so in general

$$T_{jl} = \frac{1}{2} I \delta_{jl}. \tag{2.45}$$

Substituting this result into the (approximate) expression for angular momentum (2.36) and then recognizing vorticity (2.41) yields

$$\vec{H} \approx \frac{1}{2}\epsilon_{ijk} \left.\frac{\partial u_k}{\partial x_l}\right|_g I\delta_{jl} = \frac{1}{2}\epsilon_{ijk} \left.\frac{\partial u_k}{\partial x_j}\right|_g I = \frac{1}{2} I \left.\vec{\omega}\right|_g . \tag{2.46}$$

In the limit of a very small element the approximation improves and the subscript g can be omitted.

For example take a *sphere with constant density*, then $I = \frac{2}{5}mR^2$ (as given on the last page of [3]) with m the mass of the sphere and R its radius so that

$$\vec{H} \approx \frac{1}{5} m R^2 \left.\vec{\omega}\right|_g . \tag{2.47}$$

Interestingly (2.46) shows angular momentum is directly proportional to vorticity for incompressible flows. For compressible flows where the fluid can be partitioned in spherical elements with spherically symmetric density distribution, (2.46) is also valid but it must be noted that I will vary in time and space. This clearly makes the relation more complex. For incompressible flows, density is constant and therefore it is appropriate to assume I is constant. This is true even though material elements can deform when moving with the flow, as at any instant it is possible to divide the flow in spherical elements of the same size and density. Because the numerical methods discussed later in this work aim to solve incompressible flows, their accuracy at solving vorticity corresponds to their accuracy in angular momentum.

Temporal derivative of angular momentum

Considering the angular momentum of an element with arbitrary shape to be given by (2.36), its temporal derivative is as follows (by the product rule):

$$\frac{\mathrm{d}H_i}{\mathrm{d}t} = \epsilon_{ijk} \frac{\mathrm{D}}{\mathrm{D}t} \left(\frac{\partial u_k}{\partial x_l} \right) \Big|_g T_{jl} + \epsilon_{ijk} \frac{\partial u_k}{\partial x_l} \Big|_g \frac{\mathrm{d}T_{jl}}{\mathrm{d}t}. \tag{2.48}$$

Before working out the time derivative of T_{jl}, some explanation on the different 'types' of temporal derivatives used above is at its place in the following.

For terms that depend on time only, the usual derivative $\mathrm{d}/\mathrm{d}t$ applies. This is the case for $T_{jl}(t)$: from its definition (2.42) one can see that the integration involved eliminates explicit spatial dependence. The domain of integration follows the fluid element as it moves with the flow. The same applies to $H_i(t)$. Such dependence on only time comes from a Lagrangian frame of reference, which assumes a function depends on time and (typically fixed) position in a reference configuration. That position is also fixed here, because a specific fluid element is followed. For the reference configuration it is usual to consider an initial time set to $t = 0$.

For the time derivative of the particle velocity gradient tensor $\partial u_k/\partial x_l$, the material derivative $\mathrm{D}/\mathrm{D}t$ is appropriate instead. This because velocity has an Eulerian frame of reference, which means it is a function of time and actual position (rather than position in a reference state). This is customary for describing a velocity field in fluid mechanics. In (2.5) the material derivative is expressed in terms of partial derivatives. It is the sum of the partial time derivative and convective derivative. The latter gives the effect of a particle's movement with the flow field, for example in direction of a region where density is lower due to expansion. This following of a particle shows the material derivative has a 'Lagrangian soul', even though it applies to 'Eulerian' functions. Its Lagrangian nature is strengthened by setting the current position equal to that of the element's center of gravity: $\vec{r} = \vec{r}_g(t)$. This way the Eulerian terms are linked to a Lagrangian reference location (at $t = 0$).

From the definition of T_{jl} (2.42), its time-derivative can be worked out further. Because the element can deform, the domain of integration can change over time. Therefore the first step is to apply the Reynolds transport formula [22, (7)] to write

$$\frac{\mathrm{d}T_{jl}}{\mathrm{d}t} = \frac{\mathrm{d}}{\mathrm{d}t} \int_{\tau(t)} s_j s_l \rho \, \mathrm{d}\tau = \int_{\tau(t)} \frac{\mathrm{D}}{\mathrm{D}t}(s_j s_l \rho) + s_j s_l \rho \nabla \cdot \vec{u} \, \mathrm{d}\tau. \tag{2.49}$$

Next apply the product rule twice to expand the material derivative of the triple product to obtain

$$\frac{\mathrm{d}T_{jl}}{\mathrm{d}t} = \int_\tau \frac{\mathrm{D}s_j}{\mathrm{D}t} s_l \rho + s_j \frac{\mathrm{D}s_l}{\mathrm{D}t} \rho + s_j s_l \underbrace{\left(\frac{\mathrm{D}\rho}{\mathrm{D}t} + \rho \nabla \cdot \vec{u} \right)}_{=0} \mathrm{d}\tau, \tag{2.50}$$

where explicit reference to the temporal dependence of the domain $\tau = \tau(t)$ is omitted again. The last part is zero because it represents conservation of mass (2.16). For the other terms, remember that the vector $\vec{s}(\vec{r}, t) = \vec{r} - \vec{r}_g(t)$ is just the difference between two position vectors. Each points to a location (inside the element τ) that is moving with the flow: $\vec{r}$ to a particle and $\vec{r}_g(t)$ the center of gravity. Therefore its temporal derivative can physically be interpreted as the velocity difference between these two:

$$\frac{\mathrm{D}\vec{s}}{\mathrm{D}t} = \vec{u} - \vec{u}\big|_g \approx \left(\vec{s} \cdot \nabla\right) \vec{u}\big|_g, \tag{2.51}$$

where the linear approximation of (2.34) has been used in the last step. Above result can be written in component notation by recognizing $\vec{s} \cdot \nabla = s_j \frac{\partial}{\partial x_j}$ from (2.39) and (2.40), so that

$$\frac{\mathrm{D}s_i}{\mathrm{D}t} = \left(\left(\vec{s} \cdot \nabla\right) \vec{u}\big|_g \right)_i = s_j \left. \frac{\partial u_i}{\partial x_j} \right|_g . \tag{2.52}$$

Therefore,

$$\begin{aligned} \epsilon_{ijk} \left. \frac{\partial u_k}{\partial x_l} \right|_g \frac{\mathrm{d}T_{jl}}{\mathrm{d}t} &= \epsilon_{ijk} \left. \frac{\partial u_k}{\partial x_l} \right|_g \int_\tau \left(s_p \left. \frac{\partial u_j}{\partial x_p} \right|_g s_l + s_j s_p \left. \frac{\partial u_l}{\partial x_p} \right|_g \right) \rho \, \mathrm{d}\tau \\ &= \epsilon_{ijk} \left\{ \frac{\partial u_k}{\partial x_l} \frac{\partial u_l}{\partial x_p} \right\}_g T_{pj}, \end{aligned} \tag{2.53}$$

where the first term in the integral dropped out because

$$\epsilon_{ijk} s_p \left. \frac{\partial u_j}{\partial x_p} \right|_g s_l \left. \frac{\partial u_k}{\partial x_l} \right|_g = \left(\left(\vec{s} \cdot \nabla\right) \vec{u}\big|_g \right) \times \left(\left(\vec{s} \cdot \nabla\right) \vec{u}\big|_g \right) = 0 \tag{2.54}$$

by definition of the cross product. With a small change in index notation (letting $l = m$ and $p = l$) and recognizing the symmetry $T_{jl} = T_{lj}$, (2.53) can be rewritten as

$$\epsilon_{ijk} \left. \frac{\partial u_k}{\partial x_l} \right|_g \frac{\mathrm{d}T_{jl}}{\mathrm{d}t} = \epsilon_{ijk} \left\{ \frac{\partial u_k}{\partial x_m} \frac{\partial u_m}{\partial x_l} \right\}_g T_{jl}. \tag{2.55}$$

This way the second term of (2.48) has been expressed similar to the first: a product of T_{jl} and velocity derivative(s) evaluated at the centroid, so that

$$\frac{\mathrm{d}H_i}{\mathrm{d}t} = \epsilon_{ijk} \left\{ \frac{\mathrm{D}}{\mathrm{D}t} \left(\frac{\partial u_k}{\partial x_l} \right) + \frac{\partial u_k}{\partial x_m} \frac{\partial u_m}{\partial x_l} \right\} \Bigg|_g T_{jl}. \tag{2.56}$$

After deriving an expression for the torques on the element, the angular momentum equation can be assembled with this result. But it will first be examined under certain assumptions.

Interpretation of angular momentum derivative in a special case

In case of a (currently) spherical element τ, with spherically symmetric density, a clear interpretation of (2.56) follows. Remember that in that situation, T_{jl} can be expressed as (2.45). Substituting this in (2.56) gives

$$\begin{aligned} \frac{\mathrm{d}H_i}{\mathrm{d}t} &= \frac{1}{2} \epsilon_{ijk} \left\{ \frac{\mathrm{D}}{\mathrm{D}t} \left(\frac{\partial u_k}{\partial x_l} \right) + \frac{\partial u_k}{\partial x_m} \frac{\partial u_m}{\partial x_l} \right\} \Bigg|_g I \delta_{jl} \\ &= \frac{1}{2} \left\{ \frac{D\omega_i}{Dt} + \epsilon_{ijk} \frac{\partial u_k}{\partial x_m} \frac{\partial u_m}{\partial x_j} \right\} \Bigg|_g I, \end{aligned} \tag{2.57}$$

recognizing vorticity (2.41). Tracking down derivations shows that the first and second terms of the above still correspond to the respective terms in (2.48), which formed the point of departure.

This means that under all aforementioned assumptions, the first term of (2.48) becomes

$$\epsilon_{ijk} \frac{\mathrm{D}}{\mathrm{D}t} \left(\frac{\partial u_k}{\partial x_l} \right) \Bigg|_g T_{jl} = \frac{1}{2} \frac{D\omega_i}{Dt} \Bigg|_g I. \tag{2.58}$$

Therefore it represents a contribution to the change in angular momentum due to angular acceleration of the sphere around its center of gravity. This can be considered to correspond to an instantaneous rigid-body rotation due to the constant inertia tensor.

Correspondingly, the second term of (2.48) becomes

$$\epsilon_{ijk} \frac{\partial u_k}{\partial x_l} \Bigg|_g \frac{\mathrm{d}T_{jl}}{\mathrm{d}t} = \frac{1}{2} \epsilon_{ijk} \frac{\partial u_k}{\partial x_m} \frac{\partial u_m}{\partial x_l} \Bigg|_g I \delta_{jl}, \tag{2.59}$$

which means it represents a contribution due to the sphere's deformation into an ellipsoid. This can be seen by noting two things. First, the left-hand

side contains the derivative of T_{jl} (2.42), so if it is nonzero the element must be deforming. Second, the right-hand side contains δ_{jl}, implying the derivative of T_{jl} is zero for $j \neq l$. Hence the sphere can deform but T_{jl} remains symmetric. Looking at its definition (2.42), this can only be the case when all integrals with $s_j s_l$ and $j \neq l$ in their integrand stay zero. Therefore $s_1 s_2$, $s_1 s_3$ and $s_2 s_3$ must remain planes of symmetry. Hence the spherical element can only deform into an ellipsoid with s_1, s_2 and s_3 as principal axes.

Torques on the element

The rate of change in angular momentum (2.56) must be balanced by body and surface forces producing torques as derived in the following. Consider the body force field to be the gradient of a scalar field ϕ_f:

$$\vec{g} = -\nabla\phi_f = -\rho\nabla V \qquad \text{or} \qquad g_k = -\frac{\partial \phi_f}{\partial x_k} = -\rho\frac{\partial V}{\partial x_k}, \tag{2.60}$$

where the subscript f is *not* an index. Such a body force field is called conservative. The couple it generates about the center of gravity g is given by

$$\int_\tau \vec{s}\times\vec{g}\,\mathrm{d}\tau \approx \underbrace{\int_\tau \vec{s}\times\left(-\nabla V\big|_g\right)\rho\,\mathrm{d}\tau}_{=0} + \int_\tau \vec{s}\times\left((\vec{s}\cdot\nabla)\left(-\nabla V\big|_g\right)\right)\rho\,\mathrm{d}\tau, \tag{2.61}$$

where (2.60) is substituted for $\vec{g}$ after expanding $-\nabla V$ around g for up to linear terms like (2.34). The first integral represents (2.32) multiplied by a constant vector and therefore integrates to zero. The remaining integral on the right-hand side can be written in component notation with the aid of (2.37), (2.39) and (2.40) as

$$-\epsilon_{ijk}\left.\frac{\partial^2 V}{\partial x_l \partial x_k}\right|_g \int_\tau s_j s_l \rho\,\mathrm{d}\tau = -\epsilon_{ijk}\left.\frac{\partial^2 V}{\partial x_l \partial x_k}\right|_g T_{jl}. \tag{2.62}$$

Now consider the torque caused by stresses of pressure and viscous type. These stresses generally vary in space and thereby produce a net force on a fluid element. With σ_{ij} the stress tensor and vector $\vec{n}$ the outward-pointing unit normal, the stress in that direction is given by $\sigma_{ij}n_i$ (or $\sigma_{ij}n_j$ due to symmetry of the stress tensor). This can be integrated over the element's surface

to yield the net force. By the divergence theorem this is equivalent to integrating $\partial\sigma_{ij}/\partial x_j$ over its volume. Hence this integrand is a vector that can be conceptualized as 'net force per unit volume'. An alternative derivation that leads to the same result can be found in the textbook by White [33, pp. 62–64]. Substitution of the stress tensor σ_{ij} from (2.6) in the general case $\nabla \cdot \vec{u} \neq 0$ gives

$$\nabla \cdot \sigma_{ij} = \frac{\partial \sigma_{ij}}{\partial x_j} = -\frac{\partial p}{\partial x_i} + \mu \left(\frac{\partial^2 u_i}{\partial x_j \partial x_j} + \frac{\partial^2 u_j}{\partial x_i \partial x_j} \right) + \lambda \frac{\partial^2 u_m}{\partial x_i \partial x_m}, \tag{2.63}$$

which describes a field throughout the fluid. Here it was used that

$$\frac{\partial p}{\partial x_j}\delta_{ij} = \frac{\partial p}{\partial x_i} \quad \text{and} \quad \lambda \delta_{ij} \frac{\partial}{\partial x_j}(\nabla \cdot \vec{u}) = \lambda \frac{\partial^2 u_m}{\partial x_i \partial x_m}. \tag{2.64}$$

Above force density $\nabla \cdot \sigma_{ij}$ creates a moment $\vec{s} \times (\nabla \cdot \sigma_{ij})$ around the center of gravity of the small element. The total torque follows from integrating over the element's volume. To transform the integral in the form used elsewhere in this section, $\nabla \cdot \sigma_{ij}$ will be divided by ρ. This is important for summing contributions later. Then $(\nabla \cdot \sigma_{ij})/\rho$ will be expanded up to linear terms like (2.34). This results in

$$\begin{aligned} \int_\tau \vec{s} \times \left(\nabla \cdot \sigma_{ij}\right) \, \mathrm{d}\tau &= \int_\tau \vec{s} \times \left(\frac{\nabla \cdot \sigma_{ij}}{\rho} \right) \rho \, \mathrm{d}\tau \\ &\approx \underbrace{\int_\tau \vec{s} \times \left. \frac{\nabla \cdot \sigma_{ij}}{\rho} \right|_g \rho \, \mathrm{d}\tau}_{=0} + \int_\tau \vec{s} \times \left((\vec{s} \cdot \nabla) \left. \frac{\nabla \cdot \sigma_{ij}}{\rho} \right|_g \right) \rho \, \mathrm{d}\tau, \end{aligned} \tag{2.65}$$

where again the first term integrates to zero because it amounts to (2.32) multiplied by a constant vector. The remaining integral is expressed in more detail by substituting (2.63) for $\nabla \cdot \sigma_{ij}$. Before substitution, the index i is changed into k and the repeated index j into m. This has no fundamental consequences, but allows to write the cross product with $\vec{s}$ like (2.37). Performing these steps yields

$$\int_\tau \epsilon_{ijk} s_j s_l \left\{ -\frac{\partial}{\partial x_l} \left(\frac{1}{\rho} \frac{\partial p}{\partial x_k} \right) + \nu \frac{\partial^3 u_k}{\partial x_l \partial x_m \partial x_m} + \left(\nu + \frac{\lambda}{\rho} \right) \frac{\partial^3 u_m}{\partial x_k \partial x_l \partial x_m} \right\} \Bigg|_g \rho \, \mathrm{d}\tau,$$

recognizing the possibility to express this as a product with T_{jl} (2.42) gives

$$\epsilon_{ijk}\left\{-\frac{\partial}{\partial x_l}\left(\frac{1}{\rho}\frac{\partial p}{\partial x_k}\right)+\nu\frac{\partial^3 u_k}{\partial x_l \partial x_m \partial x_m}+\left(\nu+\frac{\lambda}{\rho}\right)\frac{\partial^3 u_m}{\partial x_k \partial x_l \partial x_m}\right\}\Bigg|_g T_{jl}, \tag{2.66}$$

which is the final expression for torque produced by pressure and viscous stresses. As usual in this work, ν is considered a constant. It could therefore be taken outside the derivatives. The same applies to λ/ρ. For most flow problems it is common to use Stokes' hypothesis [33, p. 67], that is $\lambda = -2\mu/3$. Then $\lambda/\rho = -2\nu/3$.

Assembly of the angular momentum equation

Now all expressions are present to assemble an equation according to Newton's second law:

$$\begin{aligned}&\epsilon_{ijk}\left\{\frac{\mathrm{D}}{\mathrm{D}t}\left(\frac{\partial u_k}{\partial x_l}\right)+\frac{\partial u_k}{\partial x_m}\frac{\partial u_m}{\partial x_l}\right\}\Bigg|_g T_{jl} = \dots \\ &\epsilon_{ijk}\left\{-\frac{\partial^2 V}{\partial x_l \partial x_k}-\frac{\partial}{\partial x_l}\left(\frac{1}{\rho}\frac{\partial p}{\partial x_k}\right)+\nu\frac{\partial^3 u_k}{\partial x_l \partial x_m \partial x_m}+\left(\nu+\frac{\lambda}{\rho}\right)\frac{\partial^3 u_m}{\partial x_k \partial x_l \partial x_m}\right\}\Bigg|_g T_{jl},\end{aligned} \tag{2.67}$$

which is formed by equating the element's time-rate of change in angular momentum (2.56) to the sum of torque around its center of gravity due to the body force field (2.62) and the stresses (2.66).

The vorticity transport equation

Recognizing a few things finally allows to derive the vorticity transport equation from (2.67) as follows. To start with, note that (2.67) can easily be written in the form $A_{ijl}T_{jl} = 0$ by moving all terms to one side. Next remember that T_{jl} (2.42) is symmetric ($T_{jl} = T_{lj}$) but otherwise arbitrary, as it depends on whatever small element (group of particles) is considered. Therefore $A_{ijl}T_{jl} = 0$ is in general only satisfied when A_{ijl} has the anti-symmetric property $A_{ijl} = -A_{ilj}$ and the zero diagonals $A_{ijl} = 0$ for $l = j$. The latter also means that $A_{ijj} = \vec{0}$, with j a repeated index that represents summation (over elements of the product between the Levi-Civita tensor and the differential terms). Below, it will follow that $A_{ijj} = \vec{0}$ leads to the vorticity transport equation in terms of $\vec{u}$ and $\vec{\omega}$.

Some information in $A_{ijl}T_{jl} = 0$ (2.67) is lost by only considering $A_{ijj} = \vec{0}$, but this is acceptable for three reasons. First of all, the angular momentum equation following from $A_{ijj} = \vec{0}$ can be combined with the linear momentum and conservation of mass equations to form the complete system (2.2). It is 'complete' in the sense that it consists of seven equations and an equal amount of unknowns (counting components). Hence no extra equations are needed. Further, in case an element is considered that has particular symmetries (for example a sphere), with spherically symmetric density distribution, $T_{jl} = 0$ for $l \neq j$ by (2.43). Then $A_{ijl} = -A_{ilj}$ with $l \neq j$ is uninteresting in the light of $A_{ijl}T_{jl} = 0$ (2.67). In the limit of very small elements it is generally reasonable to assume a fluid flow can be split-up into such elements if desired. Finally, considering $A_{ijl} = -A_{ilj}$ for $l \neq j$ and the separate components of $A_{ijl} = 0$ for $l = j$ individually is unattractive. It would lead to a relatively complex and large set of equations with no clear (physical) interpretation.

The equation corresponding to $A_{ijj} = \vec{0}$ is obtained by recognizing several simplifications as follows. The body force term from (2.67) is zero then due to [23, A1. Vector Identities, p. 363, (11)]:

$$\epsilon_{ijk}\frac{\partial^2 V}{\partial x_j \partial x_k} = \big(\nabla \times (\nabla V)\big)_i = 0. \tag{2.68}$$

Assuming barotropic flow (meaning that density is a function of pressure only), the following can be written:

$$\frac{\partial}{\partial x_k}\left(\int^p \frac{1}{\rho(p)}\,\mathrm{d}p\right) = \frac{\partial}{\partial p}\left(\int^p \frac{1}{\rho(p)}\,\mathrm{d}p\right)\frac{\partial p}{\partial x_k} = \frac{1}{\rho(p)}\frac{\partial p}{\partial x_k}, \tag{2.69}$$

so that, again by [23, A1. Vector Identities, p. 363, (11)],

$$\epsilon_{ijk}\frac{\partial}{\partial x_j}\left(\frac{1}{\rho}\frac{\partial p}{\partial x_k}\right) = \epsilon_{ijk}\frac{\partial}{\partial x_j}\frac{\partial}{\partial x_k}\left(\int^p \frac{1}{\rho(p)}\,\mathrm{d}p\right) = 0. \tag{2.70}$$

The same vector calculus identity can be used once more to recognize the last term from (2.67) is zero:

$$\epsilon_{ijk}\frac{\partial^3 u_m}{\partial x_k \partial x_j \partial x_m} = \nu\big(\nabla \times \nabla(\nabla \cdot \vec{u})\big)_i = 0. \tag{2.71}$$

Now that it has been identified which terms from (2.67) are zero when considering $A_{ijj} = \vec{0}$, the following remains for that equation:

$$\epsilon_{ijk}\left\{\frac{\mathrm{D}}{\mathrm{D}t}\left(\frac{\partial u_k}{\partial x_j}\right) + \frac{\partial u_k}{\partial x_m}\frac{\partial u_m}{\partial x_j}\right\}\Bigg|_g = \nu\epsilon_{ijk}\left.\frac{\partial^3 u_k}{\partial x_j \partial x_m \partial x_m}\right|_g. \tag{2.72}$$

By first recognizing vorticity (2.41) and then expanding the material derivative (2.5), note that

$$\epsilon_{ijk}\frac{\mathrm{D}}{\mathrm{D}t}\left(\frac{\partial u_k}{\partial x_j}\right) \equiv \left(\frac{\mathrm{D}\vec{\omega}}{\mathrm{D}t}\right)_i = \left(\frac{\partial\vec{\omega}}{\partial t} + (\vec{u}\cdot\nabla)\vec{\omega}\right)_i . \tag{2.73}$$

Also recognizing vorticity (2.41) in the viscous term yields

$$\nu\epsilon_{ijk}\frac{\partial^3 u_k}{\partial x_j\partial x_m\partial x_m} = \nu\frac{\partial^2\omega_i}{\partial x_m\partial x_m} = \nu\left(\nabla^2\vec{\omega}\right)_i . \tag{2.74}$$

Further,

$$\epsilon_{ijk}\frac{\partial u_k}{\partial x_m}\frac{\partial u_m}{\partial x_j} \equiv \omega_i\frac{\partial u_j}{\partial x_j} - \omega_j\frac{\partial u_i}{\partial x_j} = \left(\vec{\omega}(\nabla\cdot\vec{u}) - (\vec{\omega}\cdot\nabla)\vec{u}\right)_i . \tag{2.75}$$

This equivalence is given in the paper by Chatwin [9, p. 367] and does not seem to be a commonly used identity. Therefore the author of the current work has verified it by independently writing out all terms of the left-hand side and middle for each component i. This is not very difficult but just too elaborate to include here. Finally, note the right-hand side is the middle part expressed in vector notation.

With above relations, it is possible to write (2.72) as

$$\frac{\partial\vec{\omega}}{\partial t} + (\vec{u}\cdot\nabla)\vec{\omega} = (\vec{\omega}\cdot\nabla)\vec{u} - \vec{\omega}(\nabla\cdot\vec{u}) + \nu\nabla^2\vec{\omega}. \tag{2.76}$$

Here the subscript g could be left out by remembering (2.72) is evaluated at the center of gravity g of a fluid element that could be located anywhere. Therefore it is valid at any point.

The vorticity transport equations (2.22) and (2.25) presented earlier in this text follow from above result (2.76) by making respective assumptions. Upon assuming incompressibility, $\nabla\cdot\vec{u} = 0$ and (2.22) follows. Additionally considering the flow to be planar (2D) gives (2.25). This particularly because $\vec{\omega}$ is perpendicular to $\nabla\vec{u}$ then, making $(\vec{\omega}\cdot\nabla)\vec{u}$ zero. Further, $\vec{\omega}$ can also be written as a scalar ω in the remaining equation, because there always exists a frame of reference in which this vector consists of a single component.

2.2 Proof of conservation

This section demonstrates that the conservation properties in Table 2.1 hold for the continuous Navier-Stokes formulations that describe incompressible

(and inviscid) flows. The proofs assume periodic boundary conditions (BC), because this is also assumed in the construction of the MEEVC method [25]. A detailed description of periodic BC can be found in Section 2.3.4. There are however also other suitable BC that do not violate conservation, like impermeable walls for example.

The left half of Table 2.1 applies to 2D flow, as described with (2.1). These integral invariants are also conserved by the discrete MEEVC algorithm [25]. Because conservation of linear momentum is not, it is left out of the table. Still, its continuous proof (for both 2D and 3D) can be found in Section 2.2.6. The right half of Table 2.1 applies to 3D flow, as described with (2.2). Note that enstrophy is only listed for 2D flow, while helicity is only listed for 3D flow. This a consequence of vorticity being a 'scalar' (ω) in 2D and a vector ($\vec{\omega}$) in 3D. Therefore the 3D version of enstrophy is not conserved. Also, helicity is zero for any planar (2D) flow: then velocity and vorticity are always perpendicular and hence their inner product is zero. Further note that mass

2D		3D	
Mass°	$m = \iint_\Omega \rho \, \mathrm{d}\Omega$	Mass°	$m = \iiint_\Omega \rho \, \mathrm{d}\Omega$
Kinetic en.**	$\mathcal{K} = \iint_\Omega \frac{1}{2}\rho \lVert\vec{u}\rVert^2 \, \mathrm{d}\Omega$	Kin. en.**	$\mathcal{K} = \iiint_\Omega \frac{1}{2}\rho \lVert\vec{u}\rVert^2 \, \mathrm{d}\Omega$
Vorticity*	$\mathcal{W} = \iint_\Omega \omega \, \mathrm{d}\Omega$	Vorticity**	$\vec{\mathcal{W}} = \iiint_\Omega \vec{\omega} \, \mathrm{d}\Omega$
Enstrophy**	$\mathcal{E} = \iint_\Omega \omega^2 \, \mathrm{d}\Omega$	Helicity**	$\mathcal{H} = \iiint_\Omega \vec{u} \cdot (\nabla \times \vec{u}) \, \mathrm{d}\Omega$ $= \iiint_\Omega \vec{u} \cdot \vec{\omega} \, \mathrm{d}\Omega$

Table 2.1: Flow invariants, with:
* = global conservation;
** = global conservation for inviscid case only;
° = local and global conservation independent of viscosity.

density is included in the integrals of mass and kinetic energy, but not in total vorticity, enstrophy and helicity. This is according to usual definitions. Anyway, it is always a material constant in this work (incompressible flow) and is often set to $\rho = 1$ for convenience (especially in following Chapters).

Each of the coming subsections will be dedicated to proving one of the invariants in Table 2.1. In addition, there will also be one proving conserva-

tion of linear momentum. This is however not listed in the table as it is not one of the MEEVC properties.

2.2.1 Conservation of mass (2D and 3D)

One can easily conclude that the time derivative of mass m (see Table 2.1) is zero for constant density ρ and fixed domain of integration Ω, but it should be noted that the combination of mass conservation and incompressibility only exists if the equation of continuity ($\nabla \cdot \vec{u} = 0$) is satisfied. This is clearly derived in Section 2.1.2, which starts from requiring local mass conservation in a Lagrangian framework. Note that *local conservation* of mass trivially implies *global conservation* (that is conservation over the entire domain).

Conservation of mass should hold in both a 2D discrete system based on (2.1) and a 3D one based on (2.2). This works as follows. Both (continuous) systems include the aforementioned equation of continuity ($\nabla \cdot \vec{u} = 0$). This corresponds to a simple 'conservation of velocity' statement. Also, velocity is typically a primary unknown of a corresponding discrete system, meaning that it is directly solved for. Then conservation of mass is a *primary conservation property*.

2.2.2 Conservation of energy (2D and 3D)

Let Ω be the 2D or 3D volume equalling the entire fixed domain. This non-moving domain does not necessarily contain a certain group of particles, that is particles can in general cross the boundary. The kinetic energy of the fluid instantaneously contained within that volume Ω is

$$\mathcal{K} = \int_{\Omega} \frac{1}{2}\rho\|\vec{u}\|^2 \,\mathrm{d}\Omega = \int_{\Omega} \frac{1}{2}\rho(\vec{u}\cdot\vec{u}) \,\mathrm{d}\Omega. \tag{2.77}$$

Usually, $\vec{u}$ is a variable in the discretized system, but (the integrand of) $\mathcal{K}$ is not. Conservation of $\mathcal{K}$ is then called a *secondary conservation property*.

The derivative of $\mathcal{K}$ with time is (noting that the differential with t can be taken inside the integral because the domain Ω is fixed in time and the integrand is continuously differentiable):

$$\frac{\mathrm{d}}{\mathrm{d}t}\mathcal{K} = \int_{\Omega} \rho\vec{u}\cdot\frac{\partial\vec{u}}{\partial t} \,\mathrm{d}\Omega. \tag{2.78}$$

Here the differentials are different because $\mathcal{K}$ is a function of time only, while $\vec{u}$ is a flow field property dependent on time and position. Substituting for $\partial\vec{u}/\partial t$ from (2.8) into (2.78) yields:

$$\frac{\mathrm{d}}{\mathrm{d}t}\mathcal{K} = \int_{\Omega} \left[\rho\vec{u} \cdot \left(-(\vec{u}\cdot\nabla)\vec{u} - \frac{\nabla p}{\rho} + \nu\nabla^2\vec{u} \right) \right] \mathrm{d}\Omega. \tag{2.79}$$

Assuming inviscid flow ($\nu = 0$) and rewriting gives:

$$\frac{\mathrm{d}}{\mathrm{d}t}\mathcal{K} = -\int_{\Omega} \left[\rho\vec{u} \cdot \left((\vec{u}\cdot\nabla)\vec{u} \right) + \vec{u}\cdot\nabla p \right] \mathrm{d}\Omega. \tag{2.80}$$

The next step is to further rewrite both terms in this integrand.

Let $\vec{a} = \vec{c} = \vec{u}$ in $\nabla\left(\vec{a}\cdot\vec{c}\right) = \left(\vec{a}\cdot\nabla\right)\vec{c} + \left(\vec{c}\cdot\nabla\right)\vec{a} + \vec{a}\times\left(\nabla\times\vec{c}\right) + \vec{c}\times\left(\nabla\times\vec{a}\right)$ (see [23, A1. Vector Identities, p. 363, (8)]). Thereby note that the first two terms become equal and the last two terms as well, so that the following is obtained:

$$(\vec{u}\cdot\nabla)\vec{u} = \underbrace{\frac{1}{2}\nabla(\vec{u}\cdot\vec{u})}_{\frac{1}{2}\nabla\left(\|\vec{u}\|^2\right)} - \vec{u}\times(\nabla\times\vec{u}). \tag{2.81}$$

The first term in the integrand of (2.80) can be rewritten by substitution of the above, that is

$$\rho\vec{u}\cdot\left((\vec{u}\cdot\nabla)\vec{u}\right) = \frac{1}{2}\rho\vec{u}\cdot\nabla\left(\|\vec{u}\|^2\right) - \rho\vec{u}\cdot\left(\vec{u}\times(\nabla\times\vec{u})\right). \tag{2.82}$$

The last term is zero, because the part in brackets is perpendicular to $\vec{u}$ by the cross product's definition. The first term on the right hand side can be interpreted as convection of kinetic energy density by comparison against the integrand of (2.77). It can be rewritten further by using the identity $\nabla\cdot\left(\phi\vec{a}\right) = \phi\nabla\cdot\vec{a} + \vec{a}\cdot\nabla\phi$ [23, A1. Vector Identities, p. 363, (4)] with $\phi = \|\vec{u}\|^2$, $\vec{a} = \vec{u}$ and noting $\nabla\cdot\vec{u} = 0$ (2.14) for incompressible flow. Hence, the following is obtained:

$$\rho\vec{u}\cdot\left((\vec{u}\cdot\nabla)\vec{u}\right) = \frac{1}{2}\rho\nabla\cdot\left(\|\vec{u}\|^2\vec{u}\right). \tag{2.83}$$

Similar use of $\nabla\cdot\left(\phi\vec{a}\right) = \phi\nabla\cdot\vec{a} + \vec{a}\cdot\nabla\phi$, with $\phi = p$ and $\vec{a} = \vec{u}$ also gives:

$$\vec{u}\cdot\nabla p = \nabla\cdot\left(p\vec{u}\right), \tag{2.84}$$

where $\nabla\cdot\vec{u} = 0$ (2.14) has been used again.

Now (2.83) and (2.84) are substituted back into (2.80). The result is then substituted for $\vec{a}$ in Gauss' (3D) or Green's (2D) theorem [29, pp. 1096/1127]:

$$\int_{\Omega} \nabla \cdot \vec{a} \, \mathrm{d}\Omega = \int_{\partial\Omega} \vec{a} \cdot \vec{n} \, \mathrm{d}\Gamma,$$

so that

$$\frac{\mathrm{d}}{\mathrm{d}t}\mathcal{K} = -\int_{\partial\Omega} \left[\frac{1}{2}\rho \|\vec{u}\|^2 \vec{u} + p\vec{u} \right] \cdot \vec{n} \, \mathrm{d}\Gamma = 0. \tag{2.85}$$

This integral over the boundary of the domain is zero due to periodic BC; contributions over opposite boundaries cancel. To be clear: Γ refers to a surface in the 3D case, but a 'line' boundary in the 2D case. In both cases, $\vec{n}$ is the local outward-pointing unit vector that is normal to the boundary. Global conservation of kinetic energy for inviscid flow has now been proven in 2D as well as 3D.

2.2.3 Conservation of total vorticity (2D and 3D)

First it is interesting to note that, in case of incompressible flow, vorticity conservation is equivalent to angular momentum conservation. This is so because then the angular momentum of an element is directly proportional to its vorticity (2.46). The governing Navier-Stokes equations (2.1) and (2.2) used in this work are for incompressible flow, so this is an interesting fact.

The proof of vorticity conservation for the general (3D) system (2.2), in case of inviscid flow and periodic (or otherwise suitable) BC, can be summarized by

$$\frac{\mathrm{d}}{\mathrm{d}t}\vec{\mathcal{W}} = \int_{\Omega} \frac{\partial \vec{\omega}}{\partial t} \, \mathrm{d}\Omega = \int_{\Omega} (\vec{\omega} \cdot \nabla)\vec{u} - (\vec{u} \cdot \nabla)\vec{\omega} \, \mathrm{d}\Omega = \ldots$$

$$\int_{\Omega} \nabla \times (\vec{u} \times \vec{\omega}) \, \mathrm{d}\Omega = \int_{\partial\Omega} \vec{n} \times (\vec{u} \times \vec{\omega}) \, \mathrm{d}\Gamma = \vec{0}. \tag{2.86}$$

This proof follows an approach similar to that of kinetic energy conservation (Section 2.2.2), but with the following particular steps. The time-derivative of vorticity is substituted from the vorticity transport equation (2.22) with $\nu = 0$. This is then rewritten with (2.21) in order to apply the integral theorem [23, A1. Vector Identities, p. 363, (16)]. This results in an integral over the

boundary of the domain, which integrates to zero due to periodic BC (on $\vec{u}$ and hence also on $\vec{\omega} = \nabla \times \vec{u}$). Note that total vorticity is conserved over each component separately.

Although the proof above is also valid when the flow field can be characterized as 'planar' (i.e. there exists a plane for which the velocity component normal to it is zero everywhere), a particular proof for the 2D system (2.1) that also works for viscous flow is given below. Its approach can be summarized by

$$\frac{\mathrm{d}}{\mathrm{d}t}\mathscr{W} = \int_\Omega \frac{\partial \omega}{\partial t}\,\mathrm{d}\Omega = -\int_\Omega (\vec{u}\cdot\nabla)\omega + \nu\nabla^2\omega\,\mathrm{d}\Omega = \ldots$$
$$-\int_\Omega \nabla\cdot(\omega\vec{u} + \nu\nabla\omega)\,\mathrm{d}\Omega = -\int_{\partial\Omega} (\omega\vec{u} + \nu\nabla\omega)\cdot\vec{n}\,\mathrm{d}\Gamma = 0, \quad (2.87)$$

where the time derivative of vorticity is substituted from the 2D vorticity transport equation (2.25). Further identity [23, A1. Vector Identities, p. 363, (4)] has been used with $\nabla\cdot\vec{u} = 0$, followed by Green's theorem in 2D [29, Sec. 16.5, p. 1096, (13)]. Note that, in contrary to the 3D situation above, there was no need to assume inviscid flow. Only constant viscosity and periodic boundary conditions, of which the latter causes the final integral to evaluate to zero.

2.2.4 Conservation of enstrophy (2D only)

This proof also shares the approach of that in Section 2.2.2. In summary:

$$\frac{\mathrm{d}\mathscr{E}}{\mathrm{d}t} = \int_\Omega \frac{\partial \omega^2}{\partial t}\,\mathrm{d}\Omega = \int_\Omega 2\omega\frac{\partial \omega}{\partial t}\,\mathrm{d}\Omega = -\int_\Omega (\vec{u}\cdot\nabla)(\omega^2)\,\mathrm{d}\Omega = \ldots$$
$$-\int_\Omega \nabla\cdot(\omega^2\vec{u})\,\mathrm{d}\Omega = -\int_{\partial\Omega} \omega^2(\vec{u}\cdot\vec{n})\,\mathrm{d}\Gamma = 0, \quad (2.88)$$

where the time derivative of vorticity was substituted from the 2D vorticity transport equation (2.25) with $\nu = 0$ and it was recognized that $2\omega(\vec{u}\cdot\nabla)\omega = (\vec{u}\cdot\nabla)(\omega^2)$. Above integral evaluates to zero due to again the periodic BC.

2.2.5 Conservation of helicity (3D only)

Conservation of helicity $\mathscr{H}$ inside the domain Ω under inviscid conditions is demonstrated here, from integration of helical density $h = \vec{u}\cdot\vec{\omega}$ over its

volume. Helical density is also known as longitudinal vorticity, because it can be viewed as a measure of vorticity parallel to the streamlines. Integrating over the entire, fixed domain and applying the time derivative yields

$$\frac{\mathrm{d}\mathcal{H}}{\mathrm{d}t} = \int_\Omega \frac{\partial h}{\partial t}\,\mathrm{d}\Omega = \int_\Omega \left(\frac{\partial \vec{u}}{\partial t}\cdot\vec{\omega} + \vec{u}\cdot\frac{\partial \vec{\omega}}{\partial t}\right)\mathrm{d}\Omega, \tag{2.89}$$

by application of the product rule.

Substituting from (2.8) and (2.22) for the time derivatives, in the inviscid case (because in viscous flows helicity is not conserved):

$$\frac{\partial \vec{u}}{\partial t}\cdot\vec{\omega} = -\left((\vec{u}\cdot\nabla)\vec{u}\right)\cdot\vec{\omega} - \frac{\nabla p}{\rho}\cdot\vec{\omega}, \tag{2.90a}$$

$$\vec{u}\cdot\frac{\partial \vec{\omega}}{\partial t} = -\vec{u}\cdot\left((\vec{u}\cdot\nabla)\vec{\omega}\right) + \vec{u}\cdot\left((\vec{\omega}\cdot\nabla)\vec{u}\right). \tag{2.90b}$$

These expressions can be substituted in the integrand of (2.89), but this will not make it obvious that the integral evaluates to zero. Further modification and integration by parts will demonstrate this as follows.

To get started, the right-hand side of (2.90a) is rewritten. For its first term, identity [23, A1. Vector Identities, p. 363, (8)] will be useful. It implies

$$\nabla(\vec{u}\cdot\vec{u}) = 2(\vec{u}\cdot\nabla)\vec{u} + 2\vec{u}\times\vec{\omega}, \tag{2.91}$$

where $\vec{\omega} := \nabla\times\vec{u}$ has been used. With this result,

$$\left((\vec{u}\cdot\nabla)\vec{u}\right)\cdot\vec{\omega} = \underbrace{\frac{1}{2}\nabla(\vec{u}\cdot\vec{u})}_{=\frac{1}{2}\nabla\left(\|\vec{u}\|^2\right)}\cdot\vec{\omega} - \underbrace{(\vec{u}\times\vec{\omega})\cdot\vec{\omega}}_{=0}, \tag{2.92}$$

where $(\vec{u}\times\vec{\omega})\cdot\vec{\omega} = 0$ by definition of the cross and the dot product. Substituting this result in (2.90a), its right-hand side can simply be written as the dot product between vorticity and the gradient of total pressure $\bar{p}$:

$$-\vec{\omega}\cdot\nabla\bar{p}, \tag{2.93}$$

where $\bar{p} := \frac{1}{2}\vec{u}\cdot\vec{u} + \frac{p}{\rho}$ similar to the definition (2.3) for $\rho = 1$. Subsequently applying [23, A1. Vector Identities, p. 363, (4)] and noting $\nabla\cdot\vec{\omega} = \nabla\cdot\nabla\times\vec{u} = 0$ by [23, A1. Vector Identities, p. 363, (12)], the following is obtained:

$$\frac{\partial \vec{u}}{\partial t}\cdot\vec{\omega} = -\nabla\cdot\left(\vec{\omega}\bar{p}\right), \tag{2.94}$$

a simple expression that will turn out to be useful upon integration with the divergence theorem later in this section.

Next, the right-hand side of (2.90b) is rewritten in a few steps. Note identity [23, A1. Vector Identities, p. 363, (7)] implies

$$\nabla \times (\vec{u} \times \vec{\omega}) = (\vec{\omega} \cdot \nabla)\vec{u} - (\vec{u} \cdot \nabla)\vec{\omega} + \underbrace{\vec{u}(\nabla \cdot \vec{\omega})}_{=0} - \underbrace{\vec{\omega}(\nabla \cdot \vec{u})}_{=0}, \tag{2.95}$$

where the last two terms are respectively zero because $\nabla \cdot \vec{u} = 0$ by (2.14) and $\nabla \cdot \vec{\omega} = \nabla \cdot \nabla \times \vec{u} = 0$ by [23, A1. Vector Identities, p. 363, (12)]. Note that the right-hand side of (2.90b) can now be written as $\vec{u} \cdot \big(\nabla \times (\vec{u} \times \vec{\omega})\big)$. This can be rewritten further by [23, A1. Vector Identities, p. 363, (6)] as

$$\vec{u} \cdot \big(\nabla \times (\vec{u} \times \vec{\omega})\big) = \nabla \cdot \big((\vec{u} \times \vec{\omega}) \times \vec{u}\big) + \underbrace{(\vec{u} \times \vec{\omega}) \cdot (\nabla \times \vec{u})}_{=(\vec{u}\times\vec{\omega})\cdot\vec{\omega}=0}, \tag{2.96}$$

where the last term is zero by the definitions of vorticity, the cross product and the dot product. Therefore, (2.90b) becomes

$$\vec{u} \cdot \frac{\partial \vec{\omega}}{\partial t} = \nabla \cdot \big((\vec{u} \times \vec{\omega}) \times \vec{u}\big)\,. \tag{2.97}$$

At this point (2.97) and (2.94) provide suitable expressions for substitution in (2.89). Doing so and applying Gauss' theorem to rewrite the integral into one over the boundary surface yields

$$\frac{\mathrm{d}\mathcal{H}}{\mathrm{d}t} = \int_\Omega \frac{\partial h}{\partial t}\,\mathrm{d}\Omega = \int_\Omega \nabla \cdot \big((\vec{u} \times \vec{\omega}) \times \vec{u} - \vec{\omega}\bar{p}\big)\,\mathrm{d}\Omega = \ldots$$
$$\int_{\partial\Omega} \big((\vec{u} \times \vec{\omega}) \times \vec{u} - \vec{\omega}\bar{p}\big) \cdot \vec{n}\,\mathrm{d}\Gamma = 0, \tag{2.98}$$

due to periodic BC (detailed in Section 2.3.4) on $\vec{u}$, $\vec{\omega}$ and $\bar{p}$. This completes the proof of global helicity conservation in inviscid 3D flows.

2.2.6 Conservation of linear momentum (2D and 3D)

For inviscid flow and periodic boundary conditions, the governing equations (2.2) or (2.1) conserve linear momentum as demonstrated here. This can in fact be expected from the construction of the linear momentum equation, as

it represents the balance between change in linear momentum and forces; see Section 2.1.1 and references to [33] therein. Further, remember that conservation of angular momentum was already demonstrated in Section 2.2.3.

Instead of the convective (2.8) or rotational (2.13) formulation of the linear momentum equation, the equivalent conservative formulation [25, (2)] (with $\nu = 0$, rearranged and multiplied with ρ) will be convenient:

$$\rho \frac{\partial \vec{u}}{\partial t} = -\rho \nabla \cdot (\vec{u} \otimes \vec{u}) - \rho \nabla p. \tag{2.99}$$

This can be written in component notation as

$$\rho \frac{\partial u_i}{\partial t} = -\rho \frac{\partial u_i u_j}{\partial x_j} - \rho \frac{\partial p}{\partial x_i}. \tag{2.100}$$

Then integrate the above over the domain Ω, followed by rewriting the resulting right-hand side into an integral over the domain boundary. The first term is rewritten according to the divergence theorem (generalized for a tensor field) as given by [16, p. 325, (9.3.10)]. The second term is similarly rewritten with the integral theorem [23, A1. Vector Identities, p. 363, (15)]. Together this results in (remembering ρ is a constant):

$$\rho \int_{\Omega} \frac{\partial u_i}{\partial t} \, \mathrm{d}\Omega = -\rho \int_{\partial\Omega} u_i u_j n_j + p n_i \, \mathrm{d}\Gamma = 0, \tag{2.101}$$

which is zero due to periodic BC. As the left-hand side represents the linear momentum within the domain, its conservation is now demonstrated. This for the 3D formulation (2.2) in the inviscid limit. It however also holds for the 2D formulation (2.1) in the inviscid limit, because the linear momentum equation is nearly the same there. The only difference is that certain components of $\vec{u}$ and $\vec{\omega}$ are zero.

2.3 Taylor-Green flow: basic problem description and solutions

This section gives a description of the Taylor-Green (TG) problem, because it seems most suitable for verification: it has periodic boundary conditions, an exact solution in 2D and relates to realistic turbulent flow in 3D. For future

work it could also be interesting that suitable benchmark material may be found in literature for 3D simulations.

The TG flow is characterized by its special initial conditions (IC). For these combined with the Navier-Stokes equations, a general Fourier-series expansion and even an exact solution for 2D are known. This flow is "perhaps the simplest system in which to study the generation of small scales and the resulting turbulence" [5]. This process controls the energy dynamics and hence the global structure and evolution [5] of (seemingly) many realistic flows, making TG flow a relevant test-case for the new numeric method.

2.3.1 Initial conditions

TG flow was first presented by Taylor and Green in [30]. With the sine and cosine terms swapped like in [25] (implying just a spatial shift), the IC are

$$\left.\begin{aligned} u &= A \sin ax \cos by \cos cz \\ v &= B \cos ax \sin by \cos cz \\ w &= C \cos ax \cos by \sin cz \end{aligned}\right\} \quad \text{General IC at } t = 0. \tag{2.102}$$

The constants A, B, C, a, b and c are constrained by the incompressibility constraint $\nabla \cdot \vec{u} = 0$ (2.14):

$$Aa + Bb + Cc = 0. \tag{2.103}$$

Specific values for these six constants are required for investigation of the MEEVC algorithm's numeric performance in Chapter 3. The following simplification of the general IC was introduced by Taylor and Green as a "Special Case" [30]: $a = b = c$, $A = -B$ and $C = 0$. Although the initial streamlines are of 2D nature, the flow directly becomes 3D after $t = 0$. This simplification is also made in [12, Section 8.3] and is prominent in [5]. In the latter, the authors also considered a particular case with non-zero velocities for each component. They could however not conclude it to be an improvement over the simplified case for "the study of small-scale turbulence at late times", so the dynamics are equally relevant.

Specific IC for fully 2D flow, that are equivalently simple as the special case just discussed, are obtained here as follows. Set the constants in the general 3D case (2.102) to $B = -A = 1$, $a = b = \pi$ and $C = c = 0$. This yields

the same IC as used in the MEEVC paper [25]:

$$\left.\begin{aligned} u &= -\sin\pi x\cos\pi y \\ v &= \cos\pi x\sin\pi y \end{aligned}\right\} \quad \text{Chosen IC at } t=0. \tag{2.104}$$

2.3.2 General Fourier series solution

In [30], the IC (2.102) are combined with conservation of momentum (2.7) and mass (2.14), to compute the pressure field and velocity time derivatives at $t=0$. The latter and the IC are then substituted in the following approximate integration: $\vec{u}(t)=\vec{u}_{t=0}+t(\frac{\partial\vec{u}}{\partial t})_{t=0}$. Because the terms in the resulting expression are of the same (spatially) sinusoidal type as the IC, this process may be repeated. This is done by substituting the resulting expression (instead of the IC) into the conservation laws to find $(\frac{\partial\vec{u}}{\partial t})_{t=0}$, which is then again used for approximate integration. Each iteration adds another term to the power series expansion of type $A_0+A_1t+A_2t^2+\ldots$, making it more accurate. It must be remarked though, that the analytic expressions for subsequent A_i quickly become very long.

A Fourier series solution for the Taylor-Green flow velocity components when $a=b=c=\pi$ in the IC (2.102) is similar to [5, (1.2)], with slightly different notation written as:

$$\left.\begin{aligned} u(x,y,z,t) &= \sum_{m=0}^{\infty}\sum_{n=0}^{\infty}\sum_{p=0}^{\infty}\hat{u}_{m,n,p}(t)\sin\pi mx\cos\pi ny\cos\pi pz \\ v(x,y,z,t) &= \sum_{m=0}^{\infty}\sum_{n=0}^{\infty}\sum_{p=0}^{\infty}\hat{v}_{m,n,p}(t)\cos\pi mx\sin\pi ny\cos\pi pz \\ w(x,y,z,t) &= \sum_{m=0}^{\infty}\sum_{n=0}^{\infty}\sum_{p=0}^{\infty}\hat{w}_{m,n,p}(t)\cos\pi mx\cos\pi ny\sin\pi pz \end{aligned}\right\}, \tag{2.105}$$

where the coefficients $\hat{u}$, $\hat{v}$ and $\hat{w}$ are zero unless m, n, p are either all even or all odd integers. They contain the aforementioned power series expansions in t. This solution format nicely shows how the sinusoidal terms and their periodicity characterize the solution at all times $t\geq 0$.

The vorticity vector field follows by taking the curl of velocity and shows

to have similar solution format:

$$\vec{\omega} = \nabla \times \vec{u} = \begin{bmatrix} \frac{\partial w}{\partial y} - \frac{\partial v}{\partial z} \\ \frac{\partial u}{\partial z} - \frac{\partial w}{\partial x} \\ \frac{\partial v}{\partial x} - \frac{\partial u}{\partial y} \end{bmatrix} = \dots$$
$$\pi \sum_{m=0}^{\infty} \sum_{n=0}^{\infty} \sum_{p=0}^{\infty} \begin{bmatrix} (-n\hat{w}_{m,n,p}(t) + p\hat{v}_{m,n,p}(t)) \cos \pi mx \sin \pi ny \sin \pi pz \\ (-p\hat{u}_{m,n,p}(t) + m\hat{w}_{m,n,p}(t)) \sin \pi mx \cos \pi ny \sin \pi pz \\ (-m\hat{v}_{m,n,p}(t) + n\hat{u}_{m,n,p}(t)) \sin \pi mx \sin \pi ny \cos \pi pz \end{bmatrix}. \tag{2.106}$$

The solution formats presented above are useful for identifying certain (symmetry) properties of the Taylor-Green flows they describe. These properties generally not only apply to 3-D, but also to the particular 2D situation. Upcoming sections will describe them, as they are useful for understanding the numerical test case.

2.3.3 Exact solution for a 2D case

An exact solution exists for the fully 2D case. The reason for this is that the power series expansions made up by the summations in (2.105) and (2.106) can then be written as exponentials. For the IC (2.104) this is (from [25, (68)]):

$$\left.\begin{aligned} u(x,\, y,\, t) &= -\sin(\pi x)\cos(\pi y)e^{-2\pi^2 \nu t} \\ v(x,\, y,\, t) &= \cos(\pi x)\sin(\pi y)e^{-2\pi^2 \nu t} \\ \omega(x,\, y,\, t) &= -2\pi \sin(\pi x)\sin(\pi y)e^{-2\pi^2 \nu t} \\ p(x,\, y,\, t) &= \frac{1}{4}(\cos(2\pi x) + \cos(2\pi y))e^{-4\pi^2 \nu t} \end{aligned}\right\}. \tag{2.107}$$

In [25, (68)] the exponent in p has a positive sign, but based on intuition and references like [12, Section 8.1] it should be negative as written here.

2.3.4 Periodic boundary conditions

The domain $\Omega = [0,\, 2]^3$ with periodic BC is used in this work when numerically solving a 3D TG flow with general solution given by (2.105) and (2.106). A full period is contained within Ω in each of the x-, y- and z-directions. The current section summarizes what this periodicity of the solution means and

provides some details on component values on the boundary. All applies to the 2D case as well, by leaving the z-component out.

In general, a function f is periodic on the domain $0 \leq x, y, z \leq 2$ if

$$\left.\begin{aligned} \frac{\partial^m f}{\partial x^m}(0, y, z) &= \frac{\partial^m f}{\partial x^m}(2, y, z) \\ \frac{\partial^m f}{\partial y^m}(x, 0, z) &= \frac{\partial^m f}{\partial y^m}(x, 2, z) \\ \frac{\partial^m f}{\partial z^m}(x, y, 0) &= \frac{\partial^m f}{\partial z^m}(x, y, 2) \end{aligned}\right\} \quad \text{for all } m = 0, 1, 2, \ldots, \infty. \tag{2.108}$$

From (2.105) and (2.106) it can be verified that $\vec{u}$ and $\vec{\omega}$ meet this condition. Because all terms involving $\vec{u}$ and $\vec{\omega}$ in the PDE (2.8) have the Fourier series character of these variables, p must share this and thereby have periodic BC with characteristics of (2.108) as well. However, p will have a different expression and period because (2.8) is nonlinear. An example is the 2D case of (2.107), where p has a double period compared to $\vec{u}$ and $\vec{\omega}$.

The following examples illustrate that $\vec{u}$ given by (2.105) and $\vec{\omega}$ by (2.106) are periodic and that normal velocity and tangential vorticity components are zero on the boundary. The walls of the domain are 'impermeable' ($\vec{u} \cdot \vec{n} = 0$), while in general $\vec{u} \times \vec{n} \neq 0$. For example:

$$\begin{aligned} u(0, y, z, t) &= u(2, y, z, t) = 0, \\ u(x, 0, z, t) &= u(x, 2, z, t) \in \mathbb{R}, \\ u(x, y, 0, t) &= u(x, y, 2, t) \in \mathbb{R}, \end{aligned} \tag{2.109}$$

with $\mathbb{R}$ the set of real numbers (including zero). The tangential component of vorticity is zero at all boundary faces ($\vec{\omega} \times \vec{n} = 0$), but the normal component generally is not ($\vec{\omega} \cdot \vec{n} \neq 0$). For example consider the z-component:

$$\begin{aligned} \omega_z(0, y, z, t) &= \omega_z(2, y, z, t) = 0, \\ \omega_z(x, 0, z, t) &= \omega_z(x, 2, z, t) = 0, \\ \omega_z(x, y, 0, t) &= \omega_z(x, y, 2, t) \in \mathbb{R}. \end{aligned} \tag{2.110}$$

Another typical property is that the flow stagnates at the corners of the domain $\Omega = [0, 2]^3$: all velocity and vorticity components are zero there.

In [25] and this work, the periodic BC are advantageously applied to discretization with the finite element method as follows. To reduce the order of certain derivatives, partial integration is used. The boundary integrals involved in this are zero due to the periodic BC. Besides that, the formulation

does not need modifications or extra equations to enforce specific BC. This allows to focus on discretizing the PDE with minimal clutter. It should be remarked though, that periodicity (2.108) is only applied there for derivatives up to first order at most (and that for only normal or tangential components).

2.3.5 Symmetry properties

Some special domains can be identified from the periodic Taylor-Green solution format of (2.105), which can be useful for building, understanding and checking numerical simulations. These domains are described here based on [5, Section 2] and [5, Appendix A. Symmetries of the TG flow]. They also apply to 2D upon leaving the z-component out. The solution within the *periodicity box* $0 \leq x, y, z \leq 2$ reflects a full period which, upon endless repetition (tiling) in space, describes the complete solution. For any integer k the planes $x = k$, $y = k$ and $z = k$ are stress-free and mirror-symmetric for all time [5, Appendix A. Symmetries of the TG flow]. Because there is no flow passing these planes of symmetry, it is appropriate to call the limited region $0 \leq x, y, z \leq 1$ the *impermeable box*. Within this box, axes of symmetry are $x = y = \frac{1}{2}$, $x = z = \frac{1}{2}$ and $y = z = \frac{1}{2}$ (that is the flow is invariant under angular rotations of π around these). Therefore an even smaller special domain can be identified: the *fundamental box* $0 \leq x, y, z \leq \frac{1}{2}$. Suppose a solution is known over this domain. Then it is the smallest subdomain from which the solution in unlimited space can be described using symmetries. Only for some special cases a smaller fundamental box exists.

Clearly it could be worthwhile to make use of these symmetries in numerical simulation but that is not in the research interest of this work. Solving only within the fundamental box is however sufficient to obtain the full solution. This can be quite a bit faster, because in 3D its volume is $2^3/(\frac{1}{2})^3 = 64$ times smaller than that of the periodic box. It would require non-periodic BC.

Additional symmetries exist for special choices of IC. An example is when $\theta = 0$ in the IC written in the format of [5, (1.1)], see [5, Appendix A, (A 3) and (A 4)]. It seems this is exploited in [12, Section 8.3] to solve the problem on a 2D domain and then map the results to 3D. This is however not the aim when an 'intrinsic' 3D method is developed. Still, this source might serve as a quantitative benchmark and it can be checked whether a method can capture these (additional) symmetries.

Chapter 3

The 2D MEEVC discretization

This chapter will deal with the discrete MEEVC formulation originally presented in [25] and analytically prove its conservation properties. Earlier in Chapter 2, the governing continuous equations were considered. This included proofs for the conservation of various integral invariants under appropriate conditions. A discrete formulation and the corresponding set of equations does not naturally share the same properties. In general this is influenced by the format of the continuous equations it is based on as well as various other factors. Even kinematic relations such as $\vec{\omega} = \nabla \times \vec{u}$ are not automatically valid for discrete solutions $\vec{\omega}_h$ and $\vec{u}_h$.

Hence the MEEVC formulation is considered in Section 3.1 with proofs of its discrete conservation properties in Section 3.2. In [25], the formulation itself is characterized by three aspects in particular, which may be elaborated on as follows. First of all is the use of a decoupled vorticity and velocity-pressure systems setup, where the velocity-pressure system is characterized by the use of the rotational form. This will be presented at the start of Section 3.1, including Section 3.1.1. Using both the vorticity transport and the linear momentum equations in the discretization helps to conserve integral properties of both. The second aspect characterizing the MEEVC formulation is the finite element function spaces that are chosen, for which background can be found in Section 3.1.3 and especially Section 3.1.4. Finally, the third aspect is the time integrator: a first order Gauss method as described in Section 3.1.5. It is a vital element because it conserves linear and quadratic invariants, while also allowing the uncoupling and linearization of the discrete equations.

3.1 Discrete problem description

The discrete problem formulation is derived from the set of continuous PDEs (2.1), using integration as described in [25]. The following text and equations are strongly based on this reference. Please refer to it for more details and further references supporting some of the statements in the subsections below. These subsections describe key ingredients to the discrete formulation.

The variables in the MEEVC formulation, presented below, are in finite element spaces as follows. Velocity is discretized in terms of Raviart-Thomas elements of degree N, that is $\vec{u}_h \in \mathrm{RT}_N$. Total pressure in terms of discontinuous Lagrange elements of degree $(N-1)$, that is $\bar{p}_h \in \mathrm{DG}_{N-1}$. Vorticity in terms of Lagrange elements of degree N, that is $\omega_h \in \mathrm{CG}_N$. Further the space of scalar real numbers (R_0) is used for r_0.

The core of the discrete MEEVC algorithm is to find $\omega_h^{k+1} \in \mathrm{CG}_N$, $\vec{u}_h^{k+\frac{3}{2}} \in \mathrm{RT}_N$, $\bar{p}_h^{k+1} \in \mathrm{DG}_{N-1}$ and (although not of primary interest) $r_h \in \mathrm{R}_0$ such that:

$$\begin{aligned}\left\langle \frac{\omega_h^{k+1}-\omega_h^k}{\Delta t}, \mathscr{C}_h \right\rangle_\Omega - \frac{1}{2}\left\langle \frac{\omega_h^{k+1}+\omega_h^k}{2}, \nabla\cdot\left(\vec{u}_h^{k+\frac{1}{2}}\mathscr{C}_h\right)\right\rangle_\Omega \\ +\frac{1}{2}\left\langle \nabla\cdot\left(\vec{u}_h^{k+\frac{1}{2}}\frac{\omega_h^{k+1}+\omega_h^k}{2}\right), \mathscr{C}_h\right\rangle_\Omega \\ = -\nu\left\langle \nabla\times\frac{\omega_h^{k+1}+\omega_h^k}{2}, \nabla\times\mathscr{C}_h\right\rangle_\Omega \quad \forall \mathscr{C}_h \in \mathrm{CG}_N,\end{aligned} \tag{3.1a}$$

$$\begin{aligned}\left\langle \frac{\vec{u}_h^{k+\frac{3}{2}}-\vec{u}_h^{k+\frac{1}{2}}}{\Delta t}, \vec{v}_h\right\rangle_\Omega + \left\langle \omega_h^{k+1}\times\frac{\vec{u}_h^{k+\frac{3}{2}}+\vec{u}_h^{k+\frac{1}{2}}}{2}, \vec{v}_h\right\rangle_\Omega - \left\langle \bar{p}_h^{k+1}, \nabla\cdot\vec{v}_h\right\rangle_\Omega \\ = -\nu\left\langle \nabla\times\omega_h^{k+1}, \vec{v}_h\right\rangle_\Omega \quad \forall \vec{v}_h \in \mathrm{RT}_N,\end{aligned} \tag{3.1b}$$

$$\left\langle \nabla\cdot\vec{u}_h^{k+\frac{3}{2}} + r_h^{k+1}, q_h\right\rangle_\Omega = 0 \quad \forall q_h \in \mathrm{DG_{N-1}}, \tag{3.1c}$$

$$\left\langle \bar{p}_h^{k+1}, \tilde{r}_h\right\rangle_\Omega = 0 \quad \forall \tilde{r}_h \in \mathrm{R}_0. \tag{3.1d}$$

Vorticity is treated as a scalar where possible. This is allowed by the 2D situation, where velocity has two components but vorticity only one. An exception is (the second term of) Eq. (3.1b), where vorticity is in a cross-product; a vector operation not defined for a true scalar. Here vorticity is represented as

a vector with only its third component non-zero. Representing $\vec{u}_h$ as three-element vector with zero third component makes the cross product correctly defined. By this $\vec{\omega}_h^{k+1}$ is always perpendicular to $\vec{u}_h$, as should be for planar flow.

The four equations (3.1) are solved in two steps rather than at once. First, vorticity is computed at time t^{k+1} by solving the vorticity transport equation (3.1a). Second, this 'new' vorticity is substituted in the discrete balance of linear momentum equation in rotational form (3.1b), which is solved with enforcement of mass conservation (3.1c) and leveling of pressure (3.1d). The solution of this linear system are velocity, total pressure at a new time-level as well as an auxiliary variable r_h. This variable is not of physical interest and ends up in the equation for conservation of mass (3.1c) due to the enforcement of zero integral pressure, see Section 3.1.2. It does not influence conservation of mass as r_h appears to be zero in all calculations. As it is related to the pressure constraint, it is discretized at the same time (t^{k+1}).

The two-step approach in solving is possible by 'staggered time-stepping' of the variables. Figure 3.1 shows at which time instances the variables are discretized; the equations are solved as described above. Section 3.1.5 explains the temporal discretization in more detail. Other subsections below highlight important aspects related to the spatial discretization.

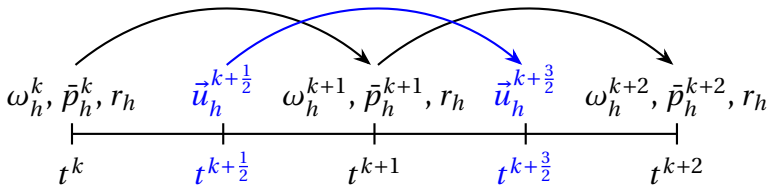

Figure 3.1: Temporal discretization of variables in staggered time stepping (modified reproduction of [25, Fig. 1]).

3.1.1 Integration by parts

The first step in deriving the discrete equations (3.1) from the continuous (2.1) is to multiply by test functions and then use integration by parts to reduce to at most first order derivatives. These test functions are similar to the trial functions (3.11) in construction, but have arbitrary weights (coef-

ficients). This is known as the Galerkin method. A solution to (3.1), being particular weights for the trial functions, must be valid for any (non-trivial) combination of weights in the test functions.

Each equation in (3.1) is obtained through multiplication with a test function existing in a particular space: 'velocity space' with $\vec{v}_h \in \mathrm{RT}_N$ for balance of linear momentum, 'vorticity space' with $\mathscr{C}_h \in \mathrm{CG}_N$ for vorticity transport, the '(total) pressure space' with $q_h \in \mathrm{DG}_{\mathrm{N}-1}$ for conservation of mass, and a space for a scalar that is constant over the domain with $r_h \in \mathrm{R}_0$.

After multiplication by test functions, integration by parts is used to reduce the order of certain derivatives:

$$\begin{aligned}
\left\langle \nabla \bar{p}, \vec{v} \right\rangle_\Omega &= -\left\langle \bar{p}, \nabla \cdot \vec{v} \right\rangle_\Omega + \overbrace{\int_{\partial\Omega} \bar{p}(\vec{v} \cdot \vec{n}) \,\mathrm{d}s}^{=0}, \\
\left\langle (\vec{u} \cdot \nabla)\omega, \mathscr{C} \right\rangle_\Omega &= -\left\langle \omega, \nabla \cdot (\vec{u}\mathscr{C}) \right\rangle_\Omega + \overbrace{\int_{\partial\Omega} \mathscr{C}\omega(\vec{u} \cdot \vec{n}) \,\mathrm{d}s}^{=0}, \\
\nu \left\langle \nabla^2 \omega, \mathscr{C} \right\rangle_\Omega &= -\nu \left\langle \nabla \times \omega, \nabla \times \mathscr{C} \right\rangle_\Omega + \nu \overbrace{\int_{\partial\Omega} \mathscr{C}(\nabla \times \omega) \times \vec{n} \,\mathrm{d}s}^{=0}.
\end{aligned} \tag{3.2}$$

Note that the boundary integrals conveniently evaluate to zero due to the periodic BC. Above equations have been used in the derivation of (3.1).

3.1.2 Computing the pressure field

Special attention is paid here to how the average level of the pressure field is fixed in the variational problem (3.1) by (3.1c) and (3.1d). This means setting

$$\int_\Omega \bar{p}_h^{k+1} \,\mathrm{d}\Omega = 0, \tag{3.3}$$

which avoids that the pressure level 'jumps around' over time-steps. Furthermore this section describes the post-processing step that is used to compute the static pressure p from the total pressure $\bar{p}$.

Fixation of total pressure level

When the MEEVC formulation as published in [25] was implemented in computer code by the author of this thesis, it was found that the pressure level

jumps around in simulations with the following reasons and consequences. The continuous balance of linear momentum equation, that is the first in (2.1), contains the pressure gradient. So that equation on its own does not say anything about the pressure level. Due to the necessary partial integration step (see Section 3.1.1) pressure appears directly in the variational formulation (3.1b) instead of its gradient in the continuous problem. But this still does not add information about its level. Neither do the boundary conditions applied in this work, as they are periodic and do not specify any preselected values. Furthermore the velocity and vorticity solutions at the new time-level link back to the known previous, and this way ultimately to their initial conditions, but with pressure that does not happen. So when the published MEEVC formulation [25] was used directly, a constant of integration could poorly be determined each time-step making that the pressure field often changed largely. Pressure thereby reached values several orders of magnitude bigger than its leveled exact solution, velocity and vorticity. This did not only made visualization inconvenient, but possibly introduced numerical error to the solutions. A deviation of the divergence of velocity from its constraint on zero may be expected. Therefore the total pressure level is fixed to zero by modifying the original formulation as explained in the following. By the way, this zero level is chosen just for convenience; physics does not require it specifically.

Setting the fixed pressure level in the variational formulation was done as follows. The constraint (3.3) itself corresponds to

$$\int_\Omega \tilde{r}_h \bar{p}_h^{k+1} \, \mathrm{d}\Omega = 0 \quad \forall \tilde{r}_h \in \mathrm{R}_0, \tag{3.4}$$

which is (3.1d). Thereby remember that R_0 is the space of scalar real numbers that are constant over the entire domain, alternatively described as the real-valued polynomial space of order zero. As (3.4) must hold for any value of $\tilde{r}_h$, it is obvious that this equation effectively enforces the pressure constraint (3.3). But with the introduction of a test function $\tilde{r}_h$ comes a corresponding trial function r_h ending up in (3.1c) as derived further below.

The extra variable r_h is of no direct physical interest but its solutions and effects to the linear system have been investigated as follows. Several numerical results were checked and all had $r_h = 0$. It is believed that r_h must always be zero, therefore the author of this thesis spent much effort on identifying additional properties of the linear system that prove this. Because of unsatis-

fying results these analyses are not included in this thesis though. Complex approaches could not be finalized and approaches based on simplified examples looked plausible but could not be proven representative for the full system. One thing is sure though: in the linear system $A\vec{x} = \vec{b}$ corresponding to the MEEVC formulation (3.1), the extra variable r_h (included as an entry in $\vec{x}$) kept the matrix A square after the system was expanded with the pressure constraint. This means there are as much equations as variables, which is necessary (but not sufficient) for always having a unique solution.

The modification of the original MEEVC formulation that fixed the pressure level was suggested and recommended by Artur Palha, first author of the MEEVC paper [25], but this came without derivation so therefore the following is an attempt to construct one. *It works but has its imperfections as will soon become clear.* It follows a Lagrange-multiplier approach where the Lagrangian to implement the pressure constraint (3.4) is formulated from trial functions as

$$L\left(r_h,\, \bar{p}_h^{k+1}\right) = \int_\Omega r_h \bar{p}_h^{k+1}\, \mathrm{d}\Omega, \tag{3.5}$$

where $r_h \in \mathrm{R}_0$ is considered the Lagrange multiplier. As it is constant, it could be drawn into the integral corresponding to the constraint. Strictly speaking $L(r_h,\, \bar{p}_h^{k+1})$ is however no Lagrangian as it misses an objective function that must be minimized subject to the constraint. It is questionable if an objective function corresponding to the MEEVC formulation could be found though, so therefore it is just assumed zero here. The addition to the formulation that fixes the pressure level can still be derived this way though by setting the derivative of $L(r_h,\, \bar{p}_h^{k+1})$ equal to zero according to the Lagrange method:

$$\begin{aligned} \lim_{\epsilon_1, \epsilon_2 \to 0} \left[L(r_h + \epsilon_1 \tilde{r}_h,\, \bar{p}_h^{k+1} + \epsilon_2 q_h) - L(r_h,\, \bar{p}_h^{k+1}) \right] = 0 \\ \forall q_h \in \mathrm{DG}_{N-1} \text{ and } \forall \tilde{r}_h \in \mathrm{R}_0, \end{aligned} \tag{3.6}$$

where $\tilde{r}_h$ and q_h in the 'incremental' terms are test functions. This equation implies that the gradient of L must be equal to the zero vector, considering that either of the test functions can be zero. Substituting (3.5) for the Lagrangian and evaluating the limit yields:

$$\int_\Omega \tilde{r}_h \bar{p}_h^{k+1}\, \mathrm{d}\Omega + \int_\Omega r_h q_h\, \mathrm{d}\Omega = 0 \quad \forall q_h \in \mathrm{DG}_{N-1} \text{ and } \forall \tilde{r}_h \in \mathrm{R}_0. \tag{3.7}$$

Finally these integrals are expressed in bracket notation for the MEEVC formulation, where the first integral becomes (3.1d) and the second ends up in (3.1c) according to the finite element spaces for the test functions.

Computation of static from total pressure

Here the equation used to compute the instantaneous static pressure field from the total pressure field in post-processing is derived. This equation, (3.10) below, also corrects the average of the static pressure field to zero for convenient visualization and comparison against exact results. Remember that this zero pressure level is associated to setting a constant of integration. The Navier-Stokes equations themselves only describe the pressure *differences*. One could wonder why the variational problem, (3.1) that is, cannot be adapted to compute static pressure directly. The reason behind this is that a non-linear term of unknowns ($\vec{u}_h \cdot \vec{u}_h$) would be introduced.

The following demonstrates that the total pressure computed by solving the variational problem (3.1) does not lead to a static pressure level that is the same as that of the exact solution used for reference. Substituting static pressure from its definition in terms of total pressure and velocity, that is $p = \bar{p} - \frac{1}{2}\vec{u} \cdot \vec{u}$, shows that its level will be at:

$$\int_\Omega p_h^{k+1} \,\mathrm{d}A = -\mathcal{K}_h^{k+1}. \tag{3.8}$$

Here it was used that the total pressure level is constrained to zero (3.3) and that $\mathcal{K} = \int_\Omega \frac{1}{2}\vec{u}\cdot\vec{u} \,\mathrm{d}A$ is the kinetic energy contained in the domain. The level of the exact solution (2.107) is different though:

$$\int_\Omega p_e \,\mathrm{d}A = 0. \tag{3.9}$$

Comparing equation (3.8) to (3.9) shows that the level of the numeric solution can be corrected by adding average kinetic energy density $\mathcal{K}_h^{k+1}/A_\Omega$ as a correction term to p_h. Here $A_\Omega = 4$ is the area over the $\Omega = [0, 2]\times[0, 2]$ domain so that the correction term integrates to $\int_\Omega \mathcal{K}_h^{k+1}/A_\Omega = +\mathcal{K}_h^{k+1}$. Therefore the corrected static pressure field is computed from the total pressure and velocity fields as follows:

$$p_h^{k+1} = \bar{p}_h^{k+1} - \frac{1}{2}\tilde{\vec{u}}_h^{k+1} \cdot \tilde{\vec{u}}_h^{k+1} + \frac{\tilde{\mathcal{K}}_h^{k+1}}{A_\Omega}. \tag{3.10}$$

This makes $\int_\Omega p_h^{k+1} \,\mathrm{d}A = 0$. The tilde indicates approximated values, as the staggered time-stepping scheme (Figure 3.1) implies $\vec{u}_h$ is not computed at t_{k+1}. Just like some terms in the variational problem, this can be done by linear interpolation: $\tilde{\vec{u}}_h^{k+1} \approx \frac{1}{2}\left(\vec{u}_h^{k+\frac{1}{2}} + \vec{u}_h^{k+\frac{3}{2}}\right)$. The resulting field is then also

used to compute $\tilde{\mathcal{K}}_h^{k+1}$. The implementation was however simplified by using velocity and kinetic energy at the latest time-step ($t^{k+\frac{3}{2}}$) instead. This is fine as the static pressure results are not of direct interest for this work and visually tend to agree with those from the exact solution.

3.1.3 A DeRham complex for function spaces

The discrete variables ($\vec{u}_h$, ω_h, $\bar{p}_h$) in the MEEVC formulation (3.1) are trial functions formed by linear combinations of the basis functions $\vec{\epsilon}_i^U(x, y)$, $\epsilon_i^Q(x, y)$ and $\epsilon_i^W(x, y)$:

$$\vec{u}_h := \sum_{i=1}^{d_U} u_i \vec{\epsilon}_i^U, \quad \bar{p}_h := \sum_{i=1}^{d_Q} p_i \epsilon_i^Q, \quad \omega_h := \sum_{i=1}^{d_W} \omega_i \epsilon_i^W, \tag{3.11}$$

where u_i, p_i and ω_i are scalar weights which generally change each time-step. The basis functions do not change over time-steps. They depend on space only and if they are continuous then this is reflected by the solutions. The number of degrees of freedom (dimensions of the problem) are d_U, d_Q and d_W. They are determined by the amount of mesh elements and the degree of the polynomial basis functions used for each mesh element.

The above trial functions span finite dimensional function spaces U_h, Q_h and W_h, which are limited by the following:

$$\vec{u}_h \in U_h \subset H(\text{div}, \Omega), \quad p_h \in Q_h \subset L^2(\Omega), \quad \omega_h \in W_h \subset H^1(\Omega). \tag{3.12}$$

This means that integrating the square of any of the indicated functions over (part of) the domain is well-defined and will always produce a finite result. Furthermore, this will also be guaranteed to hold for the square of any first order derivative of a function in $H^1(\Omega)$ and for the square of the divergence of a function in $H(\text{div}, \Omega)$. With (3.12) the MEEVC formulation (3.1) is constructed such that the derivatives included in it generally produce a function that is guaranteed to be square-integrable. For some terms in (3.1) this may not to be the case though, as discussed within Section 5.4. The square-integrability is a prerequisite for ensuring a solvable set of linear equations.

Besides their integrability, the finite element function spaces are conforming by mapping into another:

$$0 \longrightarrow W_h \xrightarrow{\nabla\times} U_h \xrightarrow{\nabla\cdot} Q_h \longrightarrow 0. \tag{3.13}$$

They form a DeRham subcomplex, which is a finite dimensional equivalent to the continuous DeRham complex in differential geometry. This characteristic forms an important requirement for obtaining a stable and accurate finite element discretization [25].

Considering the variational problem (3.1) makes it intuitive: a product of terms that are both in one of the square-integrable spaces of (3.12) must be integrable. Note from the DeRham subcomplex (3.13) that some terms contain a derivative which even puts the term it applies to in the same space as the other in the product. An example is $\left\langle \bar{p}_h^{k+1}, \nabla \cdot \vec{v}_h \right\rangle_\Omega$: the multiplier is already in the (total) pressure space Q_h, the multiplicand is cast into this space by applying the divergence operator to the term $\vec{v}_h$ in velocity space U_h. Such is not the case for all terms though, sometimes derivatives just lead to the same type: scalar or vector.

Finally, for the MEEVC formulation it should be noted that $\nabla \times \vec{u}_h$ falls outside of the DeRham subcomplex (3.13) and does not solve the vorticity transport equation. Unlike $\nabla \cdot \vec{u}_h$, $\nabla \times \vec{u}_h$ is not in $L^2(\Omega)$. So it is in general not square-integrable and thereby unsuitable for the discrete equations (3.1). The ω_h in the MEEVC method is directly computed from the discrete vorticity transport equation and does not have this problem as it is square-integrable. A further advantage is that there is proof that ω_h satisfies vorticity conservation (Section 3.2.3) and enstrophy conservation in the inviscid case (Section 3.2.4). This while $\nabla \times \vec{u}_h$ is not necessarily a solution to the (discrete) vorticity transport equation and therefore generally lacks these conservation properties. This is different from the continuous setting, where a solution $\vec{u}$ of the linear momentum equation is *always* such that its curl is a solution of the vorticity transport equation. One may refer back to Chapter 2 for more information on the continuous setting. In the discrete setting there are differences due to the finite resolution and other approximations.

3.1.4 Finite element function spaces

This section will provide more details on the finite element function spaces that are used in the MEEVC formulation (3.1).

A finite element is commonly specified by (T, $\mathscr{V}$, $\mathscr{L}$), where:

T is the *domain* of the element and is a bounded, closed subset of $\mathbb{R}^d$ with nonempty interior and piecewise smooth boundary;

$\mathscr{V}$ is a *function space* of finite dimension n on T, in this work constructed from polynomials $\mathscr{P}_q$ of degree q;

$\mathscr{L}$ is a basis $\{\ell_1, \ell_2, \ldots, \ell_n\}$ for the space $\mathscr{V}'$ dual to $\mathscr{V}$, and it are these *nodes* that represent the degrees of freedom.

This description is based on [19, Definition 3.1].

Before visualizing the finite elements used in the MEEVC discretization, it is first recalled that the following finite element function spaces are employed in the discretization (3.1):

$$W_h = \mathrm{CG}_N,\ U_h = \mathrm{RT}_N \text{ and } Q_h = \mathrm{DG}_{N-1}. \tag{3.14}$$

Figure 3.2 visualizes the $N = 1$ situation as the simplest (lowest order) example. The curved arrows show where the curl and gradient operators can be used to map from one space into another. The blue elements illustrate the degrees of freedom. For vorticity, these are each indicated by a dot with a circular arrow around it: the dot represents evaluation of a scalar function and the circular arrow adds the physical interpretation of rotation. For velocity, the degrees of freedom are indicated by straight arrows over the sides of the element. Each of these arrows represents an evaluation of the normal component of a vector function. Pressure is suggested by arrows emanating from a dot (its node). In addition, the whole interior of the triangle is colored as the pressure is constant over the entire element.

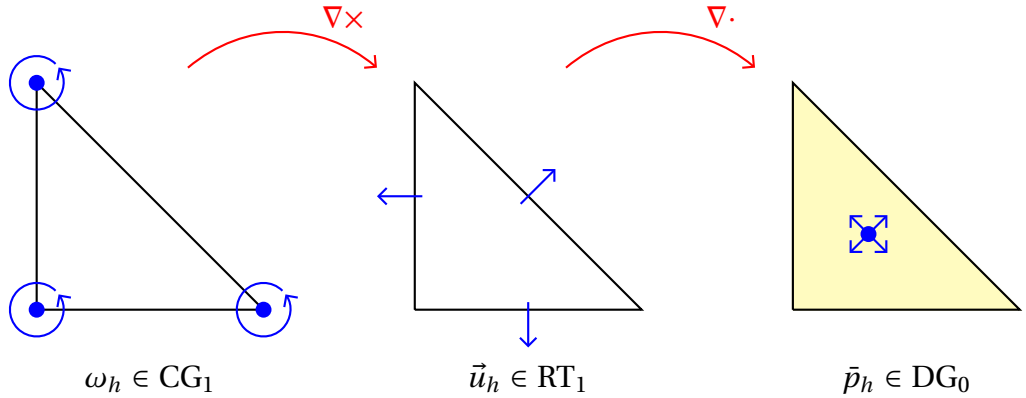

Figure 3.2: Lowest-order ($N = 1$) MEEVC finite element discretization.

While Figure 3.2 is illustrative, it is interesting to consider more properties of the spaces (3.14) and their application:

CG_N refers to the *Lagrange* element space of order N, used for vorticity. This space is particularly suitable for discrete representation of scalar functions (though vectors or tensors can be represented by taking one element per component). It is H^1-conforming and hence represents a subspace of $H^1(\Omega)$: there is not only continuity within the elements, but also across all of the inter-element boundaries. This means the discretized domain is C^0 continuous and (hence) all first order derivatives are square-integrable. All degrees of freedom are determined by point evaluation of function values. [19]

RT_N refers to the Raviart-Thomas element space of order N, used for velocity. This family of FE is especially suitable for discretizing vector fields and is $H(\mathrm{div})$-conforming, meaning that the normal components must be continuous over all (inter-element) boundaries. Velocity fluxes are therefore equal on both sides of a boundary: mass leaving one element enters into the other by the same amount. This conformity allows enforcing local and global conservation of mass, that is $\mathrm{div}(\vec{u}) = 0$. RT_N is the smallest order N polynomial space that is mapped into a $N-1$ polynomial space (DG_{N-1}) by the divergence operator. The degrees of freedom are (moments of) normal components on facets and also, for second order and higher, interior moments. [19]

DG_{N-1} is the discontinuous Lagrange element space of order $N-1$, used for pressure. DG elements are suitable for weak formulations. The abbreviation 'DG' refers to the Discontinuous Galerkin method, which uses these elements. As this name suggests, discretizations with DG elements are not in the continuous function space C^0. They are rather in $L^2(\Omega)$ only: any possible function (reconstruction) is square-integrable, but in general its derivatives are not. Within each individual element the function space is order $N-1$ polynomial, which is continuous, but at inter-element boundaries there is no general continuity enforced. Just as for the 'continuous' Lagrange element, all degrees of freedom correspond to point-wise function evaluation, but are viewed as internal to the element (in line with the discontinuous character). For example, take $N = 1$ in the MEEVC discretization. Then the triangular elements forming the discrete pressure field each have a constant scalar value (0^{th} order polynomial). This can physically be interpreted as a constant pressure within each 2D control volume. Pressure differences

between one element and its neighbors can be used to compute forces acting on this 'control volume' (as a type of numerical fluxes). [19]

3.1.5 Gauss time integration

The MEEVC discrete time integration is based on the midpoint rule, because it allows the linearized, staggered-in-time formulation and is known to conserve integral invariants. Combined with the spatial discretization described earlier, the MEEVC properties are achieved. This section will focus on the temporal discretization. Its formulation and claimed properties are mostly described along the lines of the original presentation [25] but with some critical footnotes.

Application of the midpoint rule

In order to understand the process of temporal discretization it is useful to go back to the starting point. This is a weak formulation obtained through multiplication of the equations in (2.1) with test functions, followed by (partial) integration as treated in Section 3.1.1. Furthermore the system was modified in order to fix the pressure level as described in Section 3.1.2. Two of the equations in the system contain time derivatives: the linear momentum and the vorticity transport equation. Without temporal discretization the combined system looks as follows:

$$\left.\begin{aligned}
\left\langle \frac{\partial \omega_h}{\partial t}, \mathscr{C}_h \right\rangle_\Omega - \frac{1}{2}\left\langle \omega_h, \nabla\cdot\left(\vec{u}_h\mathscr{C}_h\right)\right\rangle_\Omega + \frac{1}{2}\left\langle \nabla\cdot\left(\vec{u}_h\omega_h\right), \mathscr{C}_h\right\rangle_\Omega & \\
= -\nu\left\langle \nabla\times\omega_h, \nabla\times\mathscr{C}_h\right\rangle_\Omega \quad \forall \mathscr{C}_h \in \mathrm{CG}_N, & \\
\left\langle \frac{\partial \vec{u}_h}{\partial t}, \vec{v}_h\right\rangle_\Omega + \left\langle \omega_h\times\vec{u}_h, \vec{v}_h\right\rangle_\Omega - \left\langle \bar{p}_h, \nabla\cdot\vec{v}_h\right\rangle_\Omega & \\
= -\nu\left\langle \nabla\times\omega_h, \vec{v}_h\right\rangle_\Omega \quad \forall \vec{v}_h \in \mathrm{RT}_N, & \\
\left\langle \nabla\cdot\vec{u}_h + r_h, q_h\right\rangle_\Omega = 0 \quad \forall q_h \in \mathrm{DG}_{N-1}, & \\
\left\langle \bar{p}_h, \tilde{r}_h\right\rangle_\Omega = 0 \quad \forall \tilde{r}_h \in \mathrm{R}_0. &
\end{aligned}\right\} \tag{3.15}$$

The unknowns in (3.15) depend on time only, so the equations reduce to a system of first-order ordinary differential equations in time. This is because all terms are integrals over the spatial domain and the result only depends

on the weights of the FE basis functions. These then generally vary over the time-steps. Hence there is an initial value problem corresponding to (3.15) that is formatted similar to[1]

$$\frac{\mathrm{d}f}{\mathrm{d}t} = g(f(t)), \qquad f(0) = f^0. \tag{3.16}$$

Discretization of (3.16) with the implicit midpoint rule[2] yields, with M the number of time steps and Δt the step size:

$$\frac{f^{k+1} - f^k}{\Delta t} = g\left(\frac{f^{k+1} + f^k}{2}\right), \qquad k = 0, 1, \ldots, M. \tag{3.17}$$

The implicit midpoint rule is identical to the first-order Gauss method and conserves up to second order invariants. Gauss methods are classified under collocation methods, which in turn are a subclass of Runge-Kutta methods. The midpoint rule is second-order accurate. These and other details can be found in [14], especially (but not only) pp. 27–31, 34, 99 and 101.

A somewhat free application of the implicit numeric scheme (3.17) to (3.15) is done like in [25] as follows:

$$\left.\begin{aligned}
&\left\langle \frac{\omega_h^{k+1} - \omega_h^k}{\Delta t}, \mathscr{E}_h \right\rangle_\Omega - \frac{1}{2}\left\langle \tilde{\omega}_h^{k+\frac{1}{2}}, \nabla \cdot \left(\tilde{\vec{u}}_h^{k+\frac{1}{2}} \mathscr{E}_h\right)\right\rangle_\Omega + \frac{1}{2}\left\langle \nabla \cdot \left(\nabla \tilde{\vec{u}}_h^{k+\frac{1}{2}} \tilde{\omega}_h^{k+\frac{1}{2}}\right), \mathscr{E}_h \right\rangle_\Omega \\
&\qquad = -\nu \left\langle \nabla \times \tilde{\omega}_h^{k+\frac{1}{2}}, \nabla \times \mathscr{E}_h \right\rangle_\Omega \quad \forall \mathscr{E}_h \in \mathrm{CG}_N, \\
&\left\langle \frac{\vec{u}_h^{k+1} - \vec{u}_h^k}{\Delta t}, \vec{v}_h \right\rangle_\Omega + \left\langle \tilde{\omega}_h^{k+\frac{1}{2}} \times \tilde{\vec{u}}_h^{k+\frac{1}{2}}, \vec{v}_h \right\rangle_\Omega - \left\langle \tilde{p}_h^{k+\frac{1}{2}}, \nabla \cdot \vec{v}_h \right\rangle_\Omega \\
&\qquad = -\nu \left\langle \nabla \times \tilde{\omega}_h^{k+\frac{1}{2}}, \vec{v}_h \right\rangle_\Omega \quad \forall \vec{v}_h \in \mathrm{RT}_N, \\
&\left\langle \nabla \cdot \vec{u}_h^{k+1} + r_h^{k+\frac{1}{2}}, q_h \right\rangle_\Omega = 0 \quad \forall q_h \in \mathrm{DG}_{N-1}, \\
&\left\langle \tilde{p}_h^{k+\frac{1}{2}}, \tilde{r}_h \right\rangle_\Omega = 0 \quad \forall \tilde{r}_h \in \mathrm{R}_0,
\end{aligned}\right\} \tag{3.18}$$

[1] Note however that the problem (3.15) is actually a more complex system of equations, which makes this comparison somewhat questionable. An example of this complexity is the case of the pressure $\tilde{p}_h$, which has coefficients that vary in time but does not have a time-derivative term within (3.15) like $\mathrm{d}f/\mathrm{d}t$ in (3.16).

[2] In the MEEVC paper [25], there is also an explicit time-dependence in the midpoint rule. Its point of departure is (3.16) with $g(f(t), t)$ as right-hand side. There is however no explicit time dependence in the equations (3.15) themselves, so here the formats as presented in [14] are used.

where the divergence constraint (third equation) is applied to $\vec{u}_h$ at the new time-level because the current timelevel must already be divergence-free. Also, the following shorthand notations are used above:

$$\tilde{\vec{u}}_h^{k+\frac{1}{2}} = \frac{\vec{u}_h^{k+1} + \vec{u}_h^k}{2}, \quad \tilde{\bar{p}}_h^{k+\frac{1}{2}} = \frac{\bar{p}_h^{k+1} + \bar{p}_h^k}{2}, \quad \tilde{\omega}_h^{k+\frac{1}{2}} = \frac{\omega_h^{k+1} + \omega_h^k}{2}. \tag{3.19}$$

This corresponds to a time-stepping scheme where all variables are computed at the new time level from the current 'known' time level.

The (3.18) discrete formulation is 'heavy': it yields a coupled, non-linear and implicit system. An individual equation in the system can contain both velocity and vorticity as unknowns, also as products. Applicable iterative solvers will bring a high computational burden with them. This alone would often make common schemes favorable in practical applications, despite their possible shortcomings.

Staggered time-stepping

Staggered time-stepping comes in as a solution to above problems: a quasi-linear formulation can be obtained by applying the midpoint rule to the momentum equation at $\Delta t/2$ later than the vorticity transport equation. This way (3.1a) and (3.1b) are obtained from (3.15). The time instants at which the momentum equation is discretized are also used for conservation of mass and fixation of the pressure level, yielding (3.1c) and (3.1d). Again for velocity in (3.1c) only the newest time-level remains: when applying the divergence operator to the average of the current and new time-levels, the current is known and must already be divergence-free.

The lower diagram in Figure 3.3 gives an overview of the staggered time-stepping in the MEEVC scheme. Each arrow indicates a time-step for a variable. The order of solving the equations is as follows. First vorticity is updated with (3.1a), which contains velocity only at known time-level. Then the updated vorticity ω_h^{k+1} is used to compute velocity $\vec{u}_h^{k+\frac{3}{2}}$, pressure $\bar{p}_h^{k+1}$ and r_h^{k+1} through solving the system formed by (3.1b), (3.1c) and (3.1d). Note that both the vorticity and velocity-pressure systems are linearized by solving them in this way.

In (3.1) the averaged values $\tilde{\vec{u}}$, $\tilde{p}$ and $\tilde{\omega}$, see (3.19), are no longer used. They are either replaced by explicit averages, or considered at a single time.

Such as for pressure, which has no time-derivative in the equations so reference to a known time-level is not needed. And for vorticity in the linear momentum equation (3.1b), which is now a known at intermediate time there. In the vorticity transport equation (3.1a), a similar situation is created for velocity. That is also a known at intermediate time there.

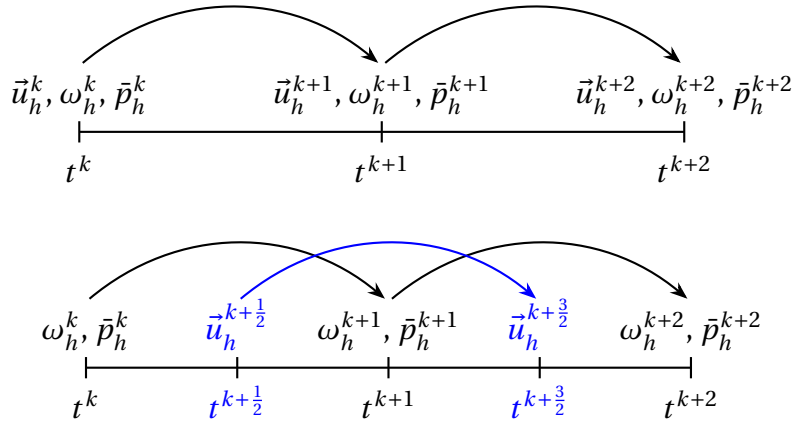

Figure 3.3: Straightforward time-stepping with all variables at the same time instant (above) versus staggered time-stepping (below), r_h excluded for clarity; reproduced from [25, Fig. 1].

To start the staggered time-stepping with (3.1), there are initial $\vec{u}_h^{\frac{1}{2}}$ and ω_h^0 needed. There is no need for pressure at a known time-level. Hence one time-step of $\Delta t/2$ with the non-linear system (3.18) is usually needed to compute $\vec{u}_h^{\frac{1}{2}}$ from the initial $\vec{u}_h^0$. For the research work considered here, $\vec{u}_h^{\frac{1}{2}}$ is estimated as the average of $\vec{u}_h^0$ and $\vec{u}_h^1$ following from the exact solution. It must be remarked though, that these discrete velocity fields are not directly interpolated from the exact solution for the following reason. Although the exact solution is divergence-free, the interpolated result would in general not be due to the approximating nature of the interpolation process. While the MEEVC method is built on assuming incompressible flow for the initial conditions, as described above, that is undesirable. A solution is to make use of the fact that for any incompressible, irrotational 2D flow there exists a stream function satisfying Laplace's equation. This involves using the initial conditions on interpolated vorticity to compute a corresponding discrete stream function, from which in turn a discrete velocity field can be computed that

automatically satisfies the incompressibility requirement.

Benefits of the MEEVC temporal discretization

Finally, this is a good place to argue why the midpoint rule and not some other method is used. Therefore its most relevant properties will be considered below, of which four are appraised desirable and one potentially undesirable. For reference, it is relevant to look back to the MEEVC formulation (3.1) and also compare it against the nonlinear formulation (3.18) or even the formulation without time discretization (3.15).

Two useful, even essential, properties are intrinsic to the midpoint rule. One is that, as a one-stage Gauss method, it conserves linear and quadratic invariants [14, p. 99 and 101]. This is just what is needed for the MEEVC properties; that is for retainment of the 2D invariants in Table 2.1. Mass and vorticity are first order (linear) invariants, kinetic energy and enstrophy second order (quadratic). Given the adequate spatial discretization and inviscid conditions, all these invariants are then conserved over time-steps because these are made with the midpoint rule. Another property of the midpoint rule is that it is symmetric [14, p. 3 and 42]. In case of inviscid flow, this symmetry allows time-reversibility of the MEEVC method as demonstrated in [25, Section 4.4]. A numerical one-step method Φ is time-reversible if $\Phi_{\Delta t} \circ \Phi_{-\Delta t} = id$ [14, Definition 1.4, p. 144]. Reverse time-steps should (eventually) make the flow return to its initial conditions.

Two other advantages are that the midpoint rule allows to decouple and linearize the system of equations. This is done by formulating the staggered time-stepping scheme (3.1), also see Figure 3.3. Rather than having a single system as in (3.18), the system is split into a vorticity part (3.1a) and a pressure-velocity (momentum) part with (3.1b), (3.1c) and (3.1d). The degrees of freedom thereby spread over two smaller systems, which are solved consecutively. It is generally faster to solve two smaller systems rather than one big combined system. Furthermore, the equations in (3.1) are linearized, because in all products of vorticity and velocity (derivatives) only one variable is unknown. Efficient numeric solvers exist for such problems. By the way: these do not rely on computing the inverse (for 'explicit' solving), as this is slow for a large linear system. Usually some form of Gaussian elimination is used. Or iterative methods, which are less demanding for problems with a large amount of unknowns.

A possible downside of the midpoint rule is however that it is limited to second order accuracy, while the spatial discretization is not. One can implement a higher-order method, but this will be a complicated endeavor as the midpoint rule is an essential element of the formulation. Some methods even involve multiple steps to make a single time-step. For now it is not worthwhile to add complexity and computational burden, while it does not add value in demonstrating the key conservation properties of the method. A practical approach is to just make the time step small enough, for example such that its associated error is comparable to that of the spatial discretization.

3.2 Algebraic proof of discrete conservation

The discrete conservation properties of the MEEVC formulation are proven algebraically in the following subsections. The approaches taken in these proofs directly follow from the MEEVC paper [25] and can also be found in [11]. Proofs arising from numerical testing are not considered here.

Aside from conservation of mass (Section 3.2.1), the proofs of conservation of kinetic energy (3.2.2), of vorticity (Section 3.2.3) and of enstrophy (Section 3.2.4) share a common approach. This is to take an equation of the discrete MEEVC formulation (3.1) and show that it is equivalent to the conservation of one of the invariants by choosing a particular test function. Thereby it may also be needed to assume inviscid flow conditions. One may however argue that it is not fair to choose a particular test function to demonstrate conservation, but the formulation is valid for *any* of the possible test functions including the particular one.

3.2.1 Conservation of mass

Mass is exactly conserved because the discrete velocity field is ensured to be point-wise divergence-free ($\nabla \cdot \vec{u}_h = 0$) by discretizing velocity in a $H(\mathrm{div})$-conforming finite element space. For more background on the requirement of divergence-free solutions and conservation of mass, see Section 2.2.1. Discretizing the velocity field as aforementioned makes it fit in the DeRham subcomplex (3.13). This means that taking the divergence of velocity maps it

into the pressure space. In other words with [25, (11)]:

$$\left\{\nabla \cdot \vec{u}_h | \vec{u}_h \in U_h\right\} \subseteq Q_h, \tag{3.20}$$

where U_h is the discrete velocity space and Q_h the discrete pressure space. Remember these spaces were specified in (3.14). All that insures that the discrete conservation of mass statement (3.1c) of the MEEVC-formulation is integrable. Furthermore the setup discussed here effectively turns this weak conservation of mass statement into a strong one: the solution is divergence-free in any point of the domain. This is independent of the solution's accuracy. In the original MEEVC paper [25], the approach discussed here is backed by literature references: [6] and [10] particularly suggest such a setup. Detailed proofs seem to be missing in these papers though.

3.2.2 Conservation of energy

Discrete kinetic energy integrated over the domain at time $t^{k+\frac{1}{2}}$ is defined to be half the $L^2(\Omega)$-norm of velocity, which upon expansion becomes

$$\mathcal{K}_h^{k+\frac{1}{2}} := \frac{1}{2}\left\langle \vec{u}_h^{k+\frac{1}{2}}, \vec{u}_h^{k+\frac{1}{2}} \right\rangle_\Omega. \tag{3.21}$$

Also, see Section 2.2.2 on energy conservation in the continuous setting.

Now take the MEEVC formulation's discrete balance of linear momentum (3.1b) in the inviscid limit ($\nu = 0$) and choose to substitute $\vec{v}_h = \frac{1}{2}\vec{u}_h^{k+\frac{3}{2}} + \frac{1}{2}\vec{u}_h^{k+\frac{1}{2}}$ for the test function. This yields

$$\begin{aligned}\frac{1}{2}\left\langle \frac{\vec{u}_h^{k+\frac{3}{2}} - \vec{u}_h^{k+\frac{1}{2}}}{\Delta t}, \vec{u}_h^{k+\frac{3}{2}} + \vec{u}_h^{k+\frac{1}{2}} \right\rangle_\Omega + \frac{1}{2}\left\langle \omega_h^{k+1} \times \frac{\vec{u}_h^{k+\frac{3}{2}} + \vec{u}_h^{k+\frac{1}{2}}}{2}, \vec{u}_h^{k+\frac{3}{2}} + \vec{u}_h^{k+\frac{1}{2}} \right\rangle_\Omega \\ -\frac{1}{2}\left\langle \bar{p}_h^{k+1}, \nabla \cdot \left(\vec{u}_h^{k+\frac{3}{2}} + \vec{u}_h^{k+\frac{1}{2}}\right)\right\rangle_\Omega = 0,\end{aligned} \tag{3.22}$$

where it is immediately clear that the third term is zero because the discrete solutions are divergence-free as just discussed in Section 3.2.1. Furthermore, the second term is also zero because the cross and dot products have the property that $(\vec{a} \times \vec{b}) \cdot \vec{b} = 0$ for any two vectors $\vec{a}$ and $\vec{b}$. Then it remains to recognize that the first term can be written as

$$\frac{1}{\Delta t}\left(\mathcal{K}_h^{k+\frac{3}{2}} - \mathcal{K}_h^{k+\frac{1}{2}}\right) \tag{3.23}$$

by expanding the product and comparing against (3.21). This means that (3.22) effectively reduces to $\mathcal{K}_h^{k+\frac{3}{2}} = \mathcal{K}_h^{k+\frac{1}{2}}$ meaning that kinetic energy is conserved over time-steps.

3.2.3 Conservation of vorticity

Discrete integrated vorticity, or total vorticity, at time t^k is simply given by

$$\mathcal{W}_h^k = \left\langle \omega_h^k, 1 \right\rangle_\Omega . \tag{3.24}$$

To describe the evolution of total vorticity in the discrete system, consider the vorticity transport equation (3.1a) and choose $\mathcal{C}_h = 1$ as test function:

$$\begin{aligned} \left\langle \frac{\omega_h^{k+1} - \omega_h^k}{\Delta t}, 1 \right\rangle_\Omega - \frac{1}{2} \left\langle \frac{\omega_h^{k+1} + \omega_h^k}{2}, \nabla \cdot \vec{u}_h^{k+\frac{1}{2}} \right\rangle_\Omega + \frac{1}{2} \left\langle \nabla \cdot \left(\vec{u}_h^{k+\frac{1}{2}} \frac{\omega_h^{k+1} + \omega_h^k}{2} \right), 1 \right\rangle_\Omega \\ = -\nu \left\langle \nabla \times \frac{\omega_h^{k+1} + \omega_h^k}{2}, \nabla \times 1 \right\rangle_\Omega . \end{aligned} \tag{3.25}$$

Here it is simple to see that the second term is zero because the discrete velocity is exactly divergence-free. Furthermore the last term drops out because the derivative of a constant is zero. Finally the third term is also zero, as can be demonstrated by rewriting it as a common integral and then applying the divergence theorem[3] for 2D:

$$\begin{aligned} \frac{1}{2} \left\langle \nabla \cdot \left(\vec{u}_h^{k+\frac{1}{2}} \frac{\omega_h^{k+1} + \omega_h^k}{2} \right), 1 \right\rangle_\Omega &= \int_\Omega \nabla \cdot \left(\vec{u}_h^{k+\frac{1}{2}} \frac{\omega_h^{k+1} + \omega_h^k}{4} \right) \mathrm{d}\Omega \\ &= \int_{\partial\Omega} \frac{\omega_h^{k+1} + \omega_h^k}{4} \vec{u}_h^{k+\frac{1}{2}} \cdot \vec{n} \, \mathrm{d}\Gamma = 0. \end{aligned} \tag{3.26}$$

Here the boundary integral is zero due to periodic boundary conditions on both $\vec{u}_h$ and ω_h. Now all terms of (3.25), except the first, are shown to be zero. Then the remaining equation (after multiplication with Δt) can be written in terms of (3.24) as $\mathcal{W}_h^{k+1} = \mathcal{W}_h^k$, meaning that total vorticity is conserved.

[3] Or also an alternative form of Green's theorem [29, pp. 1096].

3.2.4 Conservation of enstrophy

Just as before with kinetic energy and vorticity, the first step is to consider the definition of discrete enstrophy at time t^k:

$$\mathscr{E}_h^k = \frac{1}{2}\left\langle \omega_h^k, \omega_h^k \right\rangle_\Omega . \tag{3.27}$$

Then consider the discrete vorticity transport equation (3.1a) in the inviscid limit ($\nu = 0$) and substitute $\mathscr{E}_h = \frac{1}{2}\omega_h^{k+1} + \frac{1}{2}\omega_h^k$ for the test function[4] to obtain

$$\begin{aligned}\frac{1}{2}\left\langle \frac{\omega_h^{k+1} - \omega_h^k}{\Delta t}, \omega_h^{k+1} + \omega_h^k \right\rangle_\Omega - \frac{1}{4}\left\langle \frac{\omega_h^{k+1} + \omega_h^k}{2}, \nabla \cdot \left(\vec{u}_h^{k+\frac{1}{2}}(\omega_h^{k+1} + \omega_h^k)\right) \right\rangle_\Omega \\ + \frac{1}{4}\left\langle \nabla \cdot \left(\vec{u}_h^{k+\frac{1}{2}} \frac{\omega_h^{k+1} + \omega_h^k}{2}\right), \omega_h^{k+1} + \omega_h^k \right\rangle_\Omega = 0.\end{aligned} \tag{3.28}$$

Note that the last two terms on the left-hand side are in fact the same but with opposite signs, so they cancel. Then multiply the remaining equation with Δt and note that, by product expansion and comparison against (3.27), it can be written in terms of discrete enstrophy: $\mathscr{E}_h^{k+1} = \mathscr{E}_h^k$. Hence (3.28) reduces to a statement of discrete enstrophy conservation.

[4] Please do not be confused that the test function has the same symbol as enstrophy.

Chapter 4

Numeric tests with MEEVC method

In order to assess the MEEVC scheme's properties, the author of this thesis used it to perform simulations of the 2D Taylor-Green problem presented in Section 2.3. The implementation of the scheme was done by himself. Convergence as well as conservation properties under temporal and spatial refinement were verified. The following sections will present results demonstrating these qualities. Like in the test program the results are split into two groups: Section 4.1 deals with the group of tests to investigate convergence at a final time, Section 4.2 considers the group illustrating how the solution develops throughout a longer time span. But first the experimental set-up is discussed here, also using text from the authors' own project plan [34].

The simulations were performed on a reasonable laptop (with 16 GB of random-access memory) running the FEniCS finite element package. The most demanding simulations needed a few hours of runtime. FEniCS does not have a graphic interface, instead algorithms are programed into python scripts calling FEniCS routines. Thereby it must be mentioned that there was no code available to the author, nor experience with Python and FEniCS, so writing started from zero. This was a laborious process as there are many, somewhat poorly documented, versions of the FEniCS software. This made it difficult to find the correct vocabulary on multiple occasions. A helpful reference for information was the FEniCS book [21] though, containing a lot of information on (an older version of) the software with examples of possible applications. The project's website[1] contains further useful documentation and references. This includes its internet forum with questions & answers.

[1] `https://fenicsproject.org/`, checked 12 October 2021.

Despite the difficulties just mentioned, the FEniCS software environment was used due to recommendations by the authors of [11, 25]. They used it to perform the numerical simulations for those works. Relevant advantages of the software are that discretizations can be formulated in a way that is relatively close to the mathematical formulation and that the function spaces of interest are pre-programmed. Using software without these spaces in their libraries instead would have meant a lot of extra work and difficulties.

4.1 Tests for convergence at final time

The group of tests for convergence at final time show convergence rates with respect to temporal and spatial refinement as will be discussed below. They confirm the results published in the MEEVC paper [25]. Each simulation started at time $t = 0$ and stopped at a time-step near[2] 'final time' $t = 1$, with constant kinematic viscosity set to $\nu = 0.01$. The exact solution of the 2D Taylor-Green problem (2.107) was used for computing the velocity field L^2-error of the solution near final time. And indeed, the results in Figure 4.2 are comparable[3] to those published [25, Figure 3]. One may note that at the vertical axes u_h and u miss the vector arrow $\vec{u}$, but this is purely due to the software (a Python package) with which the plot was generated.

The Navier-Stokes equations with Taylor-Green initial conditions (2.104) are discretized on a $[0, 2] \times [0, 2]$ domain with a FEniCS 'crossed' mesh. Remember that more details on the Taylor-Green flow can be found in Section 2.3. The crossed mesh is square and is divided-up into $N_c \times N_c$ smaller squares of equal size, see Figure 4.1. Each of these squares has a cross inside, splitting it up into four triangles. This makes the total of triangular cells in the mesh $4N_c^2$. The crossed mesh is chosen because it was also used to obtain some of the results in the MEEVC paper [25] according to one of the

[2] Because of the staggered time-stepping, the time instants at which the velocity field is computed are shifted compared to the pressure field. Therefore it was not possible to have both ending at precisely the final time. The difference is at most half a time-step, so it becomes small when the time-step size does.

[3] Because h and p are used in the simulation results of the MEEVC paper [25], the same is done here for sake of easy comparability. Please do not confuse h with helical density or the 'h' in $\vec{u}_h$. Also note that for polynomial degree, both N and p are used as done in the MEEVC paper. The double-usage of p for both pressure and polynomial degree is potentially confusing though.

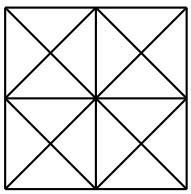

Figure 4.1: The crossed mesh for $N_c = 2$.

authors. This allows for a fair comparison against corresponding results in this section.

As a characteristic size for each cell in the mesh

$$h = 2\pi/N_c \tag{4.1}$$

is used with N_c as just described. It should be the same definition for h as in the MEEVC paper's results, which allows for easier comparison. Using $2/N_c$ seems to make more sense for a $[0, 2] \times [0, 2]$ domain though, but h is just a measure which can be chosen differently for easy comparability.

Figure 4.2a shows the velocity field L^2-error at final time of five simulations computed with time-steps $\Delta t = 1/10, 1/20, 1/40, 1/80$ or $1/160$. In

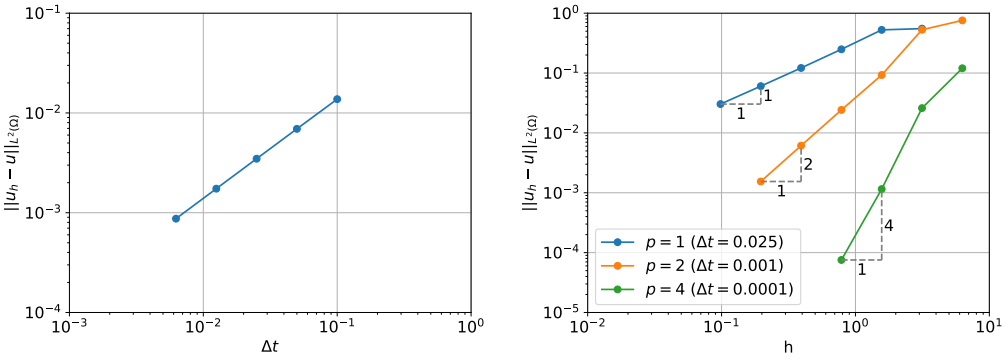

(a) Convergence with time-step Δt. (b) Convergence with mesh cell-size h.

Figure 4.2: L^2-error of the velocity field near simulation end $t = 1.0$.

each of these simulations the spatial discretization is set to a polynomial degree $p = 4$ for the finite element basis functions and the number of elements corresponding to $h \approx 0.39$. This is a relatively high level of spatial refinement for the time-step sizes just mentioned, such that the error in each result is dominated by the error due to a lack of temporal refinement. Each blue dot

in the log-log plot corresponds to a simulation result. The interpolation lines connecting them are indicative of first order convergence, that is their slope is such that making Δt ten times smaller means that the L^2-error $\|\vec{u}_h - \vec{u}\|_{L^2(\Omega)}$ (with $\vec{u}$ the exact solution) also becomes ten times smaller.

Where Figure 4.2a was created to show the effect of varying the time-step size, Figure 4.2b was created to show the effect of changing the spatial discretization. Thereby the time-step Δt was set such that it was not the bottleneck for accuracy in the set of simulations performed with a certain polynomial degree p in the spatial discretization. Of course it was also possible to use a single time-step size, set to the smallest value used here, but that would have increased simulation times and data storage unnecessarily. Looking at the plotted results, note that the approximate log-log line slopes are indicated. They correspond to optimal p^{th}-order convergence. Only for larger values of h the slopes deviate a bit from this, but some irregular behavior may be expected there as the corresponding numbers of elements are very small. In that case the initial conditions may already be poorly sampled to start with.

Besides the velocity field L^2-error of multiple simulations (Figure 4.2), it is interesting to compare two of these solutions with different levels of refinement in more detail. Therefore Figure 4.3 shows discrete velocity vectors and the pressure field in a single frame for each of these solutions. Thereby

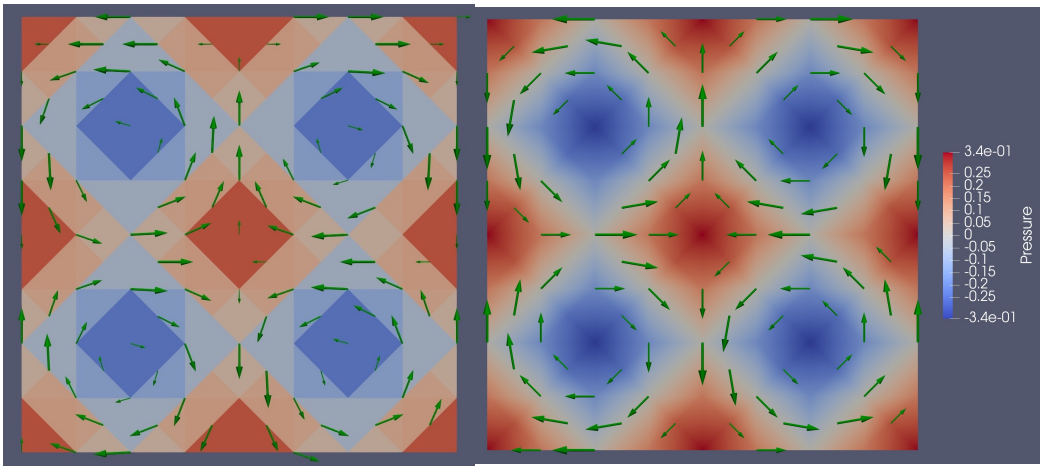

(a) $p = 1$, $\Delta t = 0.025$ and $h \approx 0.79$. (b) $p = 4$, $\Delta t = 0.0001$ and $h \approx 0.79$.

Figure 4.3: Velocity vectors and pressure field near simulation end $t = 1.0$.

the solution displayed in Figure 4.3a has a lower level of refinement, with a

first order polynomial degree for the basis functions of the 256 triangular elements ($h \approx 0.79$) making up the spatial discretization. On the other hand, the solution displayed in Figure 4.3b is built on the same number of elements but then with fourth order polynomial basis functions. It thereby has a much higher level of refinement, it is the most accurate solution included in Figure 4.2b. Still both solutions in Figure 4.3 give a good picture of what the exact solution (2.107) looks like. Even the coarser solution clearly displays most of its features. A yet more coarse solution with just 64 elements ($h \approx 1.57$) and $p = 1$ still shows some features, like the rotations, as can be seen from Figure 4.4. All this adds evidence that the MEEVC method is an effective tool for discretizing and solving Navier-Stokes flow problems.

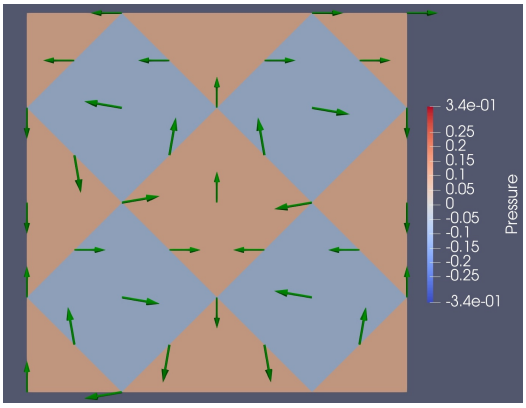

Figure 4.4: Velocity vectors and pressure field near simulation end $t = 1.0$, with a *very* coarse resolution: $p = 1$, $\Delta t = 0.025$ and $h \approx 1.57$.

4.2 Tests for development in time

Whereas Section 4.1 investigated (convergence of) results near the final time $t = 1$ of multiple simulations, this section will look at how a few simulations develop over a longer simulated time up to $t = 10$. The aim of this is to find out more about how simulations of the Taylor-Green flow problem with the MEEVC method develop over time, particularly with respect to its conservation properties and also compared to the Taylor-Green exact solution (2.107).

For this purpose, the four flow simulations with parameters as given in the legend of Figure 4.5 were performed for both the inviscid case with $\nu = 0$ and a viscous case with $\nu = 0.01$ (shown in the figure). These simulations

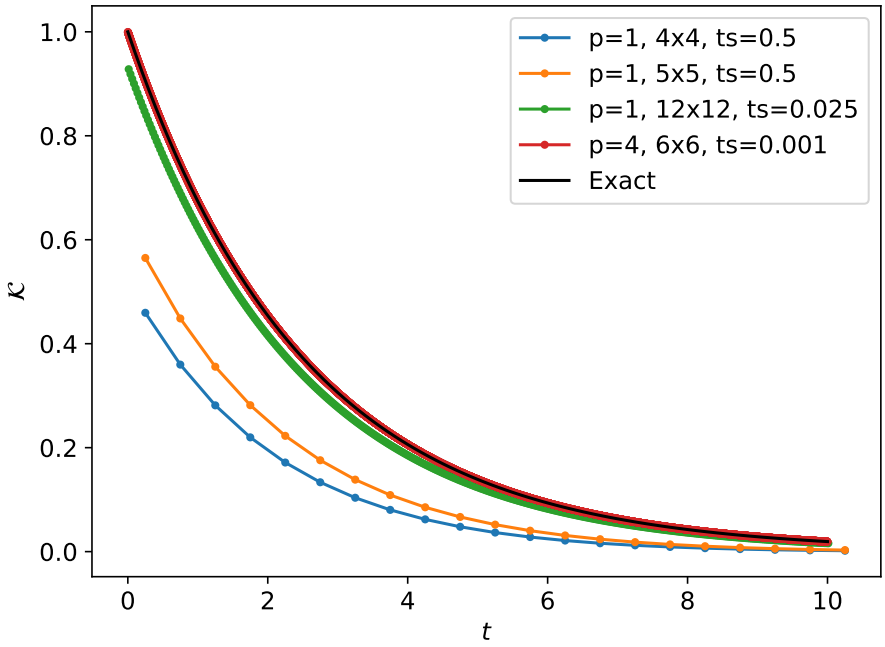

Figure 4.5: Development of kinetic energy over time for $\nu = 0.01$.

have N_c between $N_c = 4$ and $N_c = 12$, which by (4.1) respectively corresponds to $h = 1.57$ and $h = 0.52$. One may note that the first two simulations are very coarse in terms of both the spatial as well as the temporal refinement. Still these are stable to capture the kinetic energy development and make it evolve in a similar curved way through time. It is just that its values are about half of the exact solution. As will also become clear later, this is largely because the initial conditions are poorly captured by the spatial discretization. Note that, for the viscous case considered here, the kinetic energy largely decays over the time-range. Hence simulation after $t = 10$ could be less interesting.

For Figure 4.5 a linear scaling is chosen because this gives an intuitive picture of how the exact solution develops and is captured by the simulations, but the same results are plotted again in Figure 4.6 with a logarithmic scaling on the vertical axis in order to check for exponential behavior. Such can be seen for the exact solution, which has a straight line due to its exponential nature. The simulations should ideally have the same slope in order to match its decay rate. This is however not completely the case as especially the two least

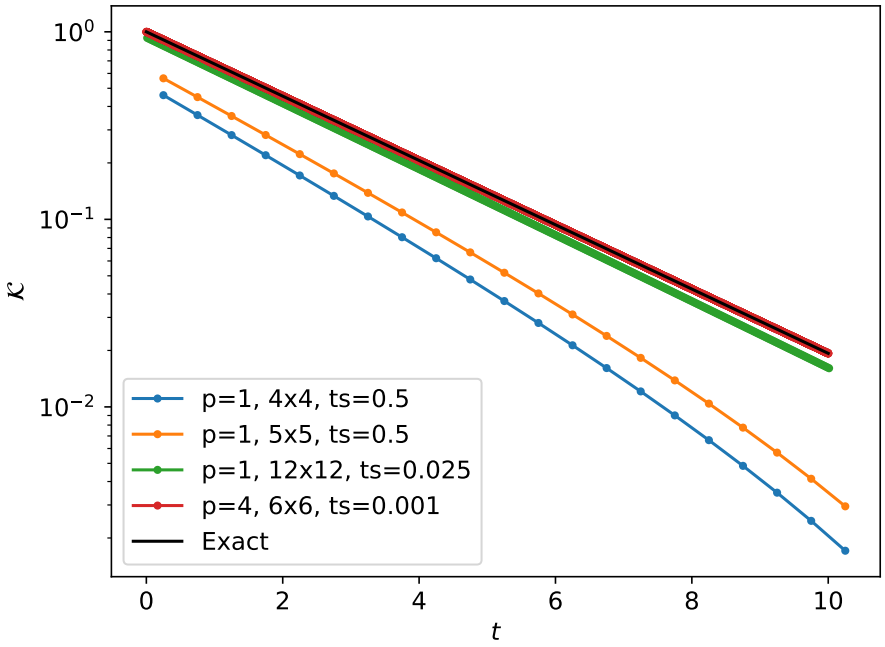

Figure 4.6: Logarithmic kinetic energy through time for $\nu = 0.01$.

refined have a somewhat steeper average slope and a slight downward bend. Therefore their decay rate increases with time and is a bit higher throughout than the exact solution. It should however be remembered that these simulations have a very coarse discretization, so some imperfection is not strange.

Before continuing with inviscid kinetic energy results, it is good to consider how the above numeric simulations perform over time from yet another perspective: Figure 4.7 shows the absolute kinetic energy error that is scaled with the instantaneous exact solution $\mathcal{K}_e(t)$. The reason for this scaling is that the solution decays strongly over time, which for the simulations considered here leads to a decreasing trend in the unscaled error that may be misleading. The scaled graph instead clearly shows that the relative error of each simulation increases over time. Note that the two lowest resolutions essentially become useless as their error nears the exact solution's magnitude. The finer resolutions perform a lot better, especially the $p = 4$ simulation. It should however be noted that its slope is a bit steeper than that of the other simulations.

Figure 4.8 shows that kinetic energy conservation is achieved when sim-

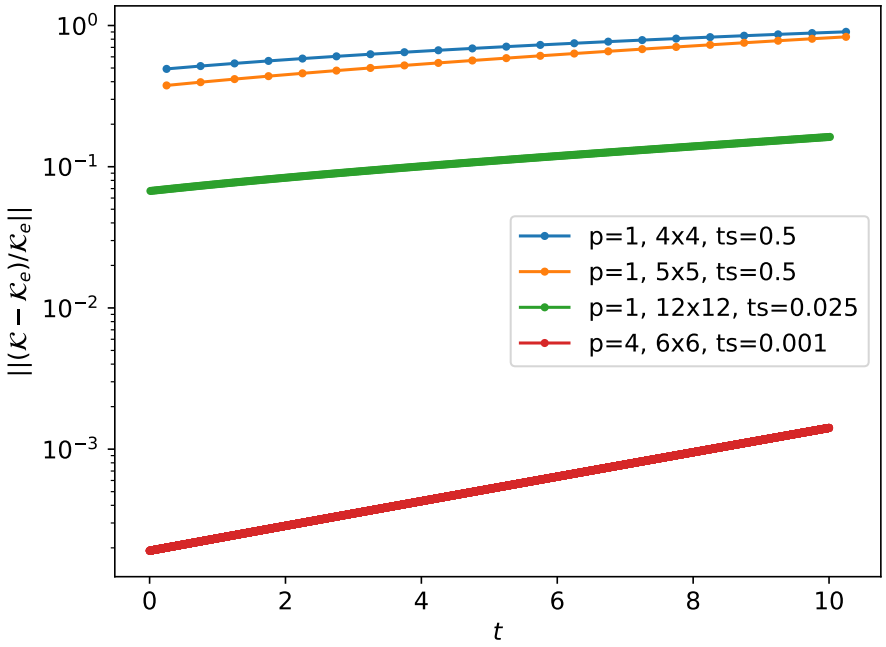

Figure 4.7: Development of the scaled kinetic energy error for $\nu = 0.01$.

ulating inviscid (Taylor-Green) flow. It displays the difference of instantaneous kinetic energy with that after the first time-step. It looks like this remains exactly zero for the $p = 1$ simulations, but Figure 4.9 shows that these also drift (although much slower). One may argue from Figure 4.8 that the results with $p = 4$ show a clearly decreasing trend, but considering that the vertical axis is scaled by 10^{-11} it would take up to nearly order 10^{11} in time until the initial kinetic energy (of order one) is destroyed. That is obviously way past the timescale of 10^1 simulated here. So kinetic energy is conserved well by the simulations but with a much higher refinement this may no longer be the case. A longer simulated time can put a further strain on conservation. Figures 4.8 and 4.9 do not show the big differences in accuracy though: the most coarse simulation has kinetic energy constant at about 0.57 from the start on, while the most refined is constant near 1.0 (the value of the exact solution). This error can completely be attributed to poor capturing of the initial conditions by the spatial discretization. It was already mentioned that this also plays a large role in Figure 4.5, where viscous flow is simulated and the error of each simulation is largely determined from the start on.

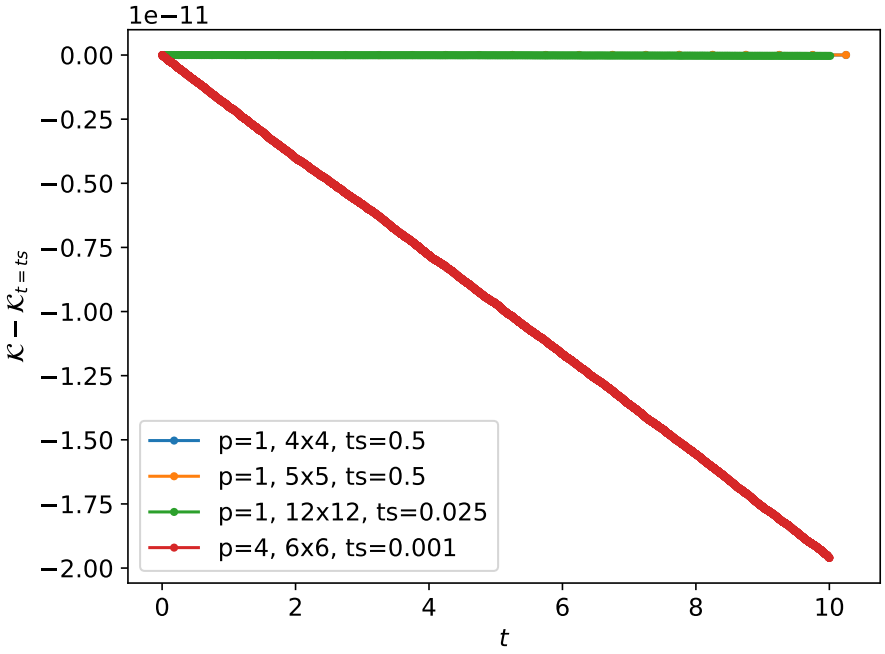

Figure 4.8: Kinetic energy drift through time for $\nu = 0$.

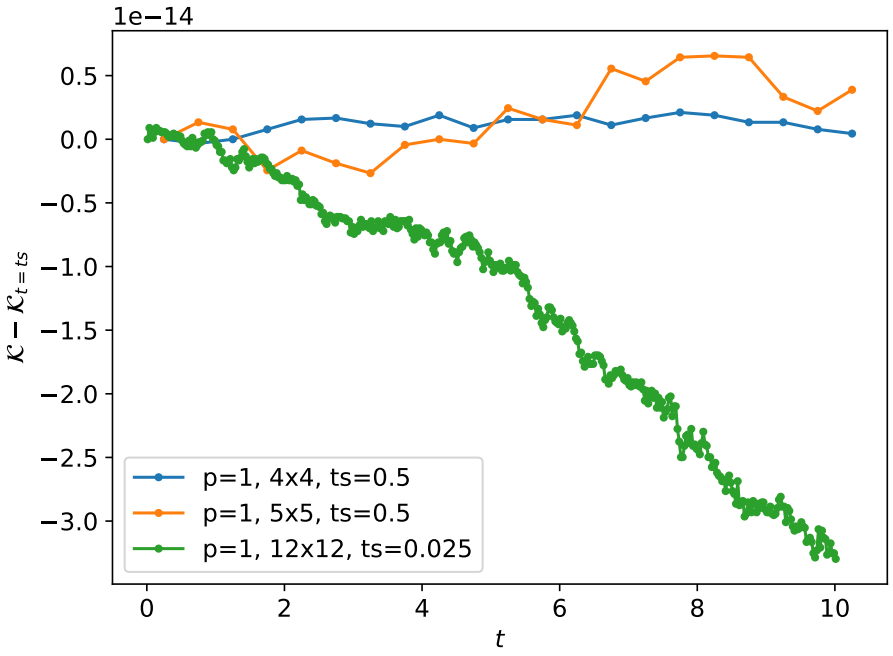

Figure 4.9: Kinetic energy drift through time for $\nu = 0$ without $p = 4$ results.

Figure 4.10 shows that local (and thereby global) conservation of mass is achieved, as the infinity norm of the divergence of the velocity field[4] is very small. For the most coarse solution, that is $p = 1$, $N_c = 4$, $\Delta t = 0.5$, it is

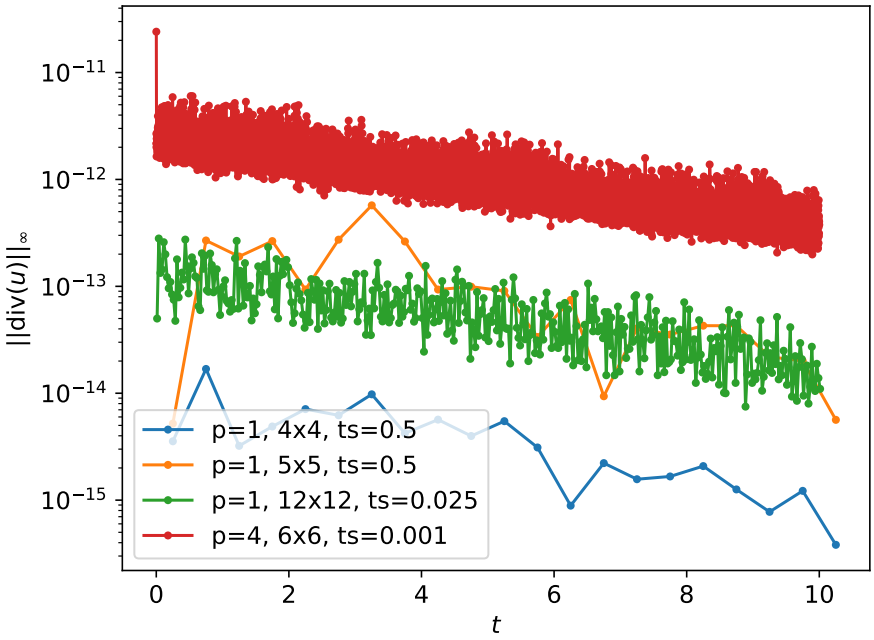

Figure 4.10: Infinity norm of velocity field divergence over time for $\nu = 0.01$.

near zero up to machine precision. Values become larger when the spatial refinement is increased, but here it must be recognized that the time-step also changes between certain simulations and that this may have some effects as well. Furthermore note that the values of $\|\nabla \cdot \vec{u}\|_\infty$ become smaller with increasing time. This is expected to be related to the diminishing of the velocity field. When simulating without viscosity, that is $\nu = 0$, the starting values near $t = 0$ are about the same as in Figure 4.10. Then they fluctuate in a constant bandwidth when time is increased: there is no decreasing (nor increasing) trend. As there are otherwise no differences of interest, this plot is omitted here.

[4]This infinity norm is the local maximum of the absolute divergence. It is approximated here by taking the following steps. First compute the divergence of the finite element velocity field and project that to the appropriate function space. Then interpolate the result to a first order polynomial function space on a refined mesh (with 100 times as many elements). Finally compute the maximum of the absolute vertex values.

The simulation results also include the enstrophy development and the graphs showing this look similar to the kinetic energy graphs in most aspects. Three of these graphs will be discussed in the following though, the first two are for $\nu = 0.01$ and the third is for $\nu = 0$. The first plot is shown in Figure 4.11 and it looks very similar to Figure 4.6. A visible difference however is that the

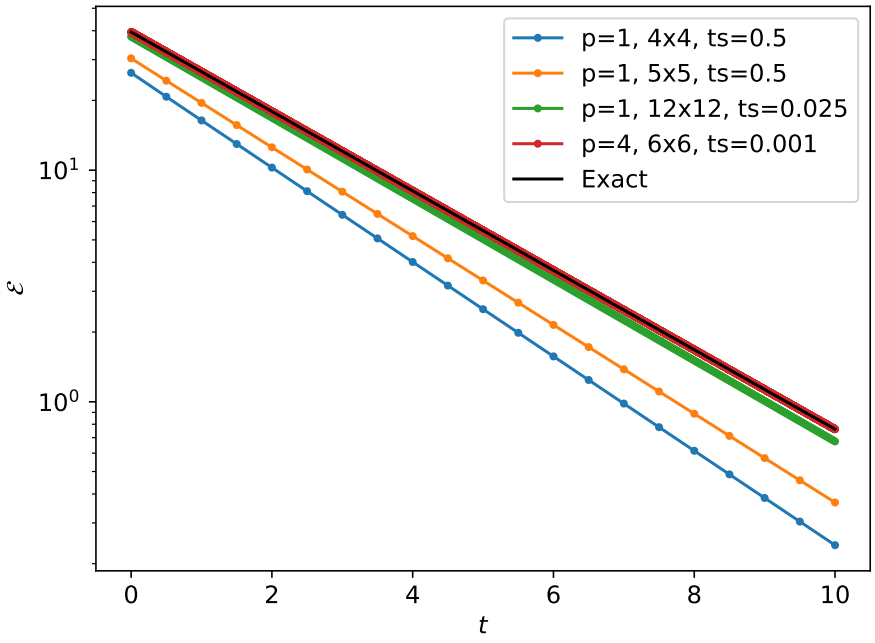

Figure 4.11: Logarithmic enstrophy through time for $\nu = 0.01$.

two least-refined simulations do not have a clear downward bend like those in the kinetic energy plot but look as straight lines instead. This is actually more desired as it corresponds to exponential decay of enstrophy, which is a characteristic of the exact solution. Still their slope is slightly steeper than that of the exact solution, so their decay rate is again a bit too high. Another interesting plot is that of enstrophy error scaled against the exact solution $\mathcal{E}_e$ in Figure 4.12, which is very similar to its kinetic energy sibling in Figure 4.7. The most eye-catching difference is that the simulation results with $p = 4$ show slower, nearly constant values. The latter means that their enstrophy error decays as quickly as the enstrophy exact solution. Finally Figure 4.13 contains a plot looking quite similar to Figure 4.8. It shows enstrophy is conserved for the simulations under inviscid conditions, as there is some growth but the values at the vertical axis are really small (order 10^{11}).

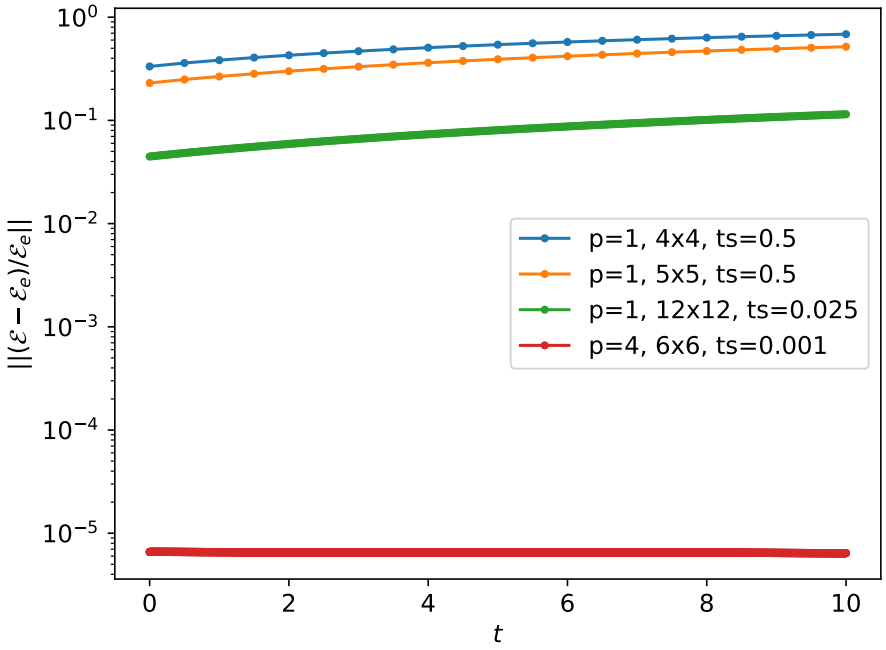

Figure 4.12: Development of the scaled enstrophy error for $\nu = 0.01$.

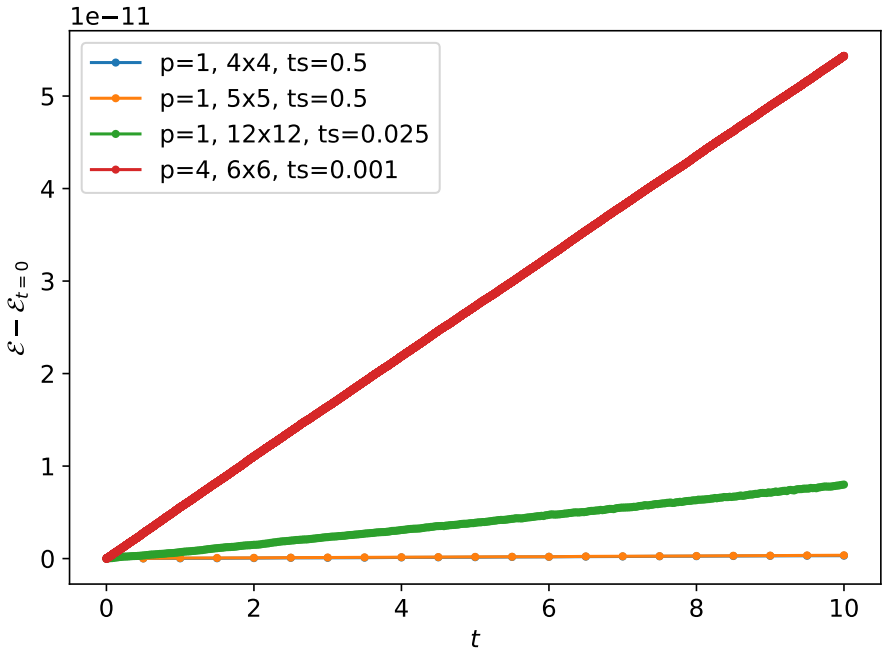

Figure 4.13: Enstrophy drift through time for $\nu = 0$.

Conservation of total vorticity is the last property to confirm from the simulation results. Section 2.2.3 shows with (2.87) that for any 2D flow with periodic boundary conditions, as considered here, the integral of vorticity over the complete domain must be constant. Figures 4.14 and 4.15 confirm that this is achieved in each simulation independent of whether the conditions are viscous or inviscid, as values drift in time but stay really close to the initial zero.

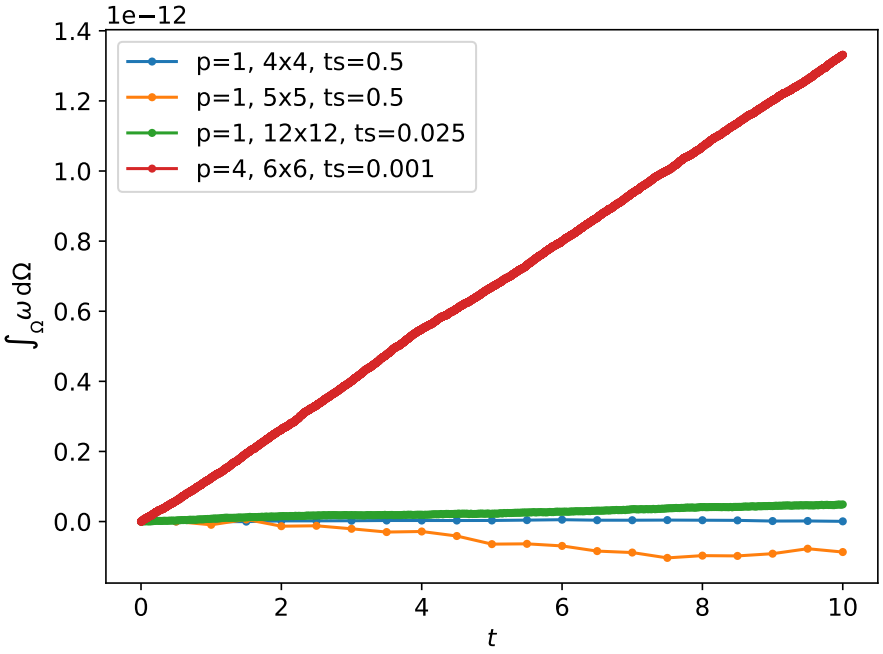

Figure 4.14: Vorticity integrated over entire domain for $\nu = 0$.

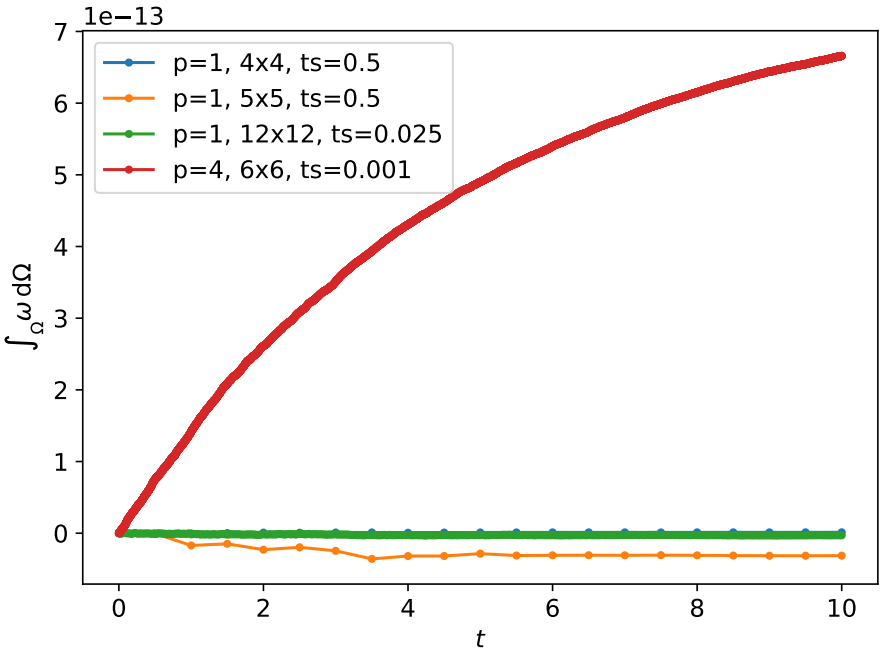

Figure 4.15: Vorticity integrated over entire domain for $\nu = 0.01$.

Chapter 5

The 3D MEHC discretization

The favorable properties of the 2D MEEVC method inspire to explore whether a promising 3D method can be constructed from similar ingredients. Several (conservation) properties of the MEEVC method have been demonstrated analytically in Chapter 3 and confirmed by test results in Chapter 4. Yet most real-life CFD problems are found in 3D, so finding a 3D CFD method that is more physics-compatible than common methods can be valuable. A new mass, energy and helicity conserving (MEHC) method is found in this chapter but is not without problems as will be reported.

Any 3D method will differ from the MEEVC method in both construction and properties. Creating a 3D 'equivalent' of the MEEVC method is impossible. The extra spatial components break the 2D assumptions from which the MEEVC formulation is derived. Even more, 3D flow is fundamentally different. There are for example other invariants as found from continuous formulations in Chapter 2. These can be reviewed from Table 2.1, with on the left side the quantities conserved in the 2D case and on the right those in 3D. It must be remarked that this list is not complete but that it contains the invariants which are identified as relevant in Section 1.2.

This chapter is structured as follows. The continuous formulation that is at the basis of the discrete MEHC formulation is presented in Section 5.1. The derivations of it are included in Section 5.2 on the MEHC method's construction, as they were made in this process. In Subsection 5.2.3 the method is summarized and Section 5.3 provides analytic proof of its discrete conservation properties. Several important aspects of the method's design and (in)effectiveness are reviewed in Section 5.4.

5.1 Continuous formulation

The discrete 2D MEEVC formulation (3.1) was derived from the continuous formulation (2.1). For the 3D MEHC formulation derived in this chapter it is not (2.2) but the following that is used:

$$\left.\begin{aligned}
&\frac{\partial \vec{u}}{\partial t} + \vec{\omega} \times \vec{u} + \nabla \bar{p} = -\nu \nabla \times \vec{\omega} \\
&\frac{\partial \vec{\omega}}{\partial t} + \nabla h - 2(\vec{\omega} \cdot \nabla)\vec{u} - \vec{u} \times (\nabla \times \vec{\omega}) = -\nu \nabla \times (\nabla \times \vec{\omega}) \\
&\frac{\partial h}{\partial t} - \nabla \cdot \left((\vec{u} \times \vec{\omega}) \times \vec{u}\right) + \nabla \cdot \left(\vec{\omega} \bar{p}\right) = -2\nu(\nabla \times \vec{\omega}) \cdot \vec{\omega} - \nu \nabla \cdot ((\nabla \times \vec{\omega}) \times \vec{u}) \\
&\nabla \cdot \vec{u} = 0
\end{aligned}\right\}. \tag{5.1}$$

This specific set of PDE's was formed in the discretization process that is described in Section 5.2 below. Herein the linear momentum equation and the divergence-free condition are unchanged from (2.2). The other two equations are derived from (2.2) as described in Section 5.2.2. One is the vorticity transport equation, which has been rewritten and now includes the gradient of helical density. For the helical density variable that thereby appears, an evolution equation is introduced. This equation can be found on the third line of (5.1).

5.2 Discrete MEHC formulation

5.2.1 Function spaces

Aiming at a physics-compatible MEHC method, function spaces conforming with the DeRham complex are chosen in the FE discretization of variables. This is in the spirit of the MEEVC method, where the DeRham subcomplex is shortly represented by (3.13) and the corresponding FE spaces in the MEEVC formulation (3.1) are as in the lower part of [2, p. 60, Table 5.1]. Each variable is thereby associated with a differential k-form such that it suits its physical interpretation. But as this is often non-unique, some room is left to choose the most appropriate place in the DeRham complex. This is then done such that particular derivatives in the formulation are supported, although there could be some interplay if the formulation itself can be adjusted appropriately.

Similarly, but then for the 3D situation, [2, p. 60, Table 5.2] shows for (a selection of) classical FE spaces how they correspond to FE differential k-forms. Focussing at the lower group in this table, which contains Nédélec elements of the first kind, the function spaces are represented as follows:

$$\begin{aligned} h_h &\in X_h = \mathrm{CG}_q \subset H^1(\Omega) \\ \vec{\omega}_h &\in W_h = \mathrm{NED}_N^{1,\mathrm{curl}} \subset H(\mathrm{curl}, \Omega) \\ \vec{u}_h &\in U_h = \mathrm{RT}_N \subset H(\mathrm{div}, \Omega) \\ \tilde{p}_h &\in Q_h = \mathrm{DG}_{N-1} \subset L^2(\Omega) \end{aligned} \tag{5.2}$$

Because $\mathrm{NED}^{1,\mathrm{div}}$ elements can be viewed as 3D extensions of RT elements, which were originally introduced by Raviart and Thomas for triangles [19, Sections 3.4.1 and 3.5], they are denoted as such here (to be consistent with FEniCS notation). The choice of including helical density as an independent variable in computations is considered within the discussions in Section 5.4.

The FE function spaces in (5.2) fit in a DeRham subcomplex as can be summarized by

$$0 \longrightarrow X_h \xrightarrow{\nabla} W_h \xrightarrow{\nabla\times} U_h \xrightarrow{\nabla\cdot} Q_h \longrightarrow 0. \tag{5.3}$$

This situation is similar to the 2D MEEVC situation of (3.13), except that there is a $H^1(\Omega)$ subspace X_h to the left of W_h.

This work will not dive further in the differential geometry background, but for the individual variables and their function spaces (5.2) the interpretation is as follows:

- the *helical density* variable is geometrically related to a point (0-form as discussed below) with orientation associated to rotation or spin;
- the *vorticity* vector-variable is interpreted as rotation around a line element (1-form);
- the *velocity* vector-variable is interpreted as a flux through a surface (2-form);
- the *pressure* variable is related to a volume (3-form) that is oriented by outward-pointing normals that can be related to the stresses.

All variables (and their spaces) are considered to be equipped with outer orientation, in case of further interest in a visualization see [31, p. 41, Table 3.1].

It must be mentioned that above interpretation of variables and their ordering in the DeRham subcomplex (5.3) is not necessarily the 'only' or 'best' way to do this, but it is a founded way by relating it to physical interpretation. One specific thing to add is that the choice to have velocity in $H(\mathrm{div}, \Omega)$ allows to have exactly divergence-free velocity fields like in the MEEVC method.

Because the helical density variable is a peculiarity of the formulation presented in this work, the following explains why it is interpreted as a 0-form. From a differential geometry perspective, it is in fact most obvious to consider helical density as the wedge product of velocity (a 2-form in this work) and vorticity (a 1-form). This would make it a 3-form. Here it then falls in the discrete Q_h space just like pressure. This is a problem as Q_h is an L^2-conforming space, which can be discontinuous in every derivative. Therefore this allocation is avoided for the formulation that is derived below and summarized in Section 5.2.3, for the following two reasons. One is that the gradient of helical density is introduced in the discrete vorticity transport equation when replacing the gradient of vorticity, which is not square-integrable as vorticity is assigned within $H(\mathrm{curl}, \Omega)$. The other reason is that ∇m_h enters the discrete helicity equation through integration by parts, with m_h the test function associated to the helical density variable. This is done in oder to avoid taking the generally not square-integrable divergence of certain other terms. Luckily there is a possibility to obtain helical density trial and test functions which' gradients are guaranteed to be square-integrable as follows. With the Hodge-$\star$ operator existing in differential geometry, the 3-form is recast into a 0-form. Then the helical density function space is in $H^1(\Omega)$, see (5.2) with preceding text, which is just what is needed here.

5.2.2 Derivation of variational formulations

Substituting trial solutions in the PDEs (2.2), multiplying with test functions, integrating and finally making the temporal discretization yields a discrete problem formulation. Many details on this process can be found in Section 3.1 on the MEEVC formulation and are not repeated here. The current subsection instead provides the specific derivations for the MEHC formulation. These rewrite the governing continuous equations followed by (partial) integration in order to guarantee that certain terms are square-integrable.

Velocity-pressure system

The discrete 3D velocity-pressure system below is nearly the same as that for 2D in (3.1b), (3.1c) and (3.1d). An important difference is that vorticity is a full vector now. Furthermore the time discretization is shifted by half a time-step here because the velocity field is updated before the vorticity field, which is an arbitrary choice though.

$$\boxed{\begin{aligned}\left\langle \frac{\vec{u}_h^{k+1}-\vec{u}_h^{k}}{\Delta t}, \vec{v}_h \right\rangle_\Omega + \left\langle \vec{\omega}_h^{k+\frac{1}{2}} \times \frac{\vec{u}_h^{k+1}+\vec{u}_h^{k}}{2}, \vec{v}_h \right\rangle_\Omega - \left\langle \bar{p}_h^{k+\frac{1}{2}}, \nabla\cdot\vec{v}_h \right\rangle_\Omega \\ = -\nu \left\langle \nabla\times\vec{\omega}_h^{k+\frac{1}{2}}, \vec{v}_h \right\rangle_\Omega \quad \forall \vec{v}_h \in \mathrm{RT}_N,\end{aligned}} \tag{5.4a}$$

$$\boxed{\left\langle \nabla\cdot\vec{u}_h^{k+1} + r_h^{k+\frac{1}{2}}, q_h \right\rangle_\Omega = 0 \quad \forall q_h \in \mathrm{DG_{N-1}},} \tag{5.4b}$$

$$\boxed{\left\langle \bar{p}_h^{k+\frac{1}{2}}, \tilde{r}_h \right\rangle_\Omega = 0 \quad \forall \tilde{r}_h \in \mathrm{R}_0.} \tag{5.4c}$$

Helicity equation

To start the derivation of a discrete evolution equation for helical density, it is good to proceed in similar fashion as in Section 2.2.5. Start from the definition of helical density $h = \vec{u}\cdot\vec{\omega}$ to express its derivative as

$$\frac{\partial h}{\partial t} = \frac{\partial \vec{u}}{\partial t}\cdot\vec{\omega} + \vec{u}\cdot\frac{\partial\vec{\omega}}{\partial t}. \tag{5.5}$$

Then express the terms on the right-hand side as follows by substituting for the time derivatives from the balance of linear momentum equation (2.8) and the vorticity transport equation (2.22) with $\rho = 1$ as in the 2D MEEVC method:

$$\frac{\partial\vec{u}}{\partial t}\cdot\vec{\omega} = -\big((\vec{u}\cdot\nabla)\vec{u}\big)\cdot\vec{\omega} - \nabla p\cdot\vec{\omega} + \nu(\nabla^2\vec{u})\cdot\vec{\omega}, \tag{5.6a}$$

$$\vec{u}\cdot\frac{\partial\vec{\omega}}{\partial t} = -\vec{u}\cdot\big((\vec{u}\cdot\nabla)\vec{\omega}\big) + \vec{u}\cdot\big((\vec{\omega}\cdot\nabla)\vec{u}\big) + \nu\vec{u}\cdot(\nabla^2\vec{\omega}). \tag{5.6b}$$

The next step is to rewrite the terms on the right-hand sides into a format that leads to a suitable discrete formulation later.

Start with (5.6a) by noting that its viscous term can be rewritten using [23, A1. Vector Identities, p. 363, (10)]:

$$\nabla^2\vec{u} = \nabla(\underbrace{\nabla\cdot\vec{u}}_{=0}) - \nabla\times(\nabla\times\vec{u}) = -\nabla\times\vec{\omega}. \tag{5.7}$$

Using this result and that the first two terms on the right hand side of (5.6a) can be written as the right-hand side of (2.94), then (5.6a) can be written as

$$\frac{\partial\vec{u}}{\partial t}\cdot\vec{\omega} = -\nabla\cdot\left(\vec{\omega}\bar{p}\right) - \nu(\nabla\times\vec{\omega})\cdot\vec{\omega}. \tag{5.8}$$

With (5.8) a suitable form of (5.6a) for later use, the following rewrites (5.6b). For its viscous term first recognize that [23, A1. Vector Identities, p. 363, (10)] this time implies

$$\nabla^2\vec{\omega} = \nabla(\underbrace{\nabla\cdot\vec{\omega}}_{=0}) - \nabla\times(\nabla\times\vec{\omega}), \tag{5.9}$$

where $\nabla\cdot\vec{\omega} = \nabla\cdot(\nabla\times\vec{u}) = 0$ by another common vector identity [23, A1. Vector Identities, p. 363, (12)]. Using this in the complete viscous term and then rewriting further with [23, A1. Vector Identities, p. 363, (6)] gives

$$\nu\vec{u}\cdot(\nabla^2\vec{\omega}) = -\nu(\nabla\times(\nabla\times\vec{\omega}))\cdot\vec{u} = -\nu\nabla\cdot((\nabla\times\vec{\omega})\times\vec{u}) - \nu(\nabla\times\vec{\omega})\cdot(\underbrace{\nabla\times\vec{u}}_{=\vec{\omega}}). \tag{5.10}$$

Using this result and that the first two terms on the right-hand side of (5.6b) can be rewritten as the right-hand side of (2.97), it is possible to rewrite (5.6b) completely as

$$\vec{u}\cdot\frac{\partial\vec{\omega}}{\partial t} = \nabla\cdot\left((\vec{u}\times\vec{\omega})\times\vec{u}\right) - \nu\nabla\cdot((\nabla\times\vec{\omega})\times\vec{u}) - \nu(\nabla\times\vec{\omega})\cdot\vec{\omega}. \tag{5.11}$$

Now (5.8) and (5.11) can be substituted into (5.5) yielding an evolution equation for helical density that should be suitable for discretization in the following:

$$\frac{\partial h}{\partial t} - \nabla\cdot\left((\vec{u}\times\vec{\omega})\times\vec{u}\right) + \nabla\cdot\left(\vec{\omega}\bar{p}\right) = -2\nu(\nabla\times\vec{\omega})\cdot\vec{\omega} - \nu\nabla\cdot((\nabla\times\vec{\omega})\times\vec{u}). \tag{5.12}$$

A step towards the spatial discretization of (5.12) is made by substituting trial functions, multiplicating with test functions $m_h \in \mathrm{CG}_N$ and integrating

over the domain. For the time derivative and the first viscous term this is sufficient:

$$\left\langle \frac{\partial h_h}{\partial t}, m_h \right\rangle_\Omega \quad \forall m_h \in \mathrm{CG}_N \tag{5.13}$$

and

$$-2\nu \left\langle (\nabla \times \vec{\omega}_h) \cdot \vec{\omega}_h, m_h \right\rangle_\Omega \quad \forall m_h \in \mathrm{CG}_N. \tag{5.14}$$

Discretization of the other terms also requires a partial integration step with [23, A1. Vector Identities, p. 364, Eq. (22)]. This in order to avoid the divergence derivative present in each of them, which in all cases produces a result that is not guaranteed to be square-integrable due to the function spaces allocated to the discrete variables (5.2). For example for the term with pressure, the partial integration looks as follows without bracket notation:

$$\iiint_\Omega m_h \nabla \cdot (\vec{\omega}_h \bar{p}_h) \,\mathrm{d}V = \underbrace{\oiint_{\partial\Omega} \vec{n} \cdot (m_h \vec{\omega}_h \bar{p}_h) \,\mathrm{d}S}_{=0 \text{ by periodic BC}} - \iiint_\Omega (\vec{\omega}_h \bar{p}_h) \cdot \nabla m_h \,\mathrm{d}V. \tag{5.15}$$

After performing spatial discretization in the way just described, a discrete evolution equation for helical density is obtained by applying temporal discretization. This is done with the midpoint rule (3.17) also used in the MEEVC formulation (see Section 3.1.5). The result is

$$\begin{aligned} &\left\langle \frac{h_h^{k+1} - h_h^k}{\Delta t}, m_h \right\rangle_\Omega + \left\langle \left(\frac{\vec{u}_h^{k+1} + \vec{u}_h^k}{2} \times \vec{\omega}_h^{k+\frac{1}{2}} \right) \times \frac{\vec{u}_h^{k+1} + \vec{u}_h^k}{2}, \nabla m_h \right\rangle_\Omega \\ &\qquad - \left\langle \vec{\omega}_h^{k+\frac{1}{2}} \bar{p}_h^{k+\frac{1}{2}}, \nabla m_h \right\rangle_\Omega \\ &= -2\nu \left\langle \left(\nabla \times \vec{\omega}_h^{k+\frac{1}{2}} \right) \cdot \vec{\omega}_h^{k+\frac{1}{2}}, m_h \right\rangle_\Omega \\ &\qquad + \nu \left\langle \left(\nabla \times \vec{\omega}_h^{k+\frac{1}{2}} \right) \times \frac{\vec{u}_h^{k+1} + \vec{u}_h^k}{2}, \nabla m_h \right\rangle_\Omega \quad \forall m_h \in \mathrm{CG}_N. \end{aligned} \tag{5.16}$$

Vorticity equation

Unfortunately, the 3D vorticity transport equation (2.22) contains the gradients of both velocity and vorticity. These are not compatible with their function spaces (5.2) and the discrete DeRham sub-complex (5.3). One of

the terms with an incompatible gradient can be rewritten with vector identity [23, A1. Vector Identities, p. 363, Eq. (8)] though, as it implies that

$$\underbrace{\nabla(\vec{u}\cdot\vec{\omega})}_{=\nabla h} = (\vec{u}\cdot\nabla)\vec{\omega} + (\vec{\omega}\cdot\nabla)\vec{u} + \vec{u}\times(\nabla\times\vec{\omega}) + \underbrace{\vec{\omega}\times(\nabla\times\vec{u})}_{=\vec{\omega}\times\vec{\omega}=\vec{0}}. \tag{5.17}$$

Substituting from this equation into (2.22) for $(\vec{u}\cdot\nabla)\vec{\omega}$ yields

$$\frac{\partial\vec{\omega}}{\partial t} + \nabla h - 2(\vec{\omega}\cdot\nabla)\vec{u} - \vec{u}\times(\nabla\times\vec{\omega}) = -\nu\nabla\times(\nabla\times\vec{\omega}), \tag{5.18}$$

so that the gradient of vorticity is no longer present. Also, the viscous term has been rewritten according to [23, A1. Vector Identities, p. 363, Eq. (10)]:

$$\nabla\times(\nabla\times\vec{\omega}) = \nabla(\underbrace{\nabla\cdot\vec{\omega}}_{=0}) - \nabla^2\vec{\omega}. \tag{5.19}$$

This will allow a partial integration step that reduces the maximum order of derivatives in the viscous term to first order as described below.

Substituting trial functions in (5.18), multiplying with test functions $\vec{\mathscr{E}}_h$, integrating over the domain and applying the midpoint rule (3.17) for time integration (see Section 3.1.5) yields this variational formulation:

$$\begin{aligned}
&\left\langle \frac{\vec{\omega}_h^{k+\frac{3}{2}} - \vec{\omega}_h^{k+\frac{1}{2}}}{\Delta t}, \vec{\mathscr{E}}_h \right\rangle_\Omega + \left\langle \nabla h_h^{k+1}, \vec{\mathscr{E}}_h \right\rangle_\Omega \\
&\qquad - \left\langle \vec{u}_h^{k+1} \times \left(\nabla \times \left(\frac{\vec{\omega}_h^{k+\frac{3}{2}} + \vec{\omega}_h^{k+\frac{1}{2}}}{2} \right) \right), \vec{\mathscr{E}}_h \right\rangle_\Omega \\
&\qquad\qquad - \left\langle \left(\left(\vec{\omega}_h^{k+\frac{3}{2}} + \vec{\omega}_h^{k+\frac{1}{2}} \right) \cdot \nabla \right) \vec{u}_h^{k+1}, \vec{\mathscr{E}}_h \right\rangle_\Omega \\
&= -\nu \left\langle \nabla \times \left(\frac{\vec{\omega}_h^{k+\frac{3}{2}} + \vec{\omega}_h^{k+\frac{1}{2}}}{2} \right), \nabla\times\vec{\mathscr{E}}_h \right\rangle_\Omega \qquad \forall \vec{\mathscr{E}}_h \in \mathrm{NED}_N^{1,\mathrm{curl}}.
\end{aligned} \tag{5.20}$$

For the viscous term, integration by parts has been applied as follows. First the integrand is rewritten by [23, A1. Vector Identities, p. 363, Eq. (6)]:

$$\nabla\cdot((\nabla\times\vec{\omega}_h)\times\vec{\mathscr{E}}_h) = (\nabla\times(\nabla\times\vec{\omega}_h))\cdot\vec{\mathscr{E}}_h - (\nabla\times\vec{\omega}_h)\cdot(\nabla\times\vec{\mathscr{E}}_h) \tag{5.21}$$

Then, upon integrating this equation over the volume Ω, its left-hand side is identified to be zero by rewriting it as an integral over the boundary surface

(divergence theorem) and applying the periodic boundary conditions:

$$\iiint_{\Omega} \nabla \cdot ((\nabla \times \vec{\omega}_h) \times \vec{\mathscr{E}}_h)\, \mathrm{d}V = \oiint_{\partial\Omega} \vec{n} \cdot \left((\nabla \times \vec{\omega}_h) \times \vec{\mathscr{E}}_h\right) \mathrm{d}S = 0 \tag{5.22}$$

Therefore, the following has been obtained (using bracket notation again):

$$\nu \left\langle \nabla \times (\nabla \times \vec{\omega}_h),\, \vec{\mathscr{E}}_h \right\rangle_{\Omega} = \nu \left\langle \nabla \times \vec{\omega}_h,\, \nabla \times \vec{\mathscr{E}}_h \right\rangle_{\Omega} \tag{5.23}$$

Finally, a comment must be given on why the convective term in (2.22) was modified as in (5.18). One may note that in the 2D situation the partial integration result (3.2), that is

$$\left\langle (\vec{u} \cdot \nabla)\omega,\, \mathscr{E} \right\rangle_{\Omega} = -\left\langle \omega,\, \nabla \cdot (\vec{u}\mathscr{E}) \right\rangle_{\Omega}, \tag{5.24}$$

was used. This is however particular for the 2D case and cannot be used in the 3D situation. The nearest relation is

$$\left\langle (\vec{u} \cdot \nabla)\vec{\omega},\, \vec{\mathscr{E}} \right\rangle_{\Omega} = -\left\langle \vec{\omega},\, (\vec{u} \cdot \nabla)\vec{\mathscr{E}} \right\rangle_{\Omega}, \tag{5.25}$$

but this is not useful as it would instead leave an undesired gradient in the test function. Hence the approach outlined earlier is preferred.

5.2.3 Summary of the MEHC method

Step 1: find $\vec{u}_h^{k+1} \in \mathrm{RT}_N$ and $\bar{p}_h^{k+\frac{1}{2}} \in \mathrm{DG}_{N-1}$ such that

$$\boxed{\begin{aligned} \left\langle \frac{\vec{u}_h^{k+1} - \vec{u}_h^{k}}{\Delta t},\, \vec{v}_h \right\rangle_{\Omega} + \left\langle \vec{\omega}_h^{k+\frac{1}{2}} \times \frac{\vec{u}_h^{k+1} + \vec{u}_h^{k}}{2},\, \vec{v}_h \right\rangle_{\Omega} - \left\langle \bar{p}_h^{k+\frac{1}{2}},\, \nabla \cdot \vec{v}_h \right\rangle_{\Omega} \\ = -\nu \left\langle \nabla \times \vec{\omega}_h^{k+\frac{1}{2}},\, \vec{v}_h \right\rangle_{\Omega} \quad \forall \vec{v}_h \in \mathrm{RT}_N, \end{aligned}} \tag{5.26a}$$

$$\boxed{\left\langle \nabla \cdot \vec{u}_h^{k+1} + r_h^{k+\frac{1}{2}},\, q_h \right\rangle_{\Omega} = 0 \quad \forall q_h \in \mathrm{DG}_{N-1},} \tag{5.26b}$$

$$\boxed{\left\langle \bar{p}_h^{k+\frac{1}{2}},\, \tilde{r}_h \right\rangle_{\Omega} = 0 \quad \forall \tilde{r}_h \in \mathrm{R}_0.} \tag{5.26c}$$

Step 2: find $h_h^{k+1} \in \mathrm{CG}_N$ such that

$$\begin{aligned}\left\langle \frac{h_h^{k+1}-h_h^k}{\Delta t}, m_h \right\rangle_\Omega + \left\langle \left(\frac{\vec{u}_h^{k+1}+\vec{u}_h^k}{2} \times \vec{\omega}_h^{k+\frac{1}{2}} \right) \times \frac{\vec{u}_h^{k+1}+\vec{u}_h^k}{2}, \nabla m_h \right\rangle_\Omega \\ - \left\langle \vec{\omega}_h^{k+\frac{1}{2}} \bar{p}_h^{k+\frac{1}{2}}, \nabla m_h \right\rangle_\Omega \\ = -2\nu \left\langle \left(\nabla \times \vec{\omega}_h^{k+\frac{1}{2}} \right) \cdot \vec{\omega}_h^{k+\frac{1}{2}}, m_h \right\rangle_\Omega \\ + \nu \left\langle \left(\nabla \times \vec{\omega}_h^{k+\frac{1}{2}} \right) \times \frac{\vec{u}_h^{k+1}+\vec{u}_h^k}{2}, \nabla m_h \right\rangle_\Omega \qquad \forall m_h \in \mathrm{CG}_N.\end{aligned} \tag{5.27}$$

Step 3: find $\vec{\omega}_h^{k+\frac{3}{2}} \in \mathrm{NED}_N^{1,\mathrm{curl}}$ such that

$$\begin{aligned}\left\langle \frac{\vec{\omega}_h^{k+\frac{3}{2}}-\vec{\omega}_h^{k+\frac{1}{2}}}{\Delta t}, \vec{\mathscr{E}}_h \right\rangle_\Omega + \left\langle \nabla h_h^{k+1}, \vec{\mathscr{E}}_h \right\rangle_\Omega \\ - \left\langle \vec{u}_h^{k+1} \times \left(\nabla \times \left(\frac{\vec{\omega}_h^{k+\frac{3}{2}}+\vec{\omega}_h^{k+\frac{1}{2}}}{2} \right) \right), \vec{\mathscr{E}}_h \right\rangle_\Omega \\ - \left\langle \left(\left(\vec{\omega}_h^{k+\frac{3}{2}}+\vec{\omega}_h^{k+\frac{1}{2}} \right) \cdot \nabla \right) \vec{u}_h^{k+1}, \vec{\mathscr{E}}_h \right\rangle_\Omega \\ = -\nu \left\langle \nabla \times \left(\frac{\vec{\omega}_h^{k+\frac{3}{2}}+\vec{\omega}_h^{k+\frac{1}{2}}}{2} \right), \nabla \times \vec{\mathscr{E}}_h \right\rangle_\Omega \qquad \forall \vec{\mathscr{E}}_h \in \mathrm{NED}_N^{1,\mathrm{curl}}.\end{aligned} \tag{5.28}$$

5.3 Algebraic proof of discrete conservation

In the following it is investigated whether the discrete formulation for 3D flow that is summarized in Section 5.2.3 conserves mass, kinetic energy and helicity (see Table 2.1). Note the latter two only apply to the inviscid case, that is in the limit of $\nu = 0$. The proofs here mostly amount to a demonstration using algebra and reasoning similar to what is done in Section 3.2 for the 2D MEEVC method.

Mass conservation

Local and global mass conservation are achieved due to the divergence-free constraint (5.26b) on incompressible flow, combined with the choice of func-

tion space such that $\vec{u} \in H(\text{div}, \Omega)$. Just as shown for the MEEVC scheme in Section 3.2.1, the flow will satisfy $\nabla \cdot \vec{u} = 0$ at any point.

Helicity conservation

Helicity is an invariant for inviscid flow (Section 2.2.5): investigations below show that this also holds for the discrete helical density variable h_h but not necessarily for the product $\vec{u}_h \cdot \vec{\omega}_h$. The latter is often more interesting though: it tells us whether the velocity and vorticity fields, which' solutions are usually of higher interest than the helical density field, are such that they incorporate helicity conservation.

Discrete helicity defined as

$$\mathscr{H}_h := \int_\Omega h_h \, \mathrm{d}\Omega \tag{5.29}$$

is shown to be constant as follows. Taking $\nu = 0$ and a constant test function $m_h = c$ in the discrete evolution equation for helical density (5.27), while noting that then $\nabla m_h = \nabla c = 0$, yields

$$\left\langle \frac{h_h^{k+1} - h_h^k}{\Delta t}, c \right\rangle_\Omega = 0. \tag{5.30}$$

This means that helicity defined as the integral of the discrete helical density variable is conserved.

Now it is also investigated if discrete helicity defined as

$$\mathscr{H}_h := \int_\Omega \vec{u}_h \cdot \vec{\omega}_h \, \mathrm{d}\Omega \tag{5.31}$$

is also constant for $\nu = 0$. An approach is to choose the discrete vorticity solution $\vec{\omega}_h^{k+\frac{1}{2}}$ as a test function in the discrete linear momentum equation (5.26a). The first integral term of the resulting equation then represents the difference of helicity at two times divided by the time-step size. This is however not exactly so, because $\vec{\omega}_h^{k+\frac{1}{2}}$ is at half the time-step between $\vec{u}_h^{k+1}$ and $\vec{u}_h^k$. Another problem is that the discrete vorticity is not in the same space as the test function $\vec{v}_h$, so some information of its solution will be changed before it can be substituted. This also means that the second integral term

in (5.26a) will not become (exactly) zero when $\vec{v}_h = \vec{\omega}_h^{k+\frac{1}{2}}$. The third integral term may not be zero either because the divergence of the discrete vorticity solution is generally nonzero. From all this it can be concluded that there is no proof of helicity conservation in the context described.

As a variant to the approach above, again directly use the definition of discrete helicity in (5.31) but now try to represent the difference in helicity at two time-steps with the discrete vorticity transport equation (5.28). Substitute velocity as a test function. This is at least as problematic, however. It rejects that there is conservation of helicity.

Another variant starts from the temporal derivative of (5.31), that is

$$\frac{\mathrm{d}\mathcal{H}_h}{\mathrm{d}t} = \int_\Omega \left(\frac{\partial \vec{u}_h}{\partial t} \cdot \vec{\omega}_h + \vec{u}_h \cdot \frac{\partial \vec{\omega}_h}{\partial t} \right) \mathrm{d}\Omega, \tag{5.32}$$

where it was used that the domain is constant. Then use both the discrete linear momentum balance (5.26a) and vorticity transport equation (5.28) to find a specific expression for this and check if it is zero. This again does not work: the integrals still appear to be nonzero without evidence that they cancel out. It can hence be concluded that helicity conservation in the product of the velocity and vorticity fields is not demonstrated this way either.

Kinetic energy conservation

The discrete linear momentum equation (5.26a) is used to compute the velocity field at the next time-step such that kinetic energy is conserved for inviscid flow, as follows. First of all the right hand side is zero because $\nu = 0$. The remaining equation must be valid for any test function $\vec{v}_h \in \mathrm{RT}_N$, so also for the choice $\vec{v}_h = \vec{u}_h^{k+1} + \vec{u}_h^k$. Furthermore any initial condition or solution must satisfy $\nabla \cdot \vec{u}_h = 0$, so the pressure integral is obviously zero as well. Then what remains is:

$$\left\langle \frac{\vec{u}_h^{k+1} - \vec{u}_h^k}{\Delta t}, \vec{u}_h^{k+1} + \vec{u}_h^k \right\rangle_\Omega + \left\langle \vec{\omega}_h^{k+\frac{1}{2}} \times \frac{\vec{u}_h^{k+1} + \vec{u}_h^k}{2}, \vec{u}_h^{k+1} + \vec{u}_h^k \right\rangle_\Omega = 0, \tag{5.33}$$

which can be rearranged to

$$\left\langle \vec{u}_h^{k+1}, \vec{u}_h^{k+1} \right\rangle_\Omega + \underbrace{\Delta t \left\langle \vec{\omega}_h^{k+\frac{1}{2}} \times \frac{\vec{u}_h^{k+1} + \vec{u}_h^k}{2}, \vec{u}_h^k + \vec{u}_h^{k+1} \right\rangle_\Omega}_{=0} = \left\langle \vec{u}_h^k, \vec{u}_h^k \right\rangle_\Omega . \tag{5.34}$$

Here the integral multiplied with Δt has a cross product inside that is perpendicular to $\vec{u}_h^{k+1} + \vec{u}_h^k$ (by definition of the cross product), hence the inner product with this particular test function is zero. This shows kinetic energy is conserved:

$$\mathcal{K}_h^{k+1} := \frac{1}{2}\left\langle \vec{u}_h^{k+1}, \vec{u}_h^{k+1} \right\rangle_\Omega = \frac{1}{2}\left\langle \vec{u}_h^{k}, \vec{u}_h^{k} \right\rangle_\Omega := \mathcal{K}_h^{k}. \tag{5.35}$$

This derivation and result is similar to that for the MEEVC method in [25], also worked out in Section 3.2.2.

5.4 Critical review of the proposed 3D method

In this chapter a 3D MEHC method has been constructed and the following is the place to critically look at its qualities. Overall, the method has been constructed with the design of the 2D MEEVC method in mind. This for example meant that conforming function spaces were chosen combined with the objective to only use admissible derivatives in the equations. A remarkable and possibly unique feature is the use of a separate helicity equation. This made it possible to conserve helicity and to remove the gradient of vorticity from the vorticity transport equation. This gradient would be outside of the DeRham complex (5.3), so it is better to avoid it.

The foremost thing to discuss is the expected efficacy of the formulation with respect to its conservation properties. In Section 5.3 it was found from algebraic analysis that MEHC is achieved, but that helicity conservation can only be proven for the helical density variable that is directly computed from its own evolution equation. When instead using the product of velocity and vorticity to compute helical density, conservation can no longer be proven. A downside of the approach of using a separate helical density variable with its own equation in the formulation is thus that the velocity and vorticity fields are not (directly) constrained, even though that are usually the parts of the solution that are of higher interest than the helical density field itself. Finding out if solutions are such that the product of velocity and vorticity does tend towards the separate helical density variable with refinement of resolution may however be a topic for later investigation. And possibly also whether this tendency exists for particular parts of the solution (where for example no strong gradients exist). Total vorticity conservation in the MEEVC method

has a similar issue to that just outlined: it holds for the vorticity field ω_h, but is not proven for $\nabla \times \vec{u}_h$ (which is in general unequal to ω_h).

An approach to MEHC that differs from the method proposed here is possible as shown in [36]. The dual-field MEHC method presented there solves for amongst others two velocity fields $\vec{u}_1$ and $\vec{u}_2$ as well as two vorticity fields $\vec{\omega}_1$ and $\vec{\omega}_2$. Both of these duals are staggered in time and each of a pair is discretized in its own function space. The dual-field formulation employs two (similar) linear momentum equations but no vorticity transport equation, nor an equation for helical density evolution. Helicity computed as $\langle \vec{u}_1, \vec{\omega}_1 \rangle_\Omega$ as well as $\langle \vec{u}_2, \vec{\omega}_2 \rangle_\Omega$ is conserved. A flaw in its MEHC properties is however that strong mass conservation is achieved in only one of the dual representations of the velocity field solution. The reported numerical tests however show that problems can be solved well, with MEHC achieved closely when ignoring the velocity field where mass conservation is only weakly enforced.

Having considered the MEHC-efficacy of the 3D method proposed here, another question must be answered: is this method correctly constructed in light of its theoretical framework? Well, not completely. An issue is that the velocity gradient in the variational formulation of the vorticity equation (5.28) is outside of the DeRham complex (5.3) and its square-integrability is not guaranteed. For example instability can therefore arise, but this may depend on the specific problem and conditions though. A similar issue that does not appear to have serious consequences exists for two terms in the MEEVC formulation (3.1). Each of these terms consists of the divergence of a product of two functions, one in velocity and one in vorticity space. Formally it is not sure what the integrability is of the space formed by such a product but this may be unproblematic due to the following. Velocity is in $H(\text{div}, \Omega)$ and vorticity, which is a scalar there, is in $H^1(\Omega)$. So both are square-integrable, also after applying relevant derivatives. Hence possibly also (the divergence of) their product. A general remark to square-integrability (L^2) of functions resulting after possible application of derivatives is that this is formally only enough when integrating a product of two such functions. A product of three or even four functions, as in the second integral term in (5.27), requires respectively L^3 or L^4 for each of these functions. In the finite dimensional case this requirement can however be less stringent as suggested in [36, Remark 1]. Whether L^2-integrability of the polynomial basis functions used is sufficient then (up to a certain level of refinement), however, is perhaps something for a researcher with specialist mathematical skills to investigate.

One could also question the role of helical density in the equations, provided that it is included as an independent variable. In the MEHC formulation proposed here, helical density has its own evolution equation. A different approach it is to consider it as a Lagrange multiplier. This is done for the velocity-vorticity-helicity (VVH) method that is presented in [24], a method which is fundamentally different in several design aspects. Its formulation consists of a vorticity-helical density and a velocity-pressure system, where helical density is considered a Lagrange multiplier for a weakly enforced $\nabla \cdot \vec{\omega}_h = 0$ constraint just as pressure is for a weak $\nabla \cdot \vec{u}_h = 0$ constraint. In terms of conservation properties this VVH method does not achieve MEHC as considered here, but it is good to mention that its approach towards helicity also exists. It should further be remarked that $\nabla \cdot \vec{\omega}_h = 0$ is not enforced at all in the discretization proposed here, although $\nabla \cdot \vec{\omega} = \nabla \cdot (\nabla \times \vec{u}) = 0$ should hold as dictated by the vector calculus rule [23, A1. Vector Identities, p. 363, (12)].

Some thoughts on the computational efficiency of the proposed formulation are as follows. The inclusion of the helicity equation (5.27) in principle has its computational costs. This load could be relatively small though: all terms except the first are known, hence an explicit system may be constructed to solve for helical density at the new time-level. Furthermore, when the helicity equation increases the quality of the formulation then this may also make it more efficient. Another efficient aspect of the proposed MEHC formulation is that it uses the staggered-in-time approach of the MEEVC formulation. This allowed to decouple the velocity-pressure and vorticity systems while also providing linearization.

The 3D algorithm proposed in this chapter has been implemented, but there are problems. To some extend the implementation is based on that of the MEEVC algorithm and thereby again uses the FEniCS package. It was used to simulate a 3D Taylor-Green problem. The output was a direct error or results that grow and at some point explode, first in the helical density field values. This suggests that trouble may arise from the helicity system. One could of course question if it is desired to use an evolution equation for helical density at all in CFD. Anyway, there may also or instead be problems in the vorticity system. Its formulation contains the most recently computed helical density as a known and vorticity closely follows (or might sometimes even lead) its growth and explosion. Furthermore, the vorticity equation contains the gradient of velocity. Remember this gradient falls outside of the DeRham

complex and can therefore give rise to the trouble. In [15] it is suggested that the discrete vortex-stretching term in its entirety, which does not appear in the 2D equations, could be a source of problems in moving from a stable 2D to a new 3D method. It seems least likely, though not impossible, that the trouble arises from the velocity-pressure-r-system. There may however be causes outside of the formulation itself. One is that there may be inadequacies in its implementation, which could require much effort, specialist knowledge or both to find out. Another cause may be that the simulations were performed with course grids. This is not expected to be a major cause of the trouble though but it does mean viscous dissipation at unresolved scales is missed. Capturing these in 3D could however mean computational demands that are too high for the computer that was used.

Chapter 6

Conclusions and perspectives

In short, this thesis started off with a study of the continuous equations for understanding of the matter, then considered the 2D MEEVC method with extensive simulation results and finally used the knowledge of these parts for the novel 3D MEHC method. Thereby the favorable properties of the MEEVC method were verified with few critical notes. The MEHC method was constructed using the MEEVC method's mimetic design philosophies. A successful implementation has not (yet) been achieved.

When it comes to the discrete formulation used for the MEEVC method, this thesis describes some theoretical support and a modification that are not to be found in the original publication [25]. It is demonstrated by extensive derivations in Section 2.1.4 that vorticity is closely related to angular momentum, which underlines its physical relevance in many flow situations. Support for adding the vorticity transport equation to the velocity-pressure system in order to enhance CFD accuracy can be found in [1]. Such is quite unsurprising in light of the aforementioned. The modification to the MEEVC method as published in [25] is the addition of a pressure constraint in the way that is described in Section 3.1.2. This was recommended by the first author of that paper as a solution against reduced accuracy. It works well but developing a stronger theoretical backing may be interesting for future work.

Part of the results from simulating Taylor-Green flows with the MEEVC method confirm the corresponding ones published in [25] and another part adds additional information as follows. As can be seen in Section 4.2, integral quantities develop correctly over a longer time span even when resolutions are extremely low. In that case there is quite some error of course,

but this is largely due to with poor sampling of the initial conditions. Such a demonstration of the MEEVC method's efficacy was not available to this extend. While the most refined simulations delivered the best accuracy, a side note must be made for these in particular when it comes to conservation. Very small diverging trends in kinetic energy, enstrophy and vorticity under inviscid conditions are visible. These trends have a negligible impact here but this could especially change when refinement is much higher. It can therefore be concluded that the MEEVC method, like any other method, has its limits. These may only come into play in extreme situations though.

A new MEHC method employing an evolution equation for helical density, which is uncommon or even unique in CFD, has been developed for this thesis. Further research will be needed though to see if this method or its approach can be successful. A theoretical issue of the method regards the integrability of certain terms in its formulation as discussed in Section 5.4, although such an issue was also identified in the MEEVC method. Yet serious consequences were not identified there. Successful simulations with the MEHC method have not been achieved and are not in the scope of this thesis. It may be something for later work to find out if certain modifications of the formulation or a better implementation in computer code can change this. The simulation results that were obtained now have relatively low resolutions and frankly showed divergence with increasing simulated time. These were not processed further for inclusion in this thesis. On the other hand, an analytic proof of the MEHC properties can be found in Section 5.3. Conservation of helicity is however only proven for the helical density variable itself, that is there is in general no helicity conservation for helical density computed from the product of velocity and vorticity. Getting an idea of how close this product can be to the separately computed helical density in practical simulations may be something for future work when there is a well-functioning implementation.

A MEHC method that does not employ a separate helical density variable and therefore lacks the related issue just discussed was presented in [36] contemporary to the development of the method in this thesis. It is clearly superior now, considering that its publication shows it functions well in solving several problems numerically. Its dual-field approach is however such that strong mass conservation is only achieved in one of the dual representations of the velocity field solution.

Bibliography

[1] M. Akbas, L. G. Rebholz, and C. Zerfas, *Optimal vorticity accuracy in an efficient velocity–vorticity method for the 2D Navier–Stokes equations*, Calcolo, 55 (2018).

[2] D. N. Arnold, R. S. Falk, and R. Winther, *Finite element exterior calculus, homological techniques, and applications*, Acta Numerica, 15 (2006), pp. 1–155.

[3] A. Bedford and W. Fowler, *Engineering Mechanics Dynamics*, Prentice Hall / Pearson, 5 ed., 2008.

[4] M. A. Belenli, L. G. Rebholz, and F. Tone, *A note on the importance of mass conservation in long-time stability of navier–stokes simulations using finite elements*, Applied Mathematics Letters, 45 (2015), pp. 98–102.

[5] M. E. Brachet, D. I. Meiron, S. A. Orszag, B. G. Nickel, R. H. Morf, and U. Frisch, *Small-scale structure of the Taylor–Green vortex*, Journal of Fluid Mechanics, 130 (1983), pp. 411–452.

[6] A. Buffa, C. de Falco, and G. Sangalli, *Isogeometric analysis: stable elements for the 2D Stokes equation*, International Journal for Numerical Methods in Fluids, 65 (2011), pp. 1407–1422.

[7] F. Capuano and D. Vallefuoco, *Effects of Discrete Energy and Helicity Conservation in Numerical Simulations of Helical Turbulence*, Flow, Turbulence and Combustion, 101 (2018), pp. 343–364.

[8] S. Charnyi, T. Heister, M. A. Olshanskii, and L. G. Rebholz, *On conservation laws of Navier–Stokes Galerkin discretizations*, Journal of Computational Physics, 337 (2017), pp. 289–308.

[9] P. C. Chatwin, *The vorticity equation as an angular momentum equation*, PCPS, (1973), pp. 365–367.

[10] B. Cockburn, G. Kanschat, and D. Schötzau, *A note on discontinuous Galerkin divergence-free solutions of the Navier–Stokes equations*, Journal of Scientific Computing, 31 (2006), pp. 61–73.

[11] G. de Diego, A. Palha, and M. Gerritsma, *Inclusion of no-slip boundary conditions in the MEEVC scheme*, Journal of Computational Physics, 378 (2019), pp. 615–633.

[12] J. A. Evans and T. J. Hughes, *Isogeometric divergence-conforming B-splines for the unsteady Navier–Stokes equations*, Journal of Computational Physics, 241 (2013), pp. 141 – 167.

[13] T. B. Gatski, *Review of incompressible fluid flow computations using the vorticity–velocity formulation*, Applied Numerical Mathematics 7, (1991), pp. 227–239.

[14] E. Hairer, C. Lubich, and G. Wanner, *Geometric Numerical Integration*, Springer-Verlag, Berlin-Heidelberg (and Geneva and Tübingen), 2 ed., 2006.

[15] T. Heister, M. A. Olshanskii, and L. G. Rebholz, *Unconditional long-time stability of a velocity–vorticity method for the 2D Navier–Stokes equations*, Numerische Mathematik, 135 (2017), pp. 143–167.

[16] F. Irgens, *Tensor Analysis*, Springer Nature, Cham (Switzerland) and Bergen (Norway), 2019.

[17] L. Jofre, O. Lehmkuhl, J. Ventosa, F. X. Trias, and A. Oliva, *Conservation properties of unstructured finite-volume mesh schemes for the Navier–Stokes equations*, Numerical Heat Transfer, Part B: Fundamentals, 65:1 (2014), pp. 53–79.

[18] T. Kajishima and K. Taira, *Computational Fluid Dynamics — Incompressible Turbulent Flows*, Springer Nature, 2017, ch. Appendix A, p. 312.

[19] R. C. Kirby, A. Logg, M. E. Rognes, and A. R. Terrel, *Common and unusual finite elements*, in Automated Solution of Differential Equations by the Finite Element Method, vol. 84 of Lecture Notes in Compu-

tational Science and Engineering, Springer-Verlag, Berlin-Heidelberg, 2012, ch. 3, pp. 95–119.

[20] W. Layton, C. C. Manica, M. Neda, M. Olshanskii, and L. G. Rebholz, *On the accuracy of the rotation form in simulations of the Navier–Stokes equations*, Journal of Computational Physics, 228 (2009), pp. 3433–3447.

[21] A. Logg, K.-A. Mardal, and G. N. Wells, eds., *Automated Solution of Differential Equations by the Finite Element Method*, vol. 84 of Lecture Notes in Computational Science and Engineering, Springer, 2012.

[22] R. Loubère, P.-H. Maire, and B. Rebourcet, *Handbook of Numerical Methods for Hyperbolic Problems*, vol. 17 of Handbook of Numerical Analysis, Elsevier, 2016, ch. 13, p. 326.

[23] D. R. Lynch, *Numerical partial differential equations for environmental scientists and engineers: a first practical course*, Springer Science+Business Media, Inc., 2005.

[24] M. A. Olshanskii and L. G. Rebholz, *Velocity-vorticity-helicity formulation and a solver for the Navier–Stokes equations*, Journal of Computational Physics, 229 (2010).

[25] A. Palha and M. Gerritsma, *A mass, energy, enstrophy and vorticity conserving (MEEVC) mimetic spectral element discretization for the 2D incompressible Navier–Stokes equations*, Journal of Computational Physics, 328 (2017), pp. 200–220.

[26] J. B. Perot, *Discrete conservation properties of unstructured mesh schemes*, Annual Review of Fluid Mechanics, 43 (2011), pp. 299–318.

[27] L. G. Rebholz, *Conservation laws of turbulence models*, Journal of Mathematical Analysis and Applications, 326 (2007), pp. 33–45.

[28] P. L. Roe, *Computational fluid dynamics—retrospective and prospective*, International Journal of Computational Fluid Dynamics, 19 (2005), pp. 581–594.

[29] J. Stewart, *Calculus: Early Transcendentals*, Thomson Brooks/Cole, 5th (international student) ed., 2003.

[30] G. I. Taylor and A. E. Green, *Mechanism of the production of small eddies from large ones*, Proceedings of the Royal Society of London A: Mathematical, Physical and Engineering Sciences, 158 (1937), pp. 499–521.

[31] E. Tonti, *The Mathematical Structure of Classical and Relativistic Physics: A General Classification Diagram*, Modeling and Simulation in Science, Engineering and Technology, Birkhäuser Basel, 2013.

[32] R. Verstappen and A. Veldman, *Symmetry-preserving discretization of turbulent flow*, Journal of Computational Physics, 187 (2003), pp. 343–368.

[33] F. M. White, *Viscous Fluid Flow*, McGraw-Hill, New York, 3rd international ed., 2006.

[34] R. Wijland, *Novelties in Conservative CFD*. Project plan for course AE4010, 2021.

[35] Wikipedia-contributor(s), *Vorticity equation*. `https://en.wikipedia.org/wiki/Vorticity_equation`, last checked 2017-09-20.

[36] Y. Zhang, A. Palha, M. Gerritsma, and L. G. Rebholz, *A mass-, kinetic energy- and helicity-conserving mimetic dual-field discretization for three-dimensional incompressible Navier-Stokes equations, part I: Periodic domains*, Journal of Computational Physics, 451 (2022).